Turbulent Flow Structures and Morphological Characteristics of Mining Affected Alluvial Channel

A Thesis Submitted

In partial fulfilment of the requirement for the degree of

Doctor of Philosophy

Submitted by

Bandita Barman

(156104012)

DEPARTMENT OF CIVIL ENGINEERING

INDIAN INSTITUTE OF TECHNOLOGY GUWAHATI

Guwahati-781039, Assam

August, 2018

Declaration of Authorship

I, Bandita Barman, declare that this thesis "Turbulent Flow Structures and Morphological Characteristics of Mining Affected Alluvial Channel" and the work presented in it are my own and have been generated by me as the result of my own original research

I confirm that:

1. This work was done wholly or mainly while in candidature for a research degree at this Institute;

2. Where any part of this thesis has previously been submitted for a degree or any other qualification at this Institute or any other institution, this has been clearly stated;

3. Where I have consulted the published work of others, this is always clearly attributed;

4. Where I have quoted from the work of others, the source is always given. With the exception of such quotations, this thesis is entirely my own work;

5. I have acknowledged all main sources of help;

6. Where the thesis is based on work done by myself jointly with others, I have made clear exactly what was done by others and what I have contributed myself;

Signed: ……

Date: ……

Department of Civil Engineering
Indian Institute of Technology Guwahati
Guwahati-781039, Assam, India

Prof. Arup Kumar Sarma
Professor
aks@iitg.ernet.in
0361-258 2409

Dr. Bimlesh Kumar
Associate Professor
bimk@iitg.ernet.in
0361-258 2420

CERTIFICATE

This is to certify that the thesis entitled **Turbulent Flow Structures and Morphological Characteristics of Mining Affected Alluvial Channel** submitted by **Bandita Barman** to the Department of Civil Engineering, Indian Institute of Technology Guwahati, is a record of bonafide research work under our supervision and is worthy of consideration for the award of the degree of Doctor of Philosophy of the Institute.

Date:

Place: Guwahati

Prof. Arup Kumar Sarma

Dr. Bimlesh Kumar

List of Publications

JOURNALS

1. Bandita Barman, Anurag Sharma, Bimlesh Kumar, and Arup Kumar Sarma, "Multiscale characterization of migrating sand wave in mining induced alluvial channel." **Ecological Engineering**, 102 (2017), 199-206. Elsevier.
2. Bandita Barman, Bimlesh Kumar, and Arup Kumar Sarma, "Turbulent flow structures and geomorphic characteristics of mining affected alluvial channel." **Earth Surface Processes and Landforms** (2018), 43(9), 1811-1824.
3. Bandita Barman, Arup Kumar Sarma, and Bimlesh Kumar. "Mining pit migration of an alluvial channel: experimental and numerical investigations." **ISH Journal of Hydraulic Engineering** (2018). Doi:10.1080/09715010.2018.1501775.
4. Bandita Barman, Bimlesh Kumar, and Arup Kumar Sarma. "Dynamic characterization of migration of mining pit in an alluvial channel." **International Journal of Sediment Research**. (Accepted).

BOOK CHAPTER

1. Bandita Barman, Bimlesh Kumar, and Arup Kumar Sarma, "Experimental study on mining pit migration." Book Title: Development of water resources in India, Series Title: Water Science Technology Library Series, Springer, Vol. 84, Chapter 26, ISBN: 978-3-319-55124-1.

CONFERENCES

1. Bandita Barman and Arup Kumar Sarma, "A study on river bed degradation due to mining of coarser top sediment layer." 6th International Conference on Computation and Simulation, IIT Bombay, 27th June- 1st July 2016.

2. Bandita Barman, Bimlesh Kumar, and Arup Kumar Sarma, "What follows after sediment mining- a preliminary investigation." 6th International and 43rd National Conference on Fluid Mechanics and Fluid Power, MNNIT Allahabad, 15th -17th December, 2016
3. Bandita Barman, Bimlesh Kumar and Arup Kumar Sarma 'Statistical Analysis of Bed Feature of an Alluvial Channel at Upstream and Downstream of Mining Pit', 44th National Conference on Fluid Mechanics and Fluid Power, Amrita University, Amritapuri Campus, Kollam, Kerala, 14th -16th December, 2017.
4. Bandita Barman, Abhishek Dixit, Arnab Kumar Pal, Bimlesh Kumar and Arup Kumar Sarma.'Characteristics of bed load in a mined alluvial channel', 22nd International Conference on Hydraulics, Water Resources and Coastal Engineering (Hydro), L. D. College of Engineering, Ahmedabad, 21st -23rd December, 2017.
5. Bandita Barman, Shivam Singh, Shankar Dev Gour, Subhashish Chamua, Bimlesh Kumar and Arup Kumar Sarma.' Review on adverse impact of river sand mining', 22nd International Conference on Hydraulics, Water Resources and Coastal Engineering (Hydro), L. D. College of Engineering, Ahmedabad, 21st -23rd December, 2017.

Acknowledgements

Completion of this Doctoral Dissertation has been a truly life-changing experience for me and it would not have been possible to do without the support and guidance that I received from many people.

First of all, I am highly indebted to my supervisors Prof. A K Sarma and Dr. Bimlesh Kumar for their guidance and supervision in completing my research work. The unconditional support gave by them always made me to clarify my doubts and I consider it as a great privilege to do my doctoral program under their guidance and to learn from their respective research expertise.

Besides my advisors, I would like to thank my thesis committee: Prof. Subashisa Dutta, Prof. Chandan Mahanta, Dr. Sreeja P. for their insightful comments, encouragement and guidance through this process; your discussion, ideas, and feedback have been absolutely invaluable.

I would like to acknowledge Department of Civil Engineering at IIT Guwahati for giving me the opportunity to pursue my PhD and does my research work.

I sincerely thank the many people who assisted to perform the experiments (Vishal Deshpande, Mahesh Patel, Anurag, Rutuja, Bazal Da, Suvam, Keshab, Arun, Bittu. Anil, Shashikant, Arnab, Abhishekh, Abhijit, Jyotismita, Vinay, Jyotirmoy). And special thanks to Anurag Sharma for encouraging me and for helping me out at the starting of my experimental work. Additionally, the help extended by summer interns, Shivam Singh, Shankar Dev Gour, Subhashish Chamua cannot be left unmentioned.

I would like to express my warm thanks to all my friends and seniors specially Hridoy Moni Kalita, Mithun Deka, Karuna Dutta, Sagarika and Raktim for helping me to learn software as well as different topics related to my research work.

I express my gratitude to my closest friends Jayshree, Uddipana and Nayantara for their unconditional friendship, support and patience throughout these years. I would like to give sincere thanks to Tinesh Pathania for staying by my side and helping me in completing this research.

Finally, I would like to thank my parents, my sisters and brother in law for their support and encouragement. I also place on record, my sense of gratitude to one and all who, directly or indirectly, have lent their helping hand in this journey.

Abstract

Sand mining in a river is an important part of civil construction work. River environment gets highly influenced by the sand mining activities. Exploitation of rivers takes place as sediment mining changes the geomorphic characteristics. Hence, the study of sand mining is important to understand the changes occurring in a river due to such activities. In this present research work, an experimental study has been conducted to analyze the impact of sand mining on morphology and the flow characteristics of the channel. Experimental investigation was carried out under different hydraulic condition in a glass sided straight recirculating flume having a bed covered by sand. Three types of sand of different median diameter 1.1mm, 0.5mm, 0.418mm were used during the experimentation. The experimental data were collected for five different shaped mining pits, having two major categories, one constructed across the whole width of the channel and another one with bank on both sides. The pit was constructed on dry bed condition.

Morphological changes of the channel bed occur due to the presence of mining pit. The channel bed shows severe degradation at downstream of the mining pit. The partial filling and migration of upstream edge is observed from the longitudinal bed profile. The cross-sectional profile also shows erosion at the bank of the pit and the erosion is expanded to the whole width of the channel and propagates downstream with time. The deposition of sediment occurs along the upstream edge of the pit and the depth of the pit decreases with time.

The turbulent structures of the flow have been analyzed for the mining region including upstream and downstream of the pit. Velocity profile shows the presence of reversal velocity at the central bottom of the pit. Results show that velocity profile for the inner zone of flow does not satisfy the modified logarithmic law at center of the pit and also at downstream edge of it. The maximum value of Reynolds shear stress occurs at the center of the pit. The Reynolds shear stress is also higher at downstream of the pit as compared to the upstream of it. The disturbance on the channel bed as a form of mining pit increases the Reynolds shear stress, turbulent intensities in the mining pit region and downstream of it as compared to the upstream section. Analysis of the bursting phenomenon shows that the contribution of sweep and ejection events to the total Reynolds shear stress is more dominant over outward and inward interaction events. The dominance of the sweep event over ejection is observed at the near-bed region from

upstream to downstream of the pit and the thickness of dominance of sweep event in the pit and downstream of the pit is found to be more than the upstream. The increase in thickness is responsible for the increase in bed material transport. The increased sediment transport capacity at the mining pit and downstream of it caused the deformation and lowering of channel bed at downstream.

The quantitative understanding of sand mining is important for sustainable development. In this context, analysis has been carried out for quantification of pit migration and the scope of numerical model for simulating pit migration is discussed. The celerity of mining pit is calculated from both physical characteristics and multi-scale statistical analysis of bed profile series. The physical characteristic of mining pit celerity shows an increase in celerity with increase in discharge into the channel. The application of multi-scale statistical analysis gives the length scale dependent celerity of mining pit. The celerity of mining pit from multi-scale analysis also shows an increasing trend with increase in discharge. However, with increase in length scale, celerity decreases. The length by width ratio of the pit plays an important role for calculating the celerity of mining pit. Both physical and statistical approaches impart increase in the mining pit celerity with increase in the length by width ratio of the pit. An empirical formulation is developed for calculating celerity or the migration speed of mining pit based on pit geometry (length by width ratio), average flow velocity and critical shear stress of bed material.

Contents

List of Figures

List of Tables

List of Abbreviations

ADV	Acoustic Doppler Velocimeter
DTM	Digital Terrain Model
GIS	Geographic Information System
MGS	Mean Grain Size
PSD	Power Spectral Density
RSS	Reynolds Shear Stress
SNR	Signal to Noise Ratio
URS	Ultrasonic Ranging System
WC	Wavelet coefficient
WCC	Wavelet cross covariance

List of Symbols

a	Scaling parameter
A	A coefficient which depends on interaction between flow and sediment particles
A_J	Jacobian matrix
b	Location parameter
B	Width of the pit
C_d	Coefficient of discharge
d_{50}	Median grain diameter
D_*	Dimensionless particle diameter
f	Frequency
F	Fluxes in x-direction
F_r	Froude number
$F_{uu}(f)$	Velocity power spectra
g	Acceleration due to gravity
h	Depth of flow
h_z	Water surface elevation
h^+	Non-dimensional flow depth
H	Hyperbolic hole region
H_n	Flow depth measured over the rectangular notch
I	Identity matrix
$I_{i,H}$	Indicator function
k	von Karman constant
L	Length of the pit
L_n	Length of the rectangular notch
m	Total number of samples for ADV data
n	Manning's constant
N	Total number of samples for bed elevation series
p	Porosity of bed material
$P_{i,H}$	Probability of occurrence of bursting events

q	Flow discharge per unit width of the channel
q_b	Dimensionless bed load transport rate
q_s	Bed load transport rate in m^2/s
Q	Flow discharge in m^3/s
Q_b	Bed load discharge in kg/s
Q_s	Quantity of sediment
R	Hydraulic radius
R_{e*}	Shear Reynolds number
s	Specific gravity
S	Source term
S_b	Bed slope
S_f	Friction slope
$S_{i,H}$	Stress function or Fractional contribution of Reynolds stress
S_w	Water surface slope
t	Time
T	Total sampling time for ADV data collection
u	Depth average longitudinal flow velocity
u_{cr}	Critical threshold velocity defined by Van Rijn (1984)
u_{*c}	Critical shear velocity
u_i, v_i, w_i,	Instantaneous velocity in the stream wise, traverse and vertical to the flow direction
U	Flow variable
$\overline{U}$	Time-averaged velocity in the stream wise direction
U_p	Pit migration speed
U_*	Total shear velocity
V	Average flow velocity
$\overline{V}$	Time-averaged velocity in traverse direction

$\overline{W}$	Time-averaged velocity vertical to the flow direction
y	Depth of the mining pit
z	Vertical distance from the bed surface
z_0	Zero velocity level
z_b	Bed elevation above datum
z^+	Non-dimensional vertical height
ω	Wave number
Δx	Sampling interval of bed elevation series
Δx_n	Spatial grid for numerical simulation
Δt	Temporal grid
Δz	Virtual bed level
φ	Dry angle of repose
θ	Shields parameter
θ_{cr}	Critical Shields parameter
ρ	Density of water
ρ_s	Density of bed material
υ	Kinematic viscosity of water
τ	Total shear stress
τ_o	Bed shear stress
τ_{0c}	Critical shear stress
τ_{uw}	Reynolds shear stress
γ	Specific weight of water
γ_s	Specific weight of sediment
σ_g	Geometric standard deviation of bed material
σ_u	Turbulence intensity in the flow direction
σ_w	Turbulence intensity vertical to the flow direction
λ_j	Eigenvalue of flux jacobian matrix

1 Introduction

1.1 Overview

Sand can be mined from various sources, such as river bed, flood plains, inland dunes, beaches, and ocean. River sand mining is a phenomenon of extracting sand from the river bed or flood plain to meet the demand of aggregates for construction and filling. One of the most extensively used sources of sand is river. Extraction of sand becomes intense in a country with rapid industrial development and urbanization. It can be used as a tool for flood control measures but unrestricted demand for construction aggregate more than restoring capacity can have adverse impacts on river environment. In the recent years, this topic is becoming popular among the engineers and scientists of different disciplines because of its adverse impacts on hydrodynamics, hydrology, morphology, environment, and ecology of the river.

Aggregates extract from the river are beneficial for any construction use as these aggregates are granulated, clean and can be easily extracted (Kondolf 1994; Rinaldi et al. 2005). Roads and buildings are constructed using sand and gravel as a common raw material, since sand is required in high-volume for construction, heavy and low cost commodity, they are brought from as close to the point of consumption as possible. Aggregates found in river are actually the sediment carried by the river, which are deposited in flood plain and river bed as bed material. In case of incising river sediment mining always has some adverse impact. It induces erosion to the river bed and bank. In case of aggrading river, controlled sediment mining from river bed and flood plain is a good practice for maintaining the flood capacity and the channel stability, but due to ineffective regulatory control and commercialization of sediment, there is possibility of occurrence of large scale uncontrolled and unplanned sediment mining (Kondolf 1994; Rinaldi et al. 2005). Riparian ecosystem as a self-sustaining environment is threatened nowadays by the indiscriminate and excessive use of riverbed sand. There is a necessity of proper planning and guidelines of mining activities to minimize the adverse impact of mining and also the economic development of the country. As per Geological Survey of India (GSI) most of the methodologies and guidelines undertaken for hard rock quarries are applicable to riverbed mining. The most applicable practices of aggregates mining are as follows,

- Dry pit mining: Dry pit mining is mainly excavated on dry stream beds and exposed channel or point bars.
- Wet pit mining: This involves mining below the water level of a perennial channel generally during the lean period. Wet pit mining may involve partial or full dewatering of working face.
- Bar skimming or scraping: Scraping of top portion of the bar deposits are called bar skimming or scraping. It is generally undertaken for sustainable mining of sand or gravel material.
- Pits on the adjacent floodplain or river terrace: Mining is done in the flood plain not in the active channel. In this case dry or wet pit mining is involved depending upon geomorphology of the area. Dry pits are located above the water table and wet pits are developed below the groundwater table in the area.

A

B

Figure 1.1 A) Flood plain mining site and B) a mining pit in Brahmaputra river flood plain near Agyathuri (Kamrup district)

Excavation of mining pit in a river bed affects the flow characteristics and disrupts the sediment transport of the river. The adverse effects of aggregate mining based on the study of literature can be broadly classified into various categories such as impact on river morphology and hydraulic structures in the river, hydrological impact, environmental, water quality and ecological impact (Collins and Dunne 1989; Collins and Dunne 1990; Rinaldi et al. 2005).

1.2 Impact on River Morphology, Hydraulic Structures, Hydrology and Hydrodynamics of the River

Morphology of the river gets affected by the in-stream and flood plain mining. Morphological impacts includes (1) erosion of channel bed which changes the bed profile of the river, (2) undercutting or collapse of banks, which can be termed as a local effect specific to particular bend or reach and occurs in response to particular modification of channel geometry, (3) increase in channel slope. It also leads to the (1) change in flow velocity, (2) failure of existing structures,

(3) upstream and downstream erosion due to increase in velocity of the stream, (4) downstream changes in patterns of deposition (Collins and Dunne 1989; Collins and Dunne 1990). Figure 1.2 shows the mining site of Mathura river of Cachar district.

Figure 1.2 Mining site of Mathura river of Cachar district

Various researchers focused on the morphological impact of sand and gravel mining and its consequences in hydraulic structures and hydrology of the river.

Bull and Scott (1974) discussed the effects of sand and gravel mining from urban stream bed in the Southern United States. They observed that both active and inactive channel mining causes local lowering of stream bed, increase in rate of replenishment of sand from the watershed, undermining of bridge pier and so on. The proper survey of mining site in inactive channel is required to find out the probability of reactivation of such channel due to the conveyance of storm discharge. They gave an example of reactivation of Tujunga Wash, the major drainage from the western San Gabriel Mountains to the extensively urbanized San Fernando Valley of southern California in the year of 1969, which causes flood in the upper reaches of the south channel. They also stated that channel deepening can accumulate more flood water but it also makes the channel bank more susceptible to the erosion.

Collins and Dunne (1989) studied on gravel transport, gravel harvesting, and channel bed degradation in rivers draining the southern Olympic Mountains, Washington, USA. They conducted sediment mass balance analysis for the three rivers, namely Humptulip, Wynoochee, and Satsop. They found decrease in the annual bedload supply at downstream from 4,000-8,000 m^3 to about 2,000- 3,000 m^3 in the Humptutips and Wynoochee rivers, but at the lower Satsop River it remains at approximately 8,000 m^3. They analyzed data from nine gauging station over a period of 55 years and found river bed degradation of about 0.03m/yr.

Collins and Dunne (1990) again studied more case histories from western United States and New Zealand and found that excessive extraction of gravel affects the pattern of the bank erosion and changes morphology of the river bed. Case studies reveal that the degradation extended to several miles upstream of the mining location. The impact of gravel mining also varies based on the different communities. For some cases, the main concern were the effects on fisheries, while in other cases agricultural or urbanized area. However, the most influencing concern they found from their case studies were flood control, effects on ground water, losses of properties and damages to the engineering structures. They also provided some important gravel mining management practice which can be carried out to reduce the adverse effects of mining. The management practice included the documentation of replacement rate from the upstream,

undisturbed bed elevation profile, historical trend of sediment transport, bar growth, bank erosion, record of gravel extraction volume, periodic monitoring program and so on.

Kondolf (1993) investigated the concept of reclamation in regulation of gravel mining in California. He observed three types of gravel mining activities such as dry pit mining, wet pit mining in the active channel and bar skimming. The concept of reclamation was mainly used for coal mines where the barren large surface mine pit was 'reclaim' by using original top soil. The mining site can be used for the productive purpose such as agriculture on later date. The concept reclamation in case of aggregate mining works for dry terrace pit and can be used as wild life habitat in wet terrace pit. However, he found that it was not a valid framework to regulate extraction in the active channel since the impact of extraction was not confined to a particular location but propagated both upstream and downstream of that location.

Lee et al. (1993) gave the example of Tan-Shui River in Taiwan where the bed elevation of the downstream reach close to the river mouth was lowered by 30-40 m below sea level. They conducted series of laboratory experiments to investigate migration and shape of rectangular mining pit of different dimension under the action of different flow conditions. The pit constructed in their experiments were spanning to the whole width of the channel. Experiments were conducted for non-equilibrium condition of sediment flow. They drained out the water from the flume after certain designated time interval to take the measurement of the bed profile near the pit. Their results showed two different migration periods, first one, named as convection period starting from the beginning of experiment until the upstream edge reached downstream pit boundary and the second one, named as the diffusion period starting from that point onwards. They observed migration of mining pit towards downstream direction. Regression equations for the description of migration speed and the pit geometry were developed from the experimental data.

Gill (1994) treated mining as a pit in an open channel flow environment and investigated the characteristics of the pit. He assumed a quasi-steady condition, regular geometrical shape mining pit spanning full width of the river, and initial depth of mining pit was sufficiently smaller than flow depth. He formulated the problem by using one dimensional Saint Venant equations along with the equilibrium bed load transport equation. The effect of suspended load was neglected. An

approximate theoretical solution was worked out for appropriate initial and boundary conditions. He observed partial filling of mining pit and downstream propagation with time.

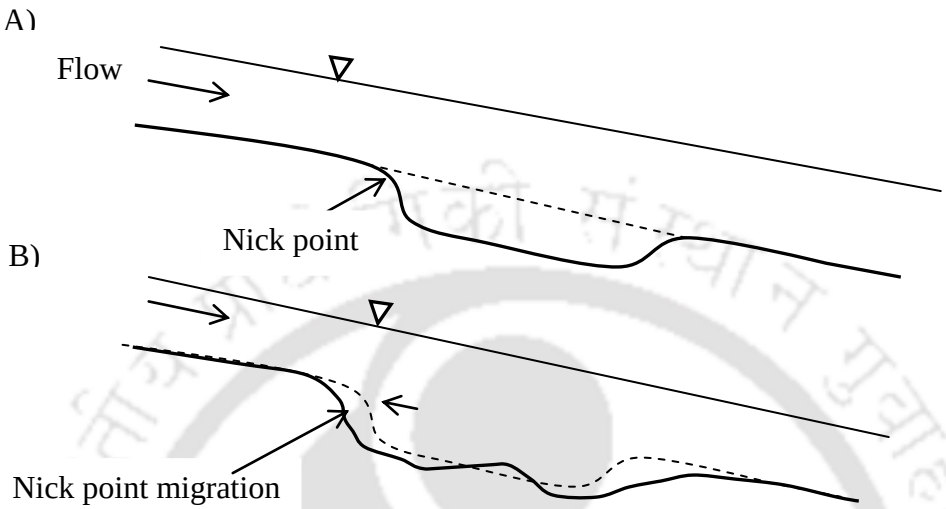

Figure 1.3 A) Formation of nick point due to pit excavation and B) migration of nick point (Kondolf 1997)

Kondolf (1997) stated that pit excavation in an active channel changes the equilibrium condition of the stream bed profile. It creates steeper gradient for the flow and thus causes nick point at the entrance. This nick point leads to the upstream erosion. Mining pit on the river bed can trap most of the bed load transported from the upstream and passes relatively clear water or hungry water to the downstream, which increases the sediment transport capacity at the downstream of the pit. Mining reduced carriage of sediment from rivers to many coastal areas, leading to beach erosion. He also reported failure of various hydraulic structures due to mining activities.

Sear and Archer (1998) investigated the stability of river bed due to the extraction of gravel in the Wooler Water, Northumberland, UK. From the historical data, they found that gravel extraction lead to the incision of river bed up to 9 m and the channel planform change to a largely single-thread sinuous channel from a laterally active wandering channel. Longitudinal and cross-sectional profiles of the Wooler Water were obtained from Northumbrian River Authority for the year of 1966, 1973, 1975, and 1995. They identified vertical instability from

these surveyed data. The analysis of gravel removal showed that extraction of gravel more than the natural restoring capacity caused downcutting of the stream. In most of the extraction site there was net gravel storage, that is, the rate of gravel transported by water was less than that of upstream supply. So removal of surplus gravel should be a good practice for maintaining the actual morphology of the river. However, it was observed by the authors that extraction of gravel caused disturbance to the armor layer of the river and the finer particles got exposed, hence significant changes in channel morphology occurred.

Neyshabouri et al. (2002) did experimental investigation on mining pit migration and variation of longitudinal profile. Like Lee et al. (1993) experiment, these authors also divided the migration speed in convection and diffusion periods and observed higher migration speed in convection period than that of diffusion period. They used rectangular shaped mining pit with various length and width ratio. The experimental investigation revealed different migration speed with respect to the different length by width ratio of the mining pit. They observed that filling rate of pit increases with increase in length or width of the pit but influence of width was observed to be more than the length. They also conducted field investigation by using the excavated pit on different sections of the river Gave-Rood in the western part of Iran. They excavated three pits, one along the center line in a straight reach and another two were on convex and concave side of the bend. They observed similarity in the trend of pit migration with experimental one for straight river reach.

Cao and Pender (2004) conducted numerical study of river mining by using shallow water conservation equations for sediment laden flow together with sediment mass conservation equation of river bed material under non-equilibrium condition. Unlike regular geometrical shaped mining pit on river bed, mentioned in the literature of Hong Yang Lee et al. (1993), and Mahammad Akram Gill (1994), a Gaussian function was used by these authors to represent the amount of sediment extracted from the river bed and continuous intervenes of this function throughout the simulation period was considered. A finite difference approach was used to simulate the flow and river bed profiles with continuous intervenes of sediment mining. They observed evident degradation within the upstream reach of the mining point and also downstream propagation of degradation with increase in magnitude of sediment mining.

Rinaldi et al. (2005) did case studies on five rivers in Italy and Southern Poland and reviewed number of documented case studies from various countries. From the case studies and various reviews they reported severe river bed degradation and channel modification. They mentioned that in-stream sediment mining induced propagation of upstream and downstream river bed degradation. They also identified management outlooks of sediment mining. They summarized the possible physical impact of sediment mining and tabulated as follows:

Table 1.1 Possible physical impact of sediment mining (Rinaldi et al., 2005)

Types of physical impacts	Main Sources
Upstream erosion	Lane (1947), Sato (1971, 1975), Kira (1972), Scott (1973), Forshage and Carter (1973), Bull and Scott (1974), Prudhomme (1975), Simons et al. (1979), Lagasse et al. (1980), Galay (1983), Chang (1988), Collins and Dunne (1989, 1990), Erskine (1990), Kondolf (1994a, 1994b, 1997), Sandecki and Avila (1997), Sear and Archer (1998), Surian and Rinaldi (2003), Marston et al. (2003)
Downstream erosion	Galay (1983), Brookes (1988), Chang (1988), Erskine (1990), Lee et al. (1993); Sandecki and Avila (1997), Rinaldi and Simon (1998), Rinaldi (2003)
Impact on hydraulic structures	Osuch (1968), Cullen and Hughes (1975), Maraga and Mortara (1981), Collins and Dunne (1990), Kondolf (1994b, 1997), Erskine (1997), Sandecki and Avila (1997), Pie´gay et al. (1997), Agnelli et al. (1998), Rinaldi and Simon (1998), Erskine and Green (2000), Marston et al. (2003), Uribelarrea et al. (2003)
Channel instability (lateral changes, changes in channel width and morphology)	Chang (1988), Collins and Dunne (1990), Petit et al. (1996), Bravard et al. (1997), Erskine (1997), Sear and Archer (1998), Erskine and Green (2000), Surian and Rinaldi (2003), Rinaldi (2003), Wyzga (2001b)
Bed armoring	Simons and Lagasse (1976)
Channel instability induced by gravel bar skimming	Collins and Dunne (1990), Kondolf (1994a)

Channel capture by off channel pit and reactivation of inactive channels	Scott (1973), Bull and Scott (1974), Dunne and Leopold (1978), Collins and Dunne (1990), Kondolf (1997)
Effects on frequency of inundation	Collins and Dunne (1990), Augustowski (1968), Wyzga (1997, 2001b)
Water table lowering	Lach (1975), Collins and Dunne (1990), Hatva (1994), Mas-Pla et al. (1999)
Changes in tidal hydrodynamics	Erskine (1990)
Sediment deficit to coastal zone	Tagliavini (1978), Gaillot and Pie´gay (1999)

Rovira et al. (2005) studied various effects of intensive gravel mining after historical gravel mining during the period of 1956-1987 in the lower Tordera River, Spain, which was mined at the rate 14 times higher than the replenishment rates. The study was done 15 years after mining ceased. From 1987 the mining was prohibited in that area due to the various adverse effects on river ecosystem and ground water. They used sediment budget approach by means of sediment transport measurement for assessing and managing present and future sediment deficits in excessively mined river. Load-rating relation method was used for the calculation of sediment yield for which relationship between discharge and suspended sediment and discharge and bedload rates were used. From their study it was found that the river was showing tendency towards aggradation of almost 3.6 mm/year on average during dry periods but they found that the estimated time for the Tordera River to recover its pre-extraction bed level would be around 420 years.

Wu and Wang (2008) used one dimensional shallow water equations over movable bed and non-equilibrium sediment transport equations to simulate morphological evolution near sediment mining pit. They assumed an initial dry bed condition without water in the mining pit and conducted fifty numerical experiments by using different flow condition, mining pit dimension, and sediment properties. The model was validated using the data of earth dam surface erosion due to the lack of measured data of in-stream mining pit evolution. Maximum head cut and tail

cut depths and lengths were established from the simulation results of those numerical experiments.

Ikhsan et al. (2009) did study on Progo River which is originated at Mt. Merapi, one of the most active volcanoes in the world. They found that sediment mining was very intensive at lower Progo River as a result of which river bed degradation occurred in this area. They conducted sediment budget analysis and also gave a concept of sustainable sediment mining by installing ground sill on the river bed. They simulated mathematical model for one dimensional bed deformation using Saint Venant equations and Exner equation. They found that bed deformation between groundsill was very fast and bed slope became milder with time.

Chen and Liu (2009) investigated impact of sand and gravel mining on river bed changes and flood zone coverage of the Rio Salado, Salt River, Arizona by using one dimensional HEC-RAS and two dimensional CCHE2D model and compared their results with field observation. They observed different results from both the models. HEC-RAS simulation showed severe head cutting at the upstream of the mining pit while CCHE2D indicated downstream degradation of river bed. The authors commented that in case of hydrodynamic simulation HEC-RAS produces similar results as CCHE2D but CCHE2D model gave more robust simulation in terms of flood zone coverage, non-uniform sediment sorting, and channel geomorphologic changes.

Vade et al. (2010) stated that the approaches that Hong Yang Lee et al. (1993), Mahammad Akram Gill (1994) described, is a static approach where pit in the initial bed was tracked afterwards in time and space. So the duration of the mining pit must be small compared to the time of river bed changes. But these authors considered the condition in which gravel mining last for several years. They presented two methods, sediment budget approach and linear diffusion model. For sediment budget approach they applied mass balance model for bed load transport, which stated that the difference between incoming and outgoing gravel equals the change in volume within the reach. For diffusion model of bed profile evolution they used Saint Venant equations, Exner equation for sediment conservation with an additional sink term. This model was an equilibrium sediment transport model. Bed load discharge was made equal to the transport capacity using bed load equation such as Meyer-Peter and Muller (MPM 1948). Diffusion equation was developed analytically assuming constant channel width and uniform bed material. In this study authors aimed to provide a methodology that can be used to quantify the

effects of gravel mining in terms of river bed degradation using diffusion coefficient. Their results matched with field data from Gallego River, Spain.

Chen et al. (2010) conducted sensitivity analysis of non-equilibrium adaptation parameters for modelling mining pit migration. They used CCHE2D, a depth-averaged two dimensional hydrodynamic and non-equilibrium sediment transport model to simulate flume experiment conducted by Lee et al. (1993) and found non-equilibrium adaptive length and coefficient. They were unable to give any empirical relationship of non-equilibrium adaptive length and coefficient, but their results showed that equilibrium and near-equilibrium schemes are not suitable for calculation of mining pit migration.

Li and Qi (2015) studied local scour induced by the upstream river bed lowering. They conducted laboratory flume experiment to study the evolution process of mining pit when the longitudinal profile of the pit was so large that the flow disturbed by the upstream slope recovers itself before reaching the downstream slope of the pit. They observed development of scour hole at the downstream of the bed-lowered river reach due to the boundary layer separation from the bed. The study also proposed regression relationship to describe the characteristics of scour hole dimensions. They also developed non-equilibrium and diffusion model to predict the bed profile at the downstream of the maximum scour depth.

Zawiejska et al. (2015) conducted investigation on the montane Czarny Dunajec River, Southern Poland to identify the impact of cobble-mining or gravel-mining and channelization of the river on the depositional pattern of the river. The study was performed in 18 km long reach with upstream channel mining section, a middle channelization section and downstream undisturbed section. They conducted field investigation by means of sampling of bar gravels in various locations. They collected 47 samples in the total study reach. The distance between the sampling collection site were 0.52 km in channelized section and 0.23 km in other sections. The data were analyzed by using both simple and multiple regression models to find out the significant relationship between the grain size parameters of bed material and the other potential controlling variables. They found the general trend of decreasing grain size towards downstream and an equation to determine mean grain size (MGS) of the bar gravel with respect the distance from the beginning of the study area (DISTANCE) and the active width of the channel (WIDTH).

$$MGS = 72.0 - 1.625 \times DISTANCE - 0.139 \times WIDTH \quad (1.1)$$

This study showed that mining of large particles from the river bed exposes the finer layer. This fine sediment gets eroded, which causes incision of the bed and the incision can propagate upstream. They did not observe sediment deficit at the downstream as finer bed material were flashed out from the incising channel section.

Ramkumar et al. (2015) studied sand mining, channel bar dynamics and sediment texture properties of the Kaveri river, South India. They documented the deterioration of natural fluvial system due to extensive sand mining and damming in the upper reaches of the river. They generated thematic map of land use land cover, lithology from remote sensing data, published information and limited field verification surveys. The field data suggested influence of long term mining activities on sediment texture by altering the grain size from coarse to fine texture. To reduce the flooding vulnerability and environmental deterioration they suggested tracking and maintaining sand bar, periodic field checking of river sand harvesting site, total sand extraction record, environmental monitoring and so on.

Brestolani et al. (2015) conducted investigation on morphological changes due to large scale gravel mining occurred during 2003-2004 in Orco River, located in the Piemonte region. They used CNR-IRPI experimental methodology based on multi-years LiDAR surveys realized in the years 2003, 2004, 2006, and 2007 to document mining and morphological response of the river to mining. They observed that incision propagates both upstream and downstream of the mining pit. A hydro-morphological one dimensional model BASEMENT was used to reproduce morphological changes happened after the gravel extraction in the time period 2004-2006. They neglected suspended load as the river was gravelly river and bed load was computed by using Mayer-Peter and Muller (1948). A satisfactory result was obtained from the model. The authors suggested that in presence of high quality river survey data, numerical hydro-morphological model can be used as a useful technique for prediction of gravel mining effects.

Calle et al. (2017) conducted a GIS- based investigation in the Rambla de la Viuda (eastern Spain) stream for assessment of morphosedimentary changes due to in-stream gravel mining. The quantification of river bed degradation was done by using LiDAR DTM and RTK-GPS (Real Time Kinematic) measurements. The geomorphological changes were identified with the

help of 13 sets of aerial photograph taken in between 1946 to 2012. The method to determine geomorphological changes included geo-referencing of aerial images, mapping of river bed unit, and analyzing the geometry of mapped unit. The mining activities were intense after 1969 and were visible in 1976 aerial data sets for the first time. The incision map showed a steady degradation of river bed since 1967 and observed almost 3.5 m degradation at present.

A great deal of previous research has focused on the morphological impact of river aggregate mining and documented erosion of the bed and the bank of the river. Kondolf (1997) reported various examples of endangered bridges, such as Capay Bridge in California, Highway 32 Bridge over Stony Greek California, Kaoping Bridge of the Kaoping River in Taiwan, exposure of the underground pipe line in San Luis Rey River of California and many other hydraulic structures. Collins and Dunne (1990) also documented various cases of failure of hydraulic structures.

Yanmaz and Cicekdag (2000) studied impact of channel mining around bridge pier. A one dimensional model for prediction of morphological changes around the bridge pier on rectangular channel under quasi-steady flow condition and for equilibrium sediment transport was developed in this study. They observed degradation of stream bed at the downstream of the mining zone and stated that extraction of large quantities of bed material for long duration would affect the foundation stability of nearby bridges or other manmade structures.

Lu et al. (2015) studied sand and gravel mining in the upstream of Yangtze River and its impacts on Three Gorges Reservoir. They analyzed the effects of mining on the deposition of reservoir by using historical data from the year of 2003 to 2012 and found decrease in deposition quantity. They observed from the data analyses that mining activity will cause serious damage to the river bed in near future as the replenishment rate from the upstream is not enough to meet the loss.

Qi and Kuai (2017) conducted experimental investigation on pier scour under the influence of head cut erosion of sand mining pit. They found that the distance between the pier and sand pit affected the contribution ratio of local scour and retrogressive scour to the total scour. The increase and decrease in the ratio also depended on the flow discharge and the hydraulic drop at the pit. They also developed a coupling calculation method for the prediction of total scour including local and retrogressive scour.

The change in river morphology subsequently affects water surface of the river. The impact of mining on hydrology and hydrodynamics are the consequence of change in morphology of the river. River mining causes degradation and widening of the river, which leads to the lowering of the ground water table in the aquifer connected to the river. It results in ground water inflow into the river that is, quantity of ground water resources decrease. Lowering of ground water table can destroy the riparian habitat (Mas-Pla et al. 1999). A Schematic diagram of lowering of ground water table due to the degradation and widening of the river is present in Figure 1. 4

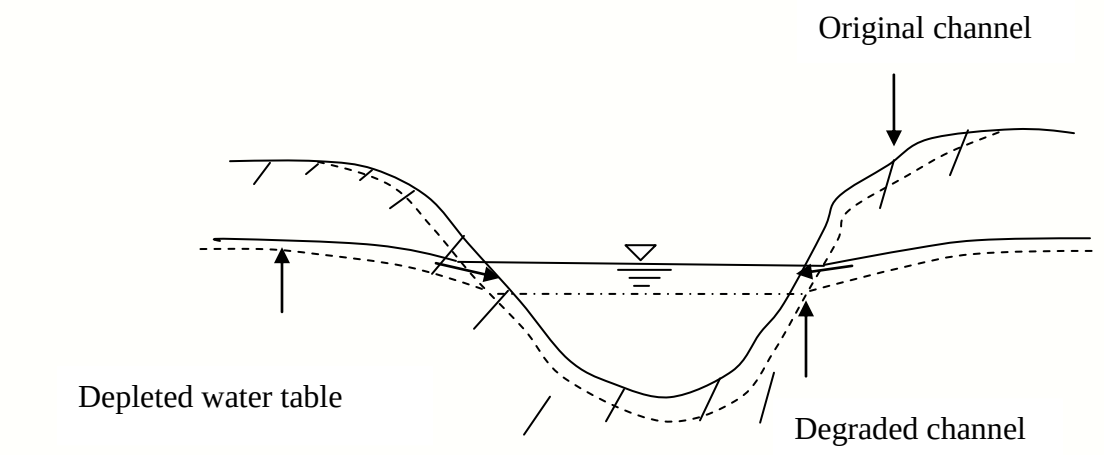

Figure 1.4 Depletion of water table due to the degradation and widening of the river

Alfrink and van Rijn (1983) developed two-equation turbulence model for flow over a trench and described the flow characteristics by using $k-\varepsilon$ turbulence model closure. They also conducted experimental study to verify their model. A fix trench with a layer of gravel of 0.006 m and a Laser Doppler Velocity meter for instantaneous velocity measurement were used by them for experimental study. They observed reversal flow at the center of the pit bottom from both experimental and numerical results.

Mas-Pla et al. (1999) stated that river morphology controls the stage of the river and, hence, the recharge to or discharge from the aquifer. The authors mentioned two types of impact of gravel mining on ground water. First one is river mining causes degradation and widening of the river, which leads to the lowering of the ground water table in the aquifer i.e quantity of ground water

resources decrease. Second one is deepening of river bed in coastal areas enhances the sea-water penetration, hence an increase of river water salinity. If there is a depression of ground water due to pumping for irrigation, then this may result in saline water intrusion into the aquifer, which threats the ground water quality. Dimensionless analytical solution for ground water flow into the river was presented using Boussinesq equation. A two dimensional finite element model using flow equation for porous media was also presented for numerical solution. Both approaches allow the estimation of the loss of total water resources from the adjoining aquifer.

Lai et al. (2014) investigated the increasing discharge ability of Poyang lake due to sand mining using surveyed and remote sensing data. The comparison of channel profile from 1998 to 2013 showed drastic increase in cross-sectional area in the Hukou Waterway immediately to the north of the lake. They also observed average decrease in bed elevation up to 9 m. Intensive sand mining created wider and deeper out flow channel for the Poyang lake, which results in drop of water level of the lake and thus increased the drought risk in the lake. They also suggested that Poyang lake water control structure to increase the lake level during the dry season is not required since it can harm the rich biodiversity in that area. They recommended prohibition of sand mining at the northern end of the lake to maintain the lake water level.

1.3 Environmental, Water Quality and Ecological Impact

Mining leads to re-suspension of streambed sediment, clearance of vegetation, and stockpiling on the streambed. Poorly planned uncontrolled dumping of overburden and chemical or fuel spills during the extraction of aggregates reduce water quality for downstream users and enhance the cost for downstream water treatment plants (Kim 2005). Deepening of a certain portion of the river bed can cause expose of finer layer of bed materials. Water flowing with high velocity over an exposed bed can cause high scouring. Turbidity of the water downstream is therefore, expected to increase and thus is a matter of concern. The increase in the turbidity of the water also reduces the light penetration, which leads to reduction of primary production. It may effect on the species attached to streambed deposits. Due to the clearance of vegetation, species of land plants decrease. It also reduces aquatic plants if mining is done on the stream bed. Most of the birds, animals, and reptiles are sensitive to noise, and therefore vehicles noise and headlight during mining operation can have adverse impacts on these species especially during the breeding season (Kim 2005). It may also create air pollution by increasing dust level in the air

due to the use of heavy vehicle for frequent transportation of material. Sediment mining causes disturbance at the bottom of the river, which is harmful to the aquatic habitat. There is a tendency of decrease in number of species as the stream bed stability decreases (Robinson and Minshall, 1986; Death and Winterbourn, 1995). Change in ecological conditions of flora and fauna due to aggregate mining further influence the livelihood of the people in that region. Figure 1.5 shows vehicle enter into the river directly, which can destroy the river environment.

Erskine (1990) studied environmental impact of sand and gravel extraction on river system. He documented that removal of sand and gravel from Brisbane river caused 3 to 5 m degradation of river bottom. He also observed that calm dredging; barging and in-stream storage of bed material must increase the turbidity of the river and proper management practice need to be implemented in that case. He obtained distinctly higher electrical conductivity and hardness, the concentrations of carbon dioxide, nitrate, sulphate and chloride at the extraction site than at the natural areas of the same esker range; however, the quality met the standard set for drinking water. He recommended management of gravel extraction and groundwater resources to reduce the risks of contamination.

Hatva (1994) monitored effects of gravel extraction on ground water during five years at 30 ground water areas of Finland. He observed changes in the channel due to the excavation of gravel, which resulted in increase in velocity, and changes in flood and tidal level. He investigated on ground water quality and quantity, pollution risk and on the use of groundwater, its usability and the need to protect it. He used almost 4000 thousand samples collected from observation pipes, wells, springs and groundwater ponds in gravel pits. He observed increase in acidity level in the seep water and increase in groundwater formation due to the accumulation of melted snow in the gravel pit. The increased acidity level in seep water also contributes to the ground water quality.

Femmer (2002) studied impact of in-stream gravel mining in Southern Missouri in the context of economic and environmental issues. In-stream gravel has very high economic value for economic growth but on the other side it has negative effects of wetland, aquatic habitat etc. It also changes the riparian vegetation, river bed texture, width and depth of the river.

Figure 1.5 Vehicle in the mining site of Mathura river of Cachar district

Santo and Sanchez (2002) had indicated various environmental impact indicators due to flood plain sand mining in the Paraiba do Sul River of southern Brazil by using GIS methodology. The extraction was started in the river in 1940, which caused number of environmental problems. The extensive mining converted the agricultural land into the open pit, open water pond. The risk of contamination of groundwater increased due to the oil spill from the equipment used during the excavation of sand and transportation. The flood plain mining also caused change in river morphology since the thin sediment lane left between the river and the pit could easily get eroded.

Kim (2005) observed that the extraction of sand or gravel from river bed can damage the water quality, ecosystem and biodiversity. They had conducted their study area in the Youngsan River located in the south-west of the Korean Peninsula. The field observation and analysis of ecosystem showed that there was a slight decrease in number of land plant species, fishes. The vehicle noise and head light also have adverse impact on birds habited since birds are very sensitive to these. So he suggested avoiding mining during the breeding periods. They observed slight increase in suspended sediment due to the mining operation and also impact of mining on fishes, mammalia, amphibia, reptilia and birds.

Padmalal et al. (2008) described the environmental effects of river sand mining from the river catchment of Vembanad lake, Southwest coast of India. They observed 40 times higher extraction of in-stream mining than the restoring capacity. Mainly two types of mining activities, pit excavation and bar skimming were practice in this area and among these two pit excavation was widespread mining practice adopted in the catchment of Vembanad lake. They observed pit excavation is more threatening than bar skimming. It can cause instability in the river bank and riparian vegetation. The various factors that got affected by the mining activities in the Vembanad lake catchment are increase in suspended particles and other pollutants such as oil, grease, etc., from vehicles used for the sand removal, ponding of water in the excavation zone and reduction in natural cleansing capacity of river water, change in flora and fauna within the river basin.

Lamelas et al. (2008) did the suitability analysis of extraction location of sand and gravel in the context of sustainable development in the surroundings of Zaragoza (Spain). They prepared extraction suitability map by considering various environmental factors with the help of spatial

decision support systems (SDSS) and geographic information system (GIS). The most suitable area for sand and gravel extraction were found to be located in the high terraces and in the terraces covered by pediments where the thickness of resource is relatively high. The other areas were most vulnerable to groundwater contamination, and beneath soils with poor irrigation characteristics. They also observed that different suitability map can be developed depending on the preference of different stakeholders and can be combined to select the most suitable one.

de Leeuw et al. (2010) studied the effects of sand mining in the Poyang lake, china. The mining in this lake started in 2001 after sand mining was banned in the Yangtze river. Mining in the Poyang lake was also banned after 2008 due to the impact on biodiversity until proper planning had been developed. They used remote sensing approach to determine the volume of extraction from the lake. Remote sensing data of 1999 and 2007 showed that mining caused in widening of the channel connecting Poyang lake to the Yangtze river. They suggested to access the environmental impact strategically and provided the first strategy by quantifying the magnitude of sand mining operation.

Ojha and Choudhary (2017) conducted investigation in Mithri River, the tributary of Luni River situated in Kosana village of Jodhpur district, Rajasthan for qualitative analysis of socio-environmental factors of sand mining. They found that soil, water, noise and air environment were within the permissible limit of as per standard except for the dust generation. However, they also observed that mining pits were responsible for damaging the land profile and shifting of the waterway.

Singh and Kumar (2017) studied the environmental and economic consequences of sand and gravel mining from piedmont and floodplain zones of Yamunanagar district in Haryana, India. They found that mining causes depletion of fertile soil, shrinkage of agricultural lands, severe land degradation, and depletion of ground water level in Gulabgarh and Shahzadpur villages, deterioration of ground water quality. They also pointed out that sand and gravel extraction was extended to almost two percent of the total geographic area and had significant economic value. So a total ban on mining activities in this area may lead to rise in price of these materials and discouragement for infrastructure development. They proposed environmentally tolerable mining policy to minimize the negative impact in the Yamunanagar district in Haryana, in general, and piedmont and floodplain zones

1.4 Need for Research

Most of the studies reviewed so far mainly concentrated on the morphological changes due to the aggregate mining in the river. Researchers also concentrated on the ecological aspect of the mining. Research methodology on this subject has been mostly involved the GIS based field investigation of gravel and sand mining. From the experimental studies conducted until now, it can be concluded that the impact analysis of sand mining has been done extensively but the research on hydrodynamic characteristics of mining pit is limited. The experimental study on sand mining to date has only tended to focused on the physical characteristics of the mining pit and has not fully explain the flow characteristics in that region. Mining pit not only changes the geomorphic characteristics of the river but also the flow characteristics. So, after extensive review of various literature, it is felt necessary to have a detailed and comprehensive research to evaluate the different flow characteristics in a mined alluvial channel. A considerable amount of sediment gets removed during the mining operation and thus, disturbs the sediment transport characteristics of the channel. It also influences the erosion process and affects the hydraulic structure present in the river. Therefore there is a need to address the sediment transport characteristics and migration of erosion in a sand mined channel, which were not discussed sufficiently in the earlier studies. Field investigation can display the actual problem but there are various practical difficulties in getting accurate and comprehensive data. In that case, a well-designed laboratory studies is preferred as a faithful method for getting detail information regarding various hydraulic parameters. This information can also be used for development of numerical model. In this present research, an experimental methodology to study the flow characteristics along with the morphological and sediment transport characteristics is needed for proper understanding of the problem.

1.5 Objectives

The main focus of this study is to investigate the impact of in-stream mining pit by conducting laboratory experiments. The main objectives are summarized as follows:

1.5.1 Geomorphic characteristics in a mining affected alluvial channel

- Study on longitudinal channel bed deformation
- Study on deformation of cross-sectional profile

1.5.2 Turbulent flow structure and bed load transport characteristics in a mining affected alluvial channel

- Explore the flow characteristics in the mining pit region
- Explore the flow characteristics at downstream of the mining pit region
- Comparison of the flow characteristics in the mining pit region and downstream of it with the upstream section.
- Study on bed load transport characteristics

1.5.3 Migration of mining pit and multi-scale characterization of migration speed

- Physical characteristics of mining pit migration
- Formulation of non-dimensional migration speed of the pit
- Investigate the celerity of mining pit from statistical analysis

1.5.4 Scope of applying numerical model for simulating pit migration

- Development of one dimensional semi coupled numerical model for rectangular and trapezoidal shaped mining pit.
- Applicability of different bed load transport formulation on pit migration.

A schematic view of present research work is as follows:

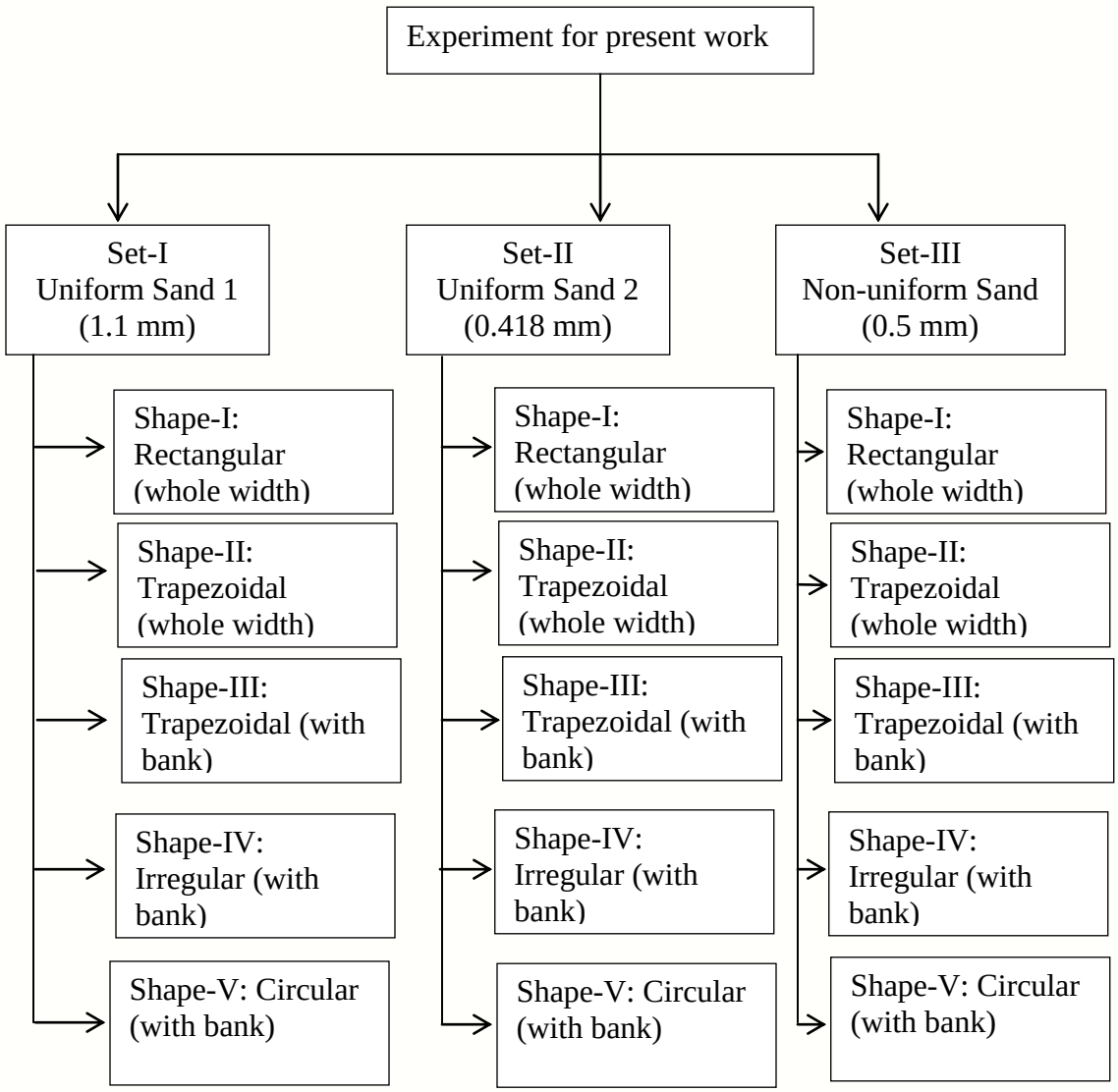

Figure 1.6 Experimental programs for present research work

1.5 Organization of Thesis

The entire work has been divided into different chapters. A brief introduction of each chapter is described as:

Chapter 1 begins with the introduction of river mining with review of literature of various pioneering researchers. It highlights various impacts of river aggregate mining. It also discussed the experimental study conducted in the field of river aggregate mining. Finally the need for research from the review of the literature has been drawn and the objectives of the present research have been outlined.

Chapter 2 describes the experimental program which includes design of experimental flume, description of various instrument used for data collection, shape of various mining pit and bed material gradation. Detailed data collection procedure and also the processing of the data with results are also presented in this chapter.

Chapter 3 presents experimental results on various morphological changes occur due to the presence of mining pit of various shape. Longitudinal and cross-sectional variation of the channel bed profile is studied and erosion of bank profile is highlighted.

Chapter 4 explores the flow characteristics in mining affected channel. The change in flow characteristics because of the construction of the pit is studied. Velocity profiles, Reynolds shear stress, turbulent intensities, quadrant analysis are calculated. The importance of development of bed load transport equation for mining affected alluvial channel is discussed and an equation is developed from experimental data. A comparison of bed load transport rate between the mining affected alluvial channel and the plain bed experiment is also presented at the end of this chapter.

Chapter 5 investigates the migration of mining pit for different length by width ratio of the pit. The physical characteristic of mining pit migration is discussed along with the multi-scale characterization of the migration speed. The migration of the pit in terms of celerity of mining pit is studied from wavelet analysis.

Chapter 6 deals with the scope of applying numerical model in pit migration. One dimensional numerical model is developed and applicability of various bed load transport equation in pit migration is discussed.

Chapter 7 presents the various important findings of this present research work. The future scope of the work is also discussed at the later part of this chapter.

2 Methodologies

2.1 Overview

One of the most popular and interesting method of studying sediment transport related problem is to conduct laboratory flume experiments. The objective of this present chapter is to describe the experimental procedure adopted in this research. All equipment related to the experiment and the materials used are discussed at the beginning of this chapter. Data collection procedure and the data processing technique are also presented along with the results. At the end of this chapter detail of the experimental program, which were planned and carried out during the period of research and the preparation of channel bed is presented.

2.2 Apparatus and Methods

Various apparatus used during the course of experiment is discussed below:

2.2.1 The flume

Experiments were conducted in a 17.2 m long, 1 m wide, and 0.72 m deep tilting recirculating flume with glass sides (Figure 2.1). Three 10 HP centrifugal pumps were used to regulate the flow into the channel. Water was first pumped into the overhead tank and a control valve was used to regulate the flow into the main channel. To minimize the effects of sudden entry of the highly turbulent flow into the flume from the overhead storage tank and to straighten the flow, a collection tank of 2.8 m long, 1.5 m wide and 1.5 m deep with wooden baffles was placed at upstream of the flume. Up to two meter from the upstream of the flume, gravel layering was used and the flume was made non porous for this length. The remaining length of the channel was made porous by placing a fine mesh of 0.1 mm sized. At the bottom of the bed, steel tube structure of 0.22 m height was placed to support the mesh arrangement. It formed a pressure chamber or seepage chamber of 15.20 m in length, 1 m wide and 0.22 m deep between the bottom of the channel and the fine mesh. Bed material was placed on the fine mesh in order to prevent its entrance into the bottom chamber. This bottom chamber was used to drain out the water from the main channel through the bed material. The depth of flow in the main channel was maintained by providing a tailgate at the downstream of the channel. A tank positioned at the downstream of the flume collects the water discharge coming from the channel and a trench

connected to the tank delivers the water to an underground tank, which can be again pumped into the overhead tank. A bed load collecting tank was placed at the downstream end of the flume to collect the bed load discharge.

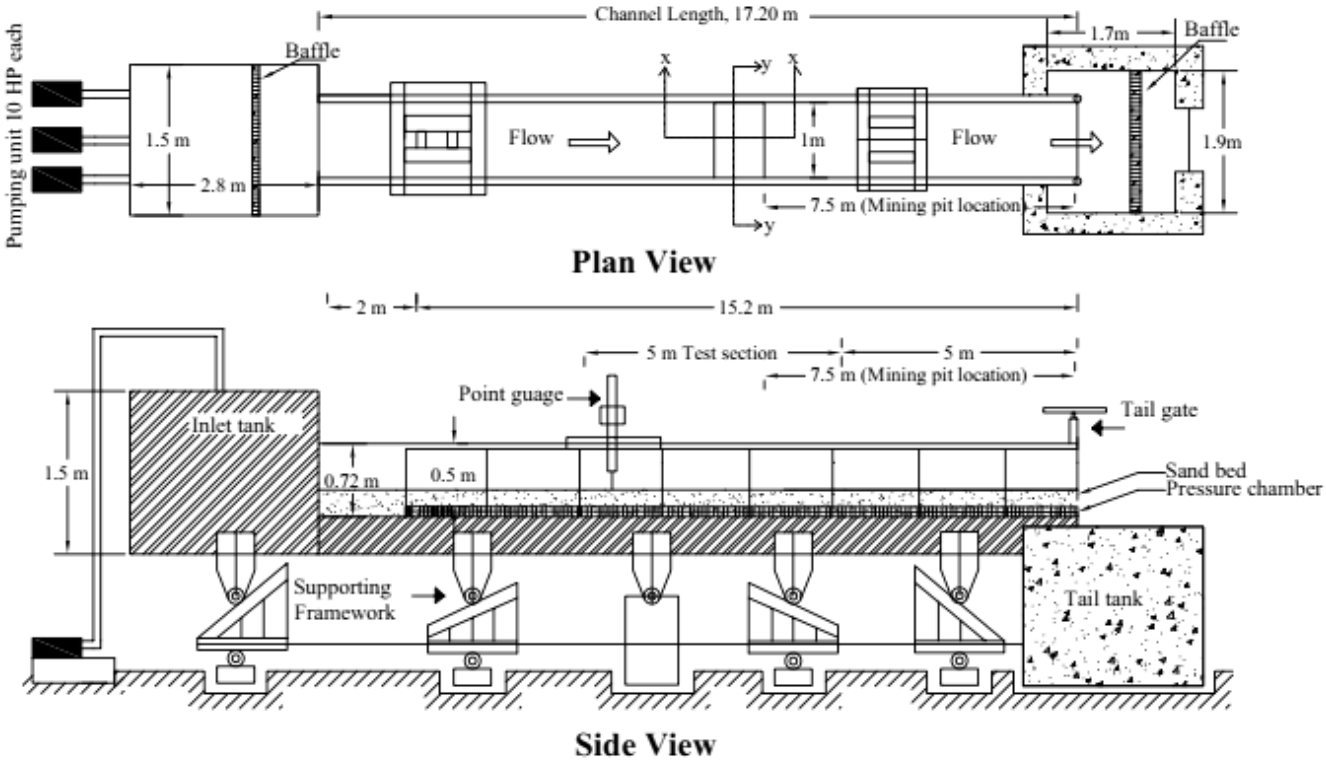

Figure 2.1 Schematic diagram of experimental set up

2.2.2 Test section

The entry and exit conditions highly affect the flow in the flume. When water is directly introduced by the pipes at the upstream end of the flume, strong circulations occurs in the flow. In order to avoid the strong circulations present in the flow due to pipes, an upstream collection tank was used to collected water at the upstream of the flume. The water was applied gradually into the upstream collection tank where couple of baffles was installed. The baffles confirm the smooth entrance of flow into the channel. Free over fall of flow occurs due to the presence of tail gate at the downstream end and causes acceleration of flow in the near bed region just upstream of the tailgate. The test section in the present experiments was considered as 5 m long in the

middle of the flume (5 m to 10 m from tail gate as shown in Figure 2.1) to minimize the effects of flow entrance and exit conditions in the channel. The flume was sufficiently long to achieve fully developed flow conditions in the test section for all the experiments.

2.2.3 Bed material

Three sets of river sand of d_{50} = 1.1 mm with geometric standard deviation 1.03, d_{50} = 0.418 mm with geometric standard deviation 1.17 and d_{50} = 0.5 mm with geometric standard deviation 1.65 were used as a bed material. The first two sets of sand were assumed as uniform since geometric standard deviation for both was less than 1.4 (Marsh et al., 2004) and the third set was non-uniform sand. The dry angle of repose (φ) for d_{50} = 1.1 mm, d_{50} = 0.418 mm and d_{50} = 0.5 mm was 31.154°, 32.5° and 32°36′ respectively. The sand size distribution curve for all three sets of sand is shown in Figure 2.2.

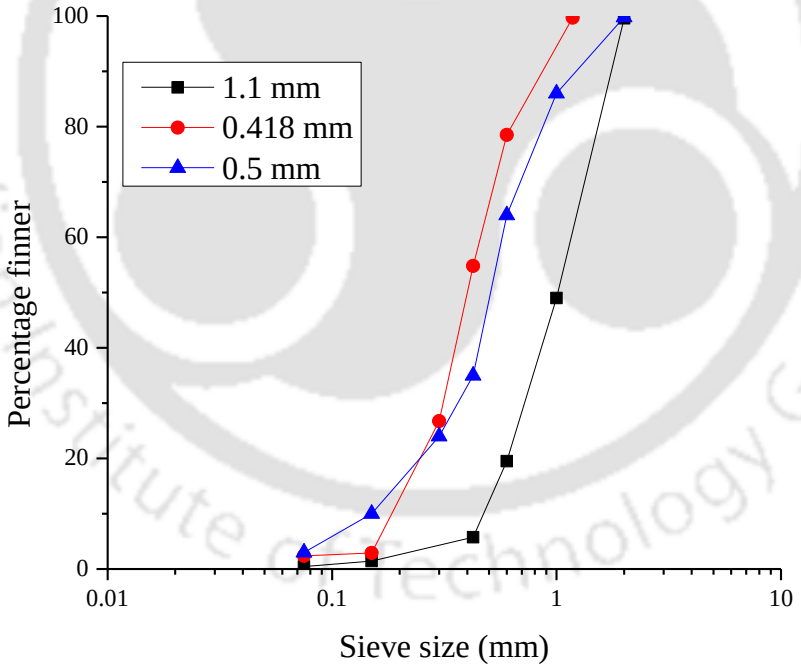

Figure 2.2 Grain size distribution curve

The critical shear velocity of bed material can be determined from Shields criterion, which provides a relationship between critical Shields parameter (θ_{cr}) and shear Reynolds number

(R_{e*}). Paphitis (2001) suggested mean threshold curve for determining critical shear velocity as follows (Behasti and Ashtaini, 2008):

$$\theta_{cr} = \frac{0.273}{1+1.2D_*} + 0.046\left(1-0.576e^{-0.02D_*}\right) \tag{2.1}$$

$$\theta_{cr} = \frac{\tau_{0c}}{(\rho_s - \rho)gd_{50}} \tag{2.2}$$

$$D_* = \left[\frac{(\rho_s - \rho)g}{\rho\upsilon^2}\right]^{1/3} d_{50} \tag{2.3}$$

where D_* is the dimensionless particle diameter, d_{50} is the median grain diameter, ρ_s is the density of bed material, g is acceleration due to gravity, υ is the kinematic viscosity of water.

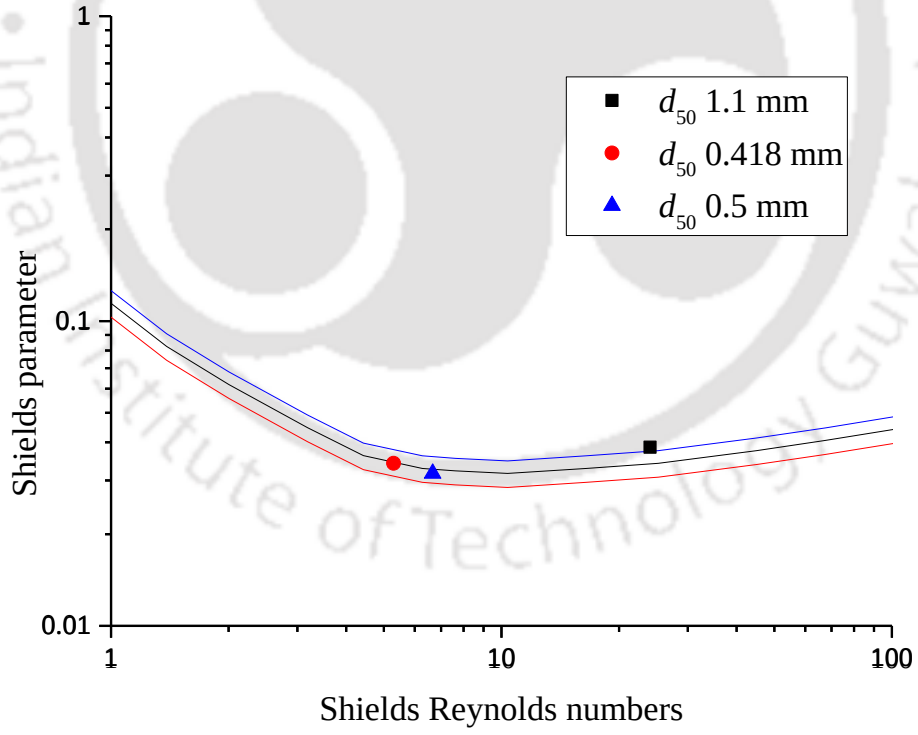

Figure 2.3 Shields diagram for critical shear stress

The critical shear velocity $u_{*_c} = \sqrt{\frac{\tau_{0c}}{\rho}}$ has been obtained as 0.0262 m/s for uniform sand with $d_{50} = 1.1$ mm, 0.0152 m/s for uniform sand with $d_{50} = 0.418$ mm. In case of non-uniform sand ($d_{50} = 0.5$ mm) representative grain diameter of the bed material d_{50} is considered by neglecting the standard deviation (Mohtar et al., 2016). The critical shear velocity is 0.016 m/s for non-uniform sand with $d_{50} = 0.5$ mm.

2.2.4 Main flow discharge

The main flow discharge (Q) was measured volumetrically with the help of a rectangular notch provided at the downstream collection tank of the flume (Figure 2.4).

Figure 2.4 Rectangular notch for the measurement of main channel discharge

The coefficient of discharge for the notch was found to be 0.82 from the equation given below:

$$Q = \frac{2}{3} C_d L_n \sqrt{2g} H_n^{\frac{3}{2}} \tag{2.4}$$

2.2.5 Flow depth

A digital point gauge attached to a moving trolley was used to measure the flow depth in the flume (Figure 2.5). We get a resolution of ± 0.01 mm from its liquid crystal display. It can be set to zero at any operating range to check the relative level difference. The depth of flow was obtained from the difference between the water surface level and the bed level.

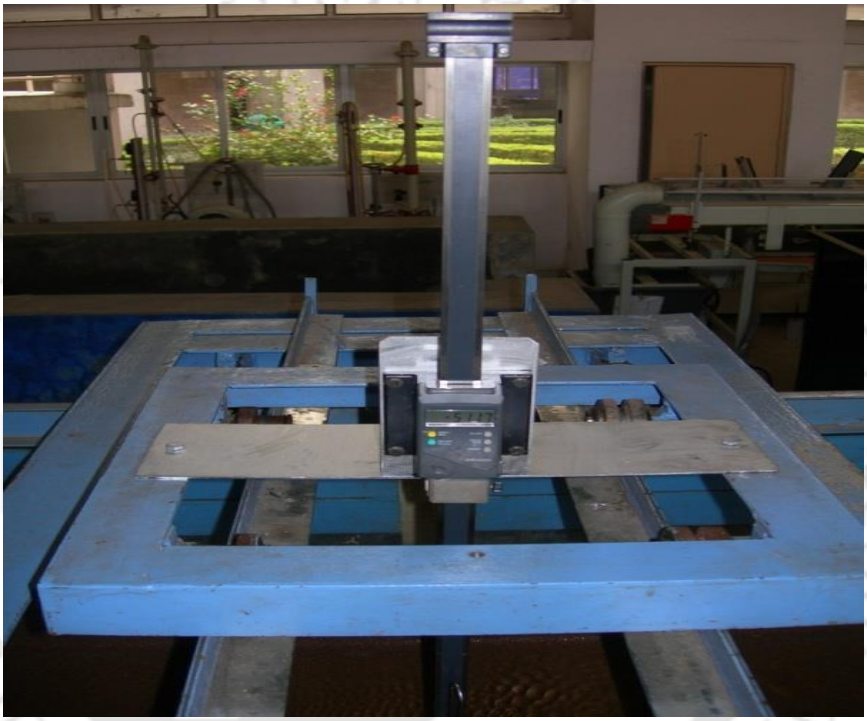

Figure 2.5 Digital point gauge for flow measurement

2.2.6 Water surface elevation

A Pitot-static tube fixed to a digital manometer which was further attached to a moving trolley was used to measure the water surface slope in all the experiments. Two batteries of 12 Volts each connected in series were used to power the digital manometer. The outer tube consisting of static pressure holes when connected to digital manometer gave the piezometric height at that point. Water surface slope was measured by moving the trolley in the stream-wise direction. The arrangement of the Pitot-static tube and digital manometer are shown in Figure 2.6.

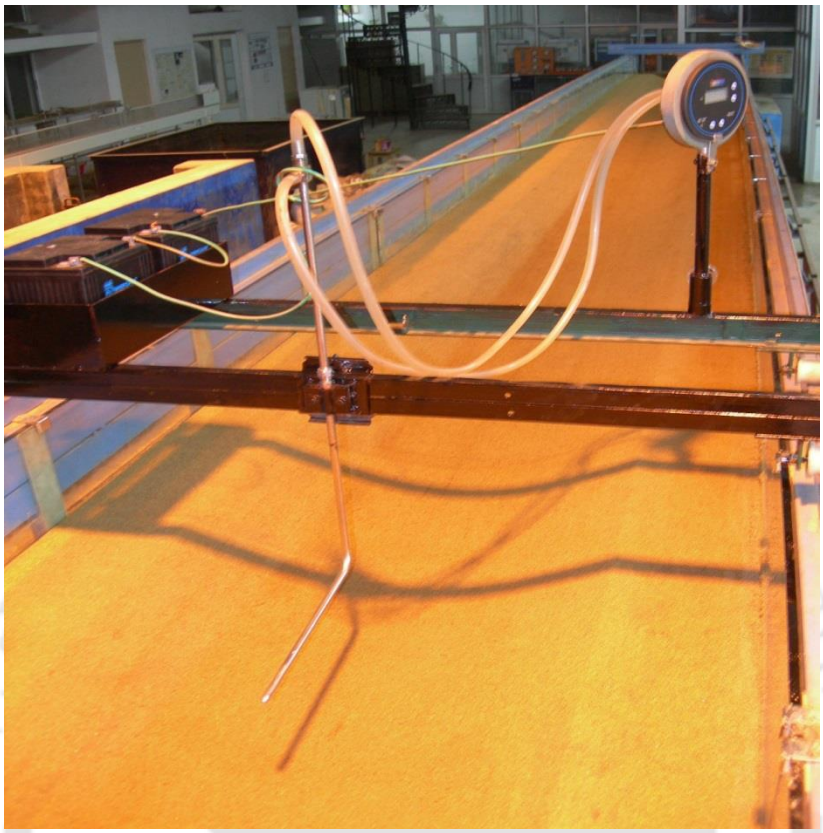

Figure 2.6 Arrangement of the Pitot-static tube and digital manometer

2.2.7 Bed slope

The laboratory flume used for the experimentation was a tilting flume. The slope of the flume can be measured with the help of Total Station. It is combination of theodolite and electronic distance measurement, which can simultaneously read horizontal and vertical position of a particular point. Total station consists of two components, a machine mounted on a tripod stand and a "target" prism on a metal staff. The machine part of the Total Station consists of a lens somewhat like a telescopic rifle-sight with cross-hairs which are focused on the prism. The whole instrument revolves horizontally and the lens pivots vertically too.

2.2.8 Flow velocity

Instantaneous velocity of flow can be measured by using Acoustic Doppler Velocimeter. It uses Doppler effect to measure velocity. The Doppler effect is the change in frequency of a wave or an event when either the source or an observer is on motion. The effect causes changes in pitch.

For example, the sound is different when a vehicle sounding a siren approaches, passes and recedes from an observer. The received frequency is higher during the approach, identical at the instant of passing by, and lower during the recession as compared to the emitted frequency. The change in the pitch will give an idea of how fast the vehicle is moving. The ADV works on this same principle to measure the velocity of water in three dimensions (Figure 2.7).

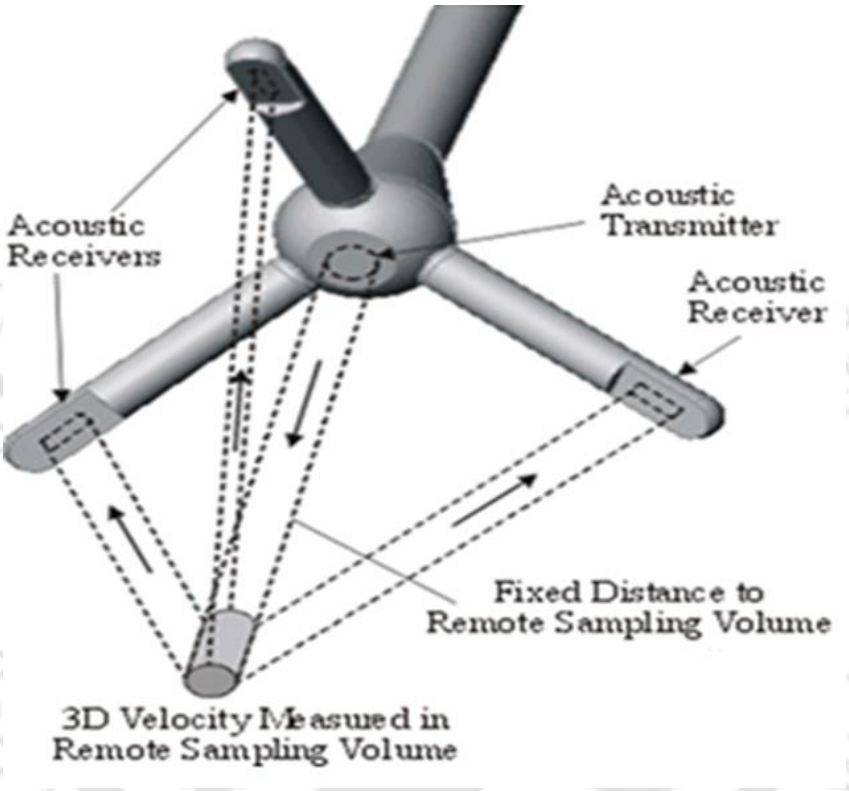

Figure 2.7 ADV prob with acoustic transmitter and receivers

The device emits a beam of acoustic pulses at a fixed frequency from a transmitter probe and three receiving probes record the change in frequency of the returned sound. The returned sound is not reflected from water. When the device emits acoustic pulse into the flow, it intercepts suspended or seeding particles in water which move with same average velocity as that of water. The ADV can calculate the velocity of the water in the *x*, *y*, and *z* directions. For measurement of instantaneous velocity, a downward looking three beam, 16 MHz microADV developed by SonTek has been used in this research (Figure 2.8).

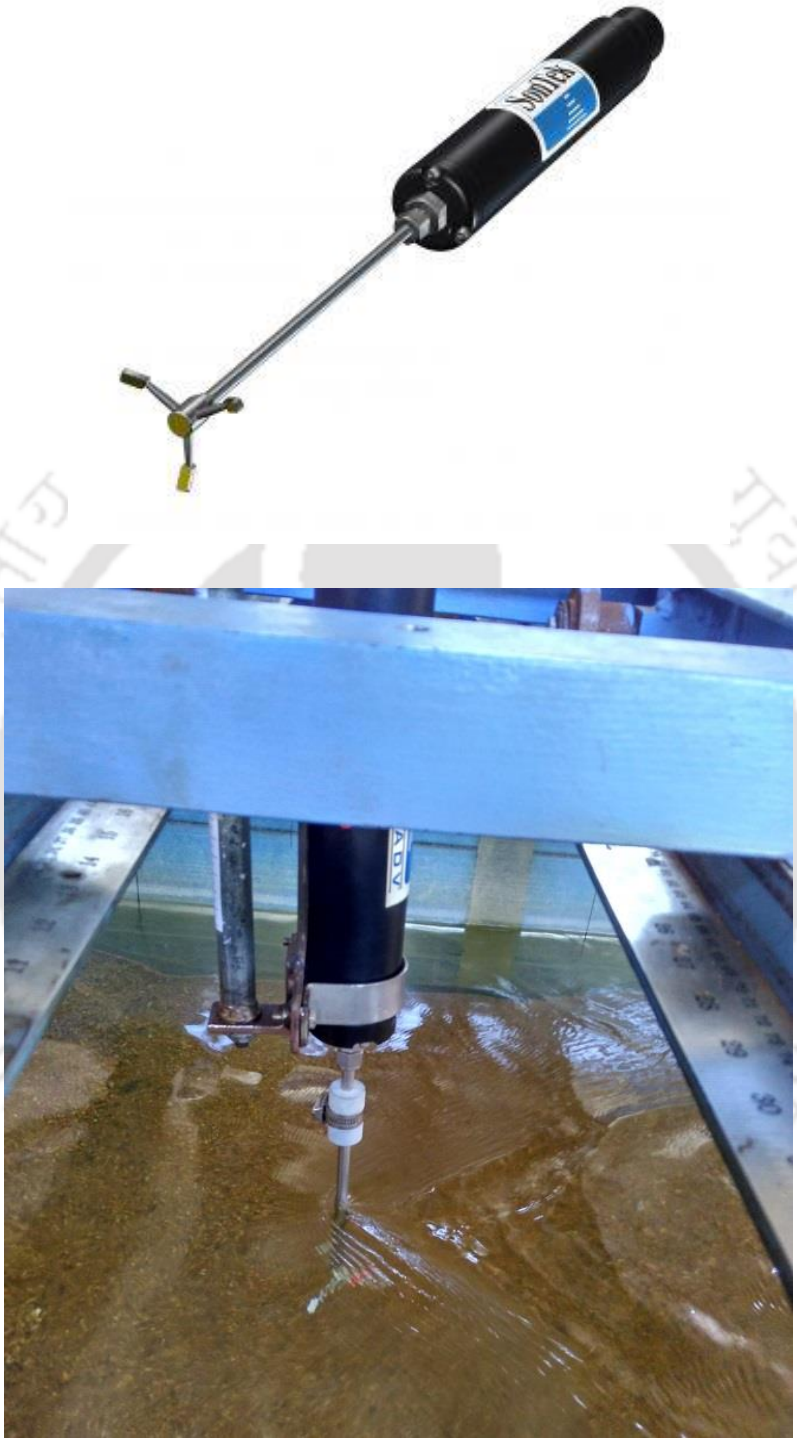

Figure 2.8 16 MHz microADV developed by SonTek

This instrument has a high acoustic frequency of 16 MHz and allows sampling rate up to 50Hz. The remote sampling volume for 16 MHz microADV developed by SonTek is less than 0.1 cc and located at a vertical distance of 5 cm below the central transducer. It also gives the distance of the central transducer from the boundary. The velocity data was collected in computer by using HorizonAdv, which gives a flexible and dynamic user interface for data collection (Figure 2.9). In the present experiment, data were collected along the centerline of the channel at various distances of 7 m, 7.5 m, 7.9 m, and 8.4 m from the downstream end of the flume. At each section, measurements were carried out at the various flow depth for at least 180 s. The vertical axis is considered zero (z= 0) at bed level and positive upward. Signal to noise ratio (SNR) for all the experiment was maintained at 15 or above and 70% correlation between the transmitted and the received signal was suggested as a termination value. However, at the near-bed region, a lower correlation of 65% was used (Despande and Kumar, 2016).

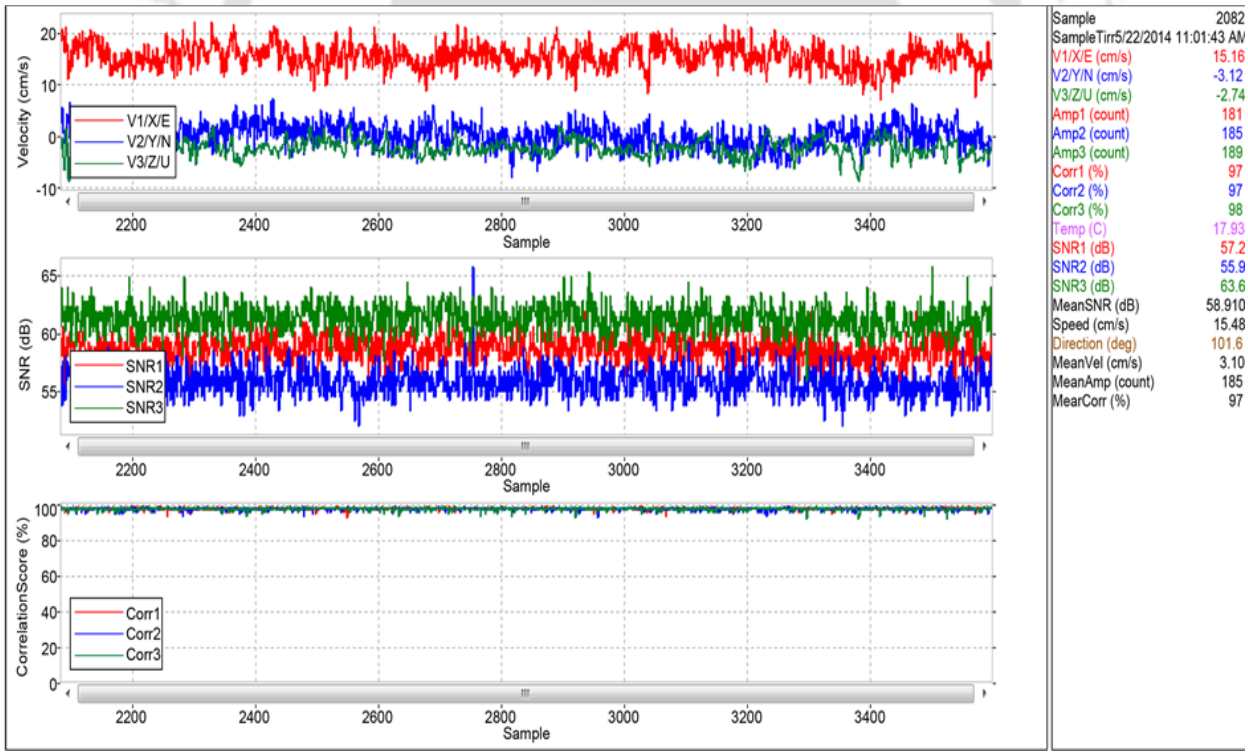

Figure 2.9 User interface of Horizon ADV

Time-averaged flow velocity at the different vertical distance of a section can be calculated from the following equation.

$$\left.\begin{aligned}\overline{U} &= \frac{1}{m}\sum_{i=1}^{m} u_i \\ \overline{V} &= \frac{1}{m}\sum_{i=1}^{m} v_i \\ \overline{W} &= \frac{1}{m}\sum_{i=1}^{m} w_i\end{aligned}\right\} \quad (2.5)$$

$\overline{U}$ and u_i are the time-averaged velocity and instantaneous velocity in the stream wise direction. m is the number of samples. Similarly, $\overline{V}$, v_i and $\overline{W}$, w_i are also the time-averaged velocity and instantaneous velocity in traverse and vertical to the flow direction. Reynolds shear stress τ_{uw} was obtained from

$$\left.\begin{aligned}\tau_{uw} &= -\rho\overline{u'w'} \\ \overline{u'w'} &= \frac{1}{m}\sum_{i=1}^{m}\left(u_i-\overline{U}\right)\left(w_i-\overline{W}\right)\end{aligned}\right\} \quad (2.6)$$

Here, u' and w' represent the fluctuating components of velocities in the flow direction and vertical to the flow direction respectively. ρ is the water density.

Time series data of velocity obtained from SonTek ADV was filtered with the acceleration threshold method for spike removal (Goring and Nikora, 2002). A threshold value of 1 to 1.5 was used based on trial and error method (Despande and Kumar, 2016). After spike removal, velocity power spectra should satisfy the Kolmogorov's -5/3 hypothesis in the inertial sub range (Lacey and Roy, 2008). Figure 2.10 shows unfiltered and filtered velocity power spectra ($F_{uu}(f)$) at z= 8 mm, where f is the frequency and z is the vertical depth from the bed. From Figure 2.10 it is observed that velocity power spectra of filtered data shows good agreement with Kolmogorov's -5/3 hypothesis.

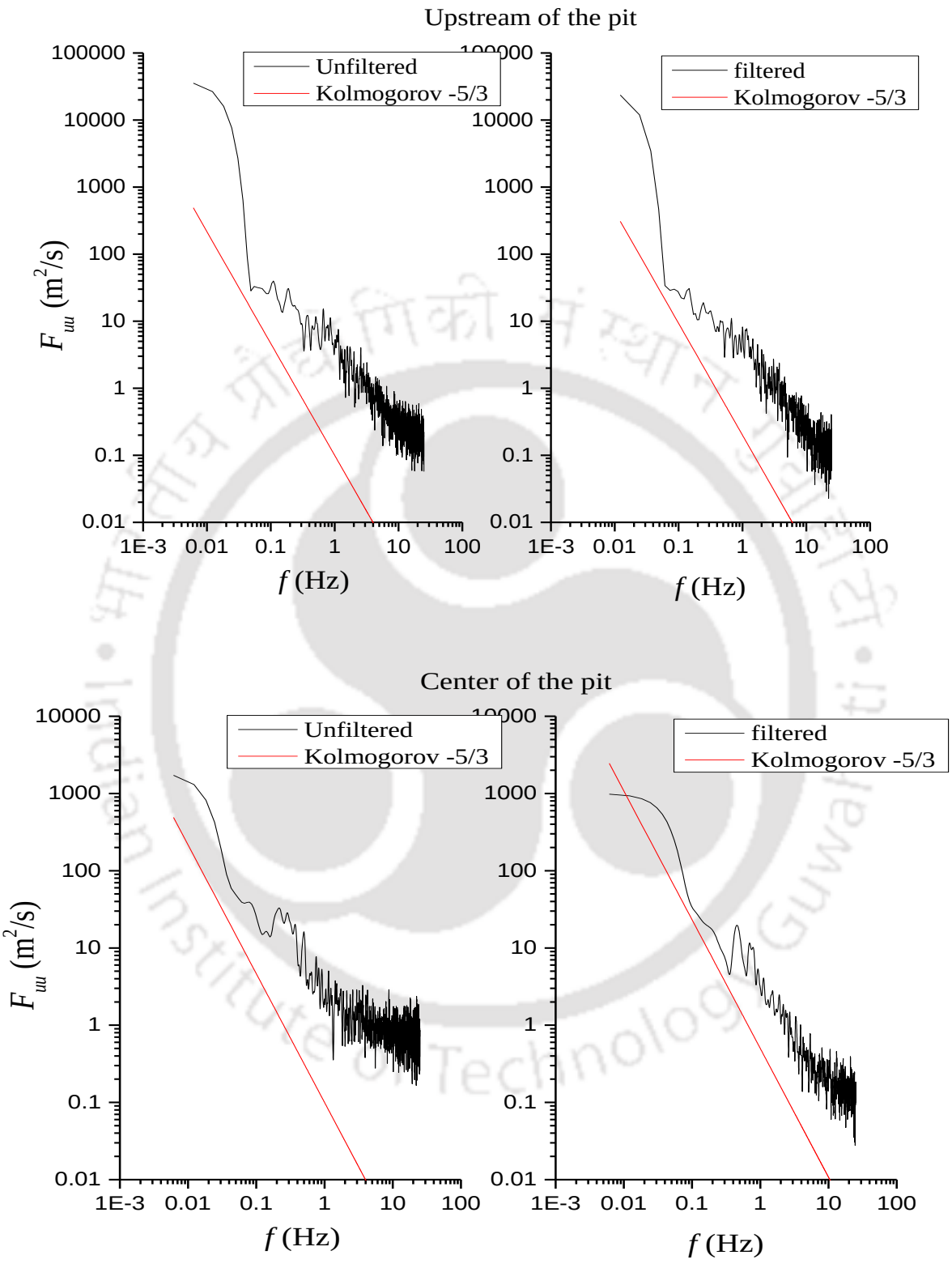

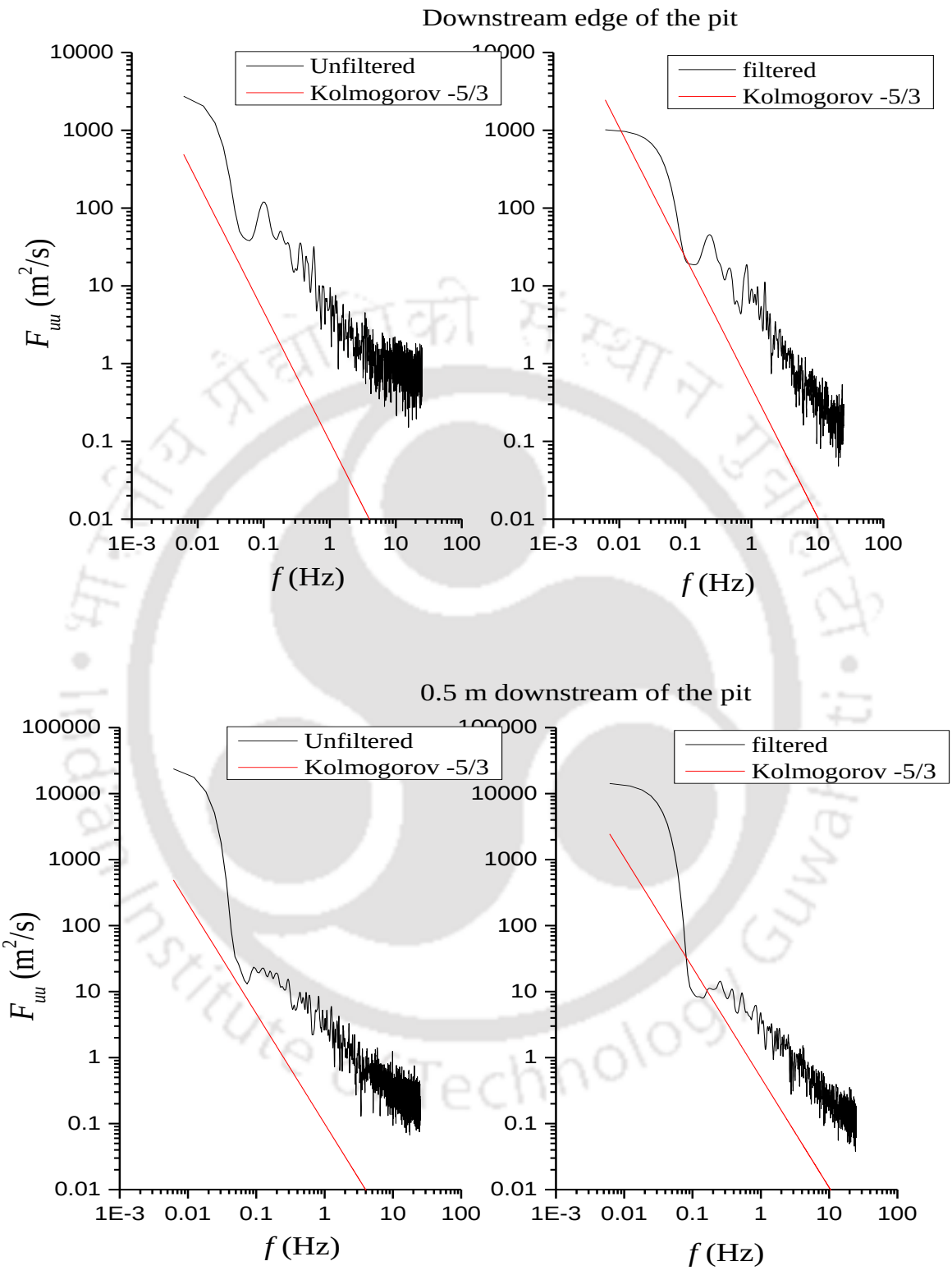

Figure 2.10 Velocity power spectra with Kolmogorov's -5/3 law

2.2.9 Ultrasonic ranging system (URS)

In order to interpret the effect of the mining pit on bed morphology, bed profiles were captured by a Seatak instrument with seven transducers (Figure 2.11). The instrument consists of a trolley system having seven transducers resting on the rail of the laboratory flume and moves with constant speed. It uses 5 MHz ultrasound to estimate the distance to a target. The wavelength of 5 MHz sound wave is 0.3 mm in water. In this instrument the transducer acts as both transmitter and receiver. The transducer first transmits a pulse of 10 microsecond duration, then it travels through the water and reflected off a target. The reflected signal travels back to the transducer and detected by the electronics. The system is having 0.1 mm resolution and the accuracy is ± 0.2 mm (if several pings are processed per return).

A)

B)

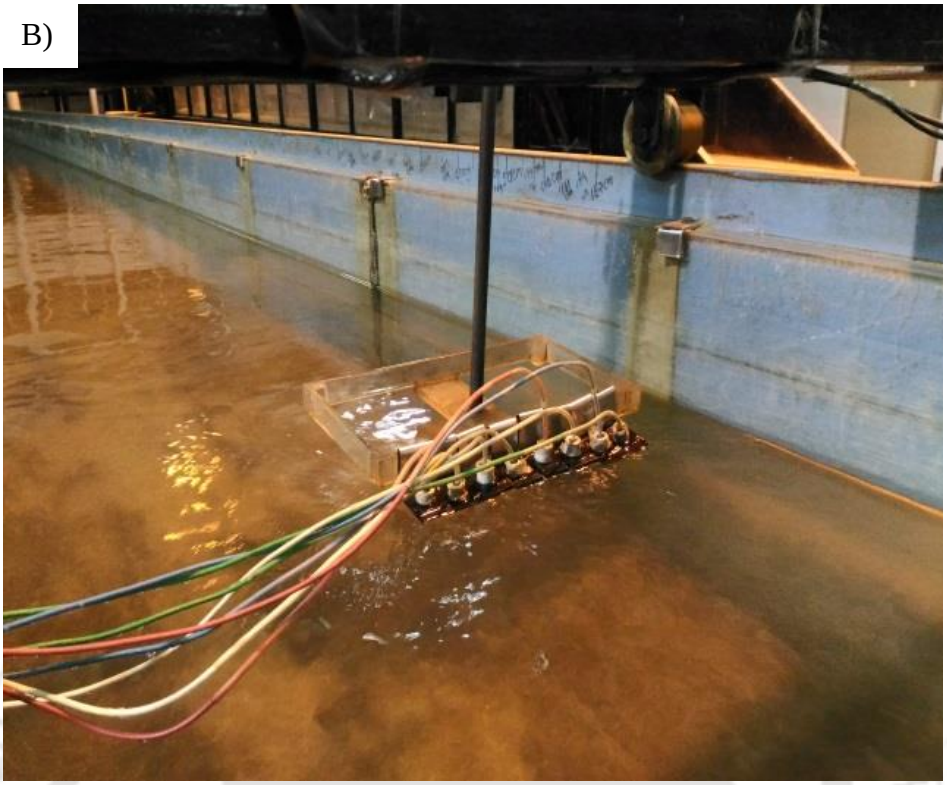

Figure 2.11 A) Ultrasonic ranging system and B) the trolley with transducers

2.3 Bed Preparation

21 cm thick layer of sand was place above the fine mesh of 0.1 mm sized. Sand was first disturbed to remove the air from the sand. It was then levelled by using a cutter attaches to a moving trolley. After levelling, the bed was flooded with water for compaction without allowing any movement of bed material. The water was then drained out and required shape of the pit was constructed on the dry bed condition. The main flow discharge was initiated after construction of the pit. Same procedure was repeated for each run of experiments. Snapshot of bed preparation is presented in Figure 2.12.

A)

B)

Figure 2.12 A) Bed preparation, B) Prepared plain bed after compacted with water

2.4 Experimental Program

The experimental program consists of three sets of experiment with five different shaped mining pit as mentioned in Figure 1.6.

Shape-I: Rectangular pit with vertical side was constructed along the whole width of the channel. Extraction volume and length by width ratio were 0.05 m^3 and 0.5 respectively (Figure 2.13).

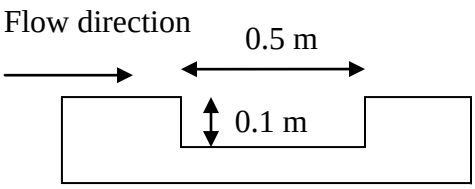

Longitudinal section x-x

Figure 2.13 Line diagram and snapshot of rectangular mining pit

Shape-II: Trapezoidal pit was constructed along the whole width of the channel. The side slope of the pit was 32°. Extraction volume and length by width ratio were 0.066 m^3 and 0.82 respectively (Figure 2.14).

Figure 2.14 Line diagram and snapshot of trapezoidal mining pit

Shape-III: Trapezoidal pit with bank value 10 cm on each side was constructed with side slope 32°. Extraction volume and length by width ratio were 0.0465 m^3 and 1.025 respectively (Figure 2.15).

Figure 2.15 Line diagram and snapshot of trapezoidal mining pit with bank

Shape-IV: Irregular pit geometry as shown in Figure 2.16 was constructed with vertical sides. Extraction volume and length by width ratio were 0.055 m^3 and 2.5 respectively. For the irregular shaped pit, length by width ratio was calculated by taking the extreme point of length and width of the pit, hence considering the maximum disturbance to the channel.

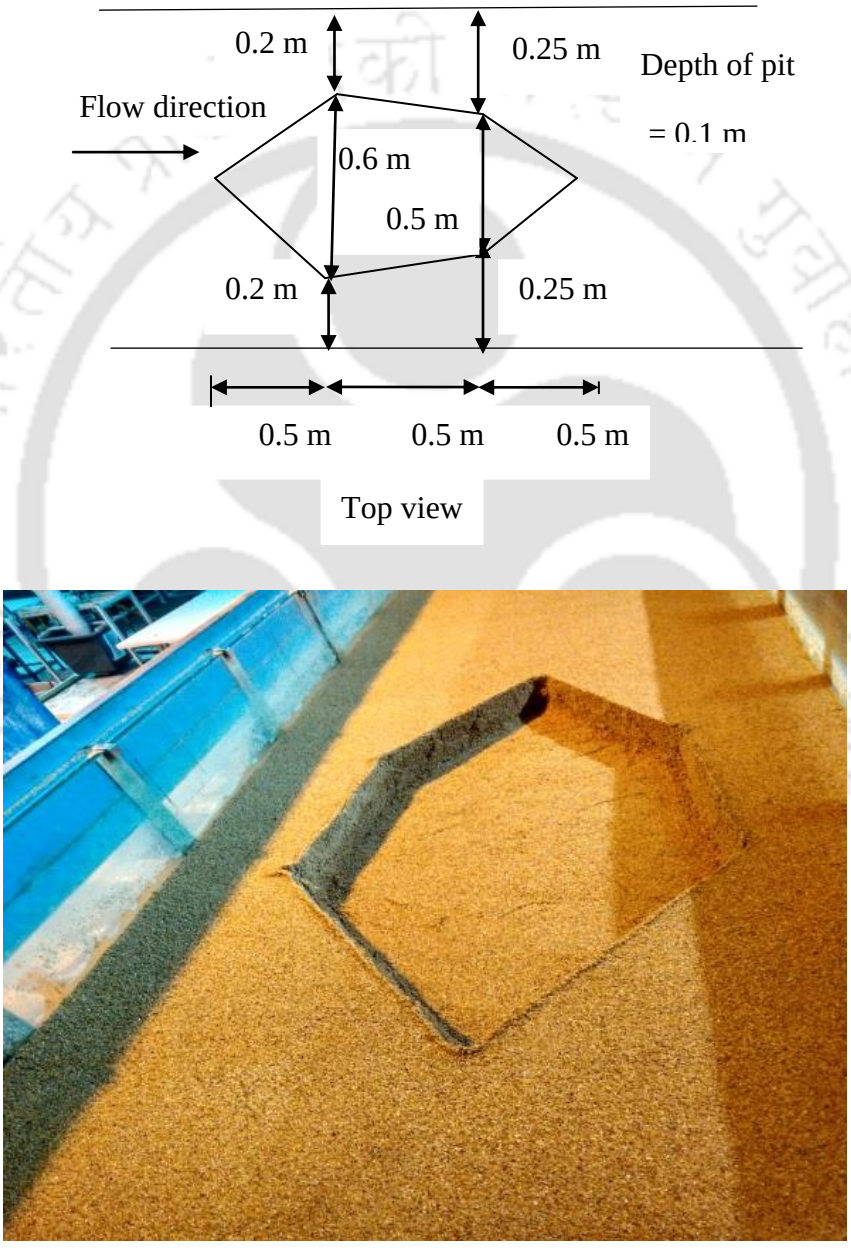

Figure 2.16 Line diagram and snapshot of irregular mining pit with bank

Shape-V: Circular pit with diameter 40 cm was constructed with vertical sides. Bank value was kept as 30 cm on each side. Extraction volume and length by width ratio were 0.01256 m^3 and 1 respectively (Figure 2.17).

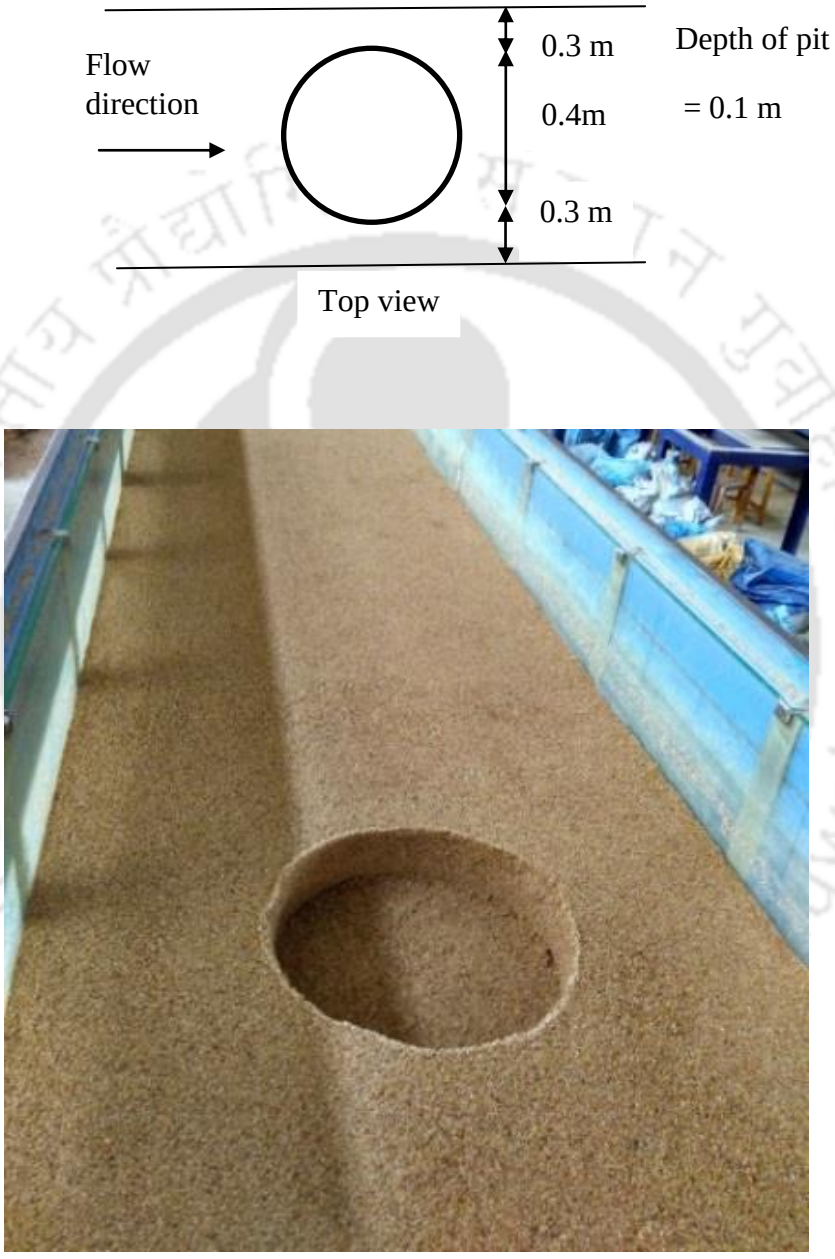

Figure 2.17 Line diagram and snapshot of circular mining pit with bank

Hydraulic conditions for all the experiments are presented in table 2.1

Table 2.1 Hydraulic conditions of different experiments

Discharge Q, m^3/s		Average Velocity V, m/s		Flow depth m	Froude No.	Reynolds No.
Q1	0.0442	V1	0.448	0.0987	0.455	30740
Q2	0.0472	V2	0.379	0.1246	0.343	31497
		V3	0.465	0.1014	0.467	32712
Q3	0.0503	V4	0.399	0.126	0.359	33499
		V5	0.484	0.1038	0.48	34730
Q4	0.0535	V6	0.418	0.128	0.373	35500
		V7	0.496	0.1079	0.482	36674
Q5	0.0567	V8	0.445	0.1276	0.398	37675
		V9	0.461	0.123	0.420	37954
		V10	0.481	0.118	0.447	38261
		V11	0.493	0.115	0.465	38448
		V12	0.515	0.1101	0.496	38756

3 Geomorphic Characteristics in a Mining Affected Alluvial Channel

3.1 Introductions

Over-excavation of sand can result in lowering of bed elevation. Collins and Dunne (1989) carried out extensive case studies in rivers of the southern Olympic Mountains, Washington, USA with data from nine gauging stations over a period of 55 years to investigate the impact of gravel mining and they found that the river bed degraded to about 0.03m/yr. Rinaldi et al. (2005) also documented change of channel morphology in terms of bed and bank erosion due to mining of aggregates from the river and categorized the adverse impact of mining as morphological, hydrological, ecological and environmental impact. The change in morphology of rivers can change the environment and ecology of the river system. The Lower Tordera River, Spain experienced intensive gravel mining during the period of 1956-1987 and sediment mass balance study of this river showed that the estimated time for the river to restore its pre-extraction bed level would be around 420 years (Rovira et al., 2005). Mining of gravel also causes flashing out of finer material from the incised channel section and can change the depositional pattern of the river (Zawiejska et al., 2015).

Earlier investigation on river aggregate mining showed incision of river bed due to huge mining activities and the propagation of incision in both upstream and downstream of the mining zone (Rinaldi et al., 2005; Brestolani et al., 2015; Zawiejska et al., 2015). Mining pit on the river bed can trap most of the bed load transported from the upstream and passes relatively clear water or hungry water to the downstream, which increases the sediment transport capacity at the downstream of the pit (Kondolf, 1997).Erosion of river bed and bank due to mining can endanger the stability of the hydraulic structure of the river. Kondolf (1997) reported various examples of endangered bridges, such as Capay Bridge in California, Highway 32 Bridge over Stony Greek California, Kaoping Bridge of the Kaoping River in Taiwan, exposure of the underground pipe line in San Luis Rey River of California and many other hydraulic structures. Collins and Dunne (1990) also documented various cases of failure of hydraulic structures. Lu et al. (2015) found in their study that sand and gravel mining in the upstream of the Yangtze River caused a decrease in deposition quantity of the Three Gorges Reservoir and stated that serious damage to the river bed would occur in the near future. Investigation of the impact of sand and

gravel mining by Chen and Liu (2009) on river bed changes and flood zone coverage of the Rio Salado, Salt River, Arizona showed severe head cutting at the upstream of the mining pit and downstream degradation of the river bed.

Unplanned sand mining threatens to the nature by exploiting river system, whereas planned and controlled mining can be used for maintaining flood capacity and channel stability (Kondolf 1994). Ikhsan et al. (2009) found that sediment mining was very intensive at lower Progo River as a result of which river bed degradation occurred in this area. They conducted sediment budget analysis and gave a concept of sustainable sediment mining by installing ground sill on the river bed. Prediction and maintenance of mining volume is important for sustainable development. Van Rijn (1986) proposed a mathematical model for the prediction of suspended sediment transport and sedimentation rate in a dredged channel and produced a set of graphs for the estimation of trapping efficiency. A mathematical model of mining pit developed by Gill (1994) on the sand bed channel showed downstream erosion and shifting of the upstream edge to downstream. Gill (1994) neglected suspended sediment in his study and assumed bed deformation occurs only because of bed load transport. Numerical modelling of sand mining also showed severe downstream erosion and migration of upstream edge (Cao and Pender, 2004; Wu and Wang, 2008). Vade et al. (2010) developed a linear diffusion model to quantify gravel mining and verified their model by using historical data on river bed degradation of Gallego River, Spain. They observed that gravel mining caused incision of more than 5 m in the river bed.

Experimental investigation carried out by Lee et al. (1993) is evident for downstream erosion and sedimentation of the mining pit with migration of the upstream edge under the bed load transport condition. Lee et al. (1993) experimentally showed two different migration periods, first one, named as convection period starting from the beginning of experiment until the upstream edge reached downstream pit boundary and the second one, named as the diffusion period starting from that point onwards. Regression equations postulated by Lee et al. (1993) for the description of migration speed and pit geometry, showed highest scour depth at the end of the convection period. The experimental investigation also revealed different migration speed with respect to the different length and width ratio of the mining pit and influence of width was observed to be more than the length (Neyshabouri et al., 2002). Neyshabouri et al. (2002) also

conducted field investigation by using the excavated pit on different sections of a river reach and observed similarity in the trend of pit migration with experimental results for straight reach. Previous experimental and field investigation showed severe change in river morphology due to aggregate mining; hence it is important to investigate the morphological impact of mining with more details. In this chapter morphological changes of channel bed under channel mining condition have been investigated.

3.2 Morphological Characteristics of Rectangular Mining Pit (Shape-I)

Bed elevation profile along the centerline of the channel is as shown in Figure 3.1 for average velocity V8 and V10 of Set-III.

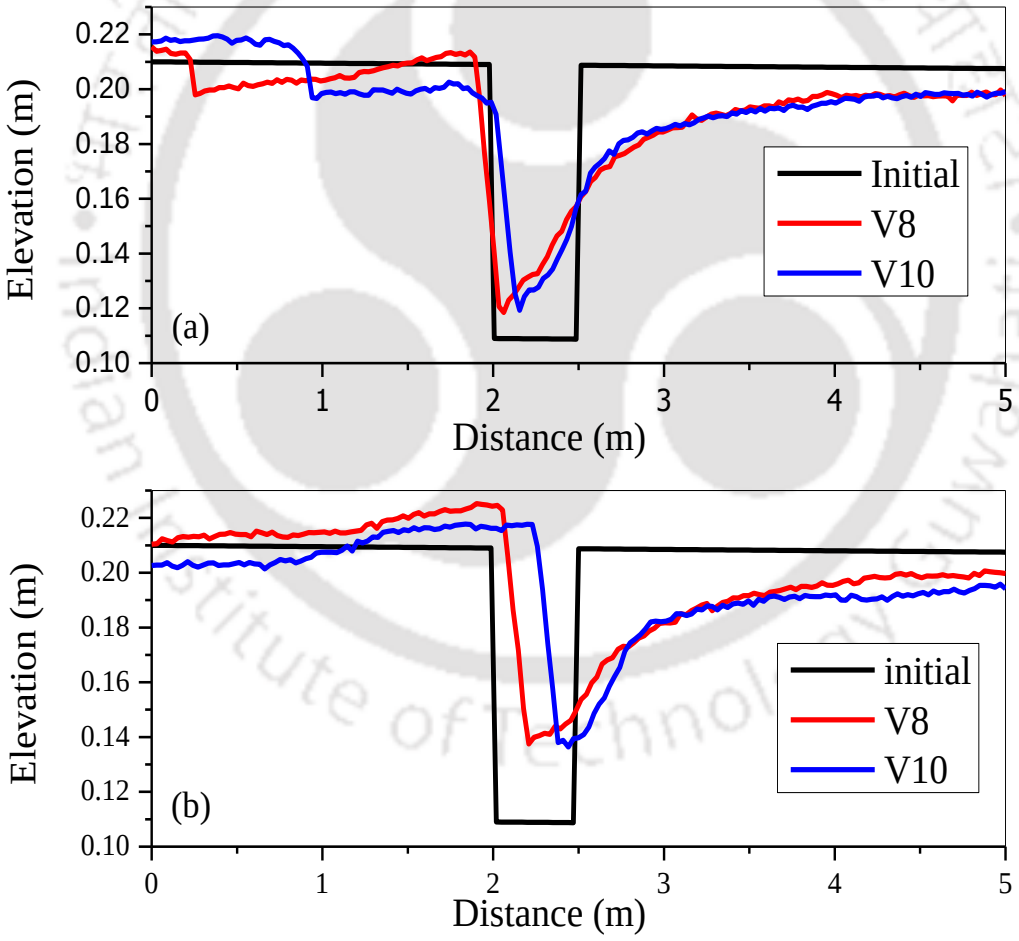

Figure 3.1 Bed elevation profile along the centerline of the channel (a) at 4 hours (b) at 7 hours

Bed elevation profiles in Figure 3.1 clearly represent erosion of channel bed at the downstream of the pit, which was postulated by many researchers in previous study. There is also increase in migration of upstream edge of the pit with increase in flow velocity. Upstream edge is migrating towards the downstream direction with increase in time and partial filling of mining pit is occurred (Gill, 1994). The upstream edge maintains an angle while migrating downstream. The slope of upstream face of the mining pit was measured and shown in the table 3.1.It is observed that the angles are near to the angle of repose of the bed material, which is 32°36´.

Table 3.1 Upstream face angle of mining pit at different hydraulic condition

Experiments	Upstream face angle
V1	30°20´
V2	34°56´
V3	30°10´
V4	30°6´
V5	30°51´
V6	32°39´
V7	33°7´
V8	33°6´
V9	31°44´
V10	30°9´
V11	30°17´
V12	30°47´

However, at downstream the edge is completely washed out and no such angle is maintained (Figure 3.2, Figure 3.3), which gives a clear picture of downstream erosion. The surface plot of

initial bed profile and 4 hours bed profile for rectangular pit (Shape-I) is presented in Figure 3.2 and snapshot of bed profile is presented in Figure 3.3.

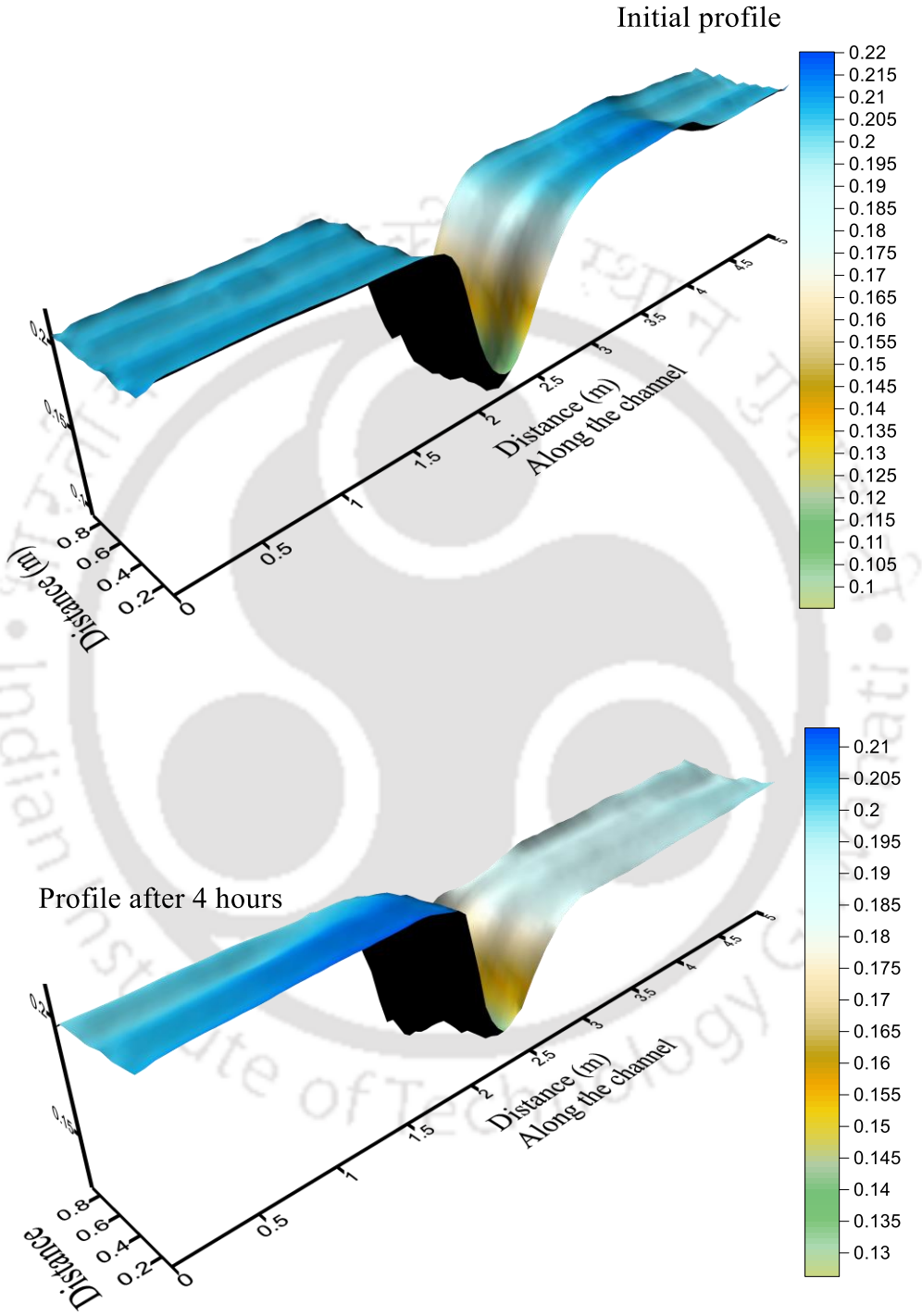

Figure 3.2 Bed surface plot for Shape-I of V12 after Initial and 4 hours of flow.

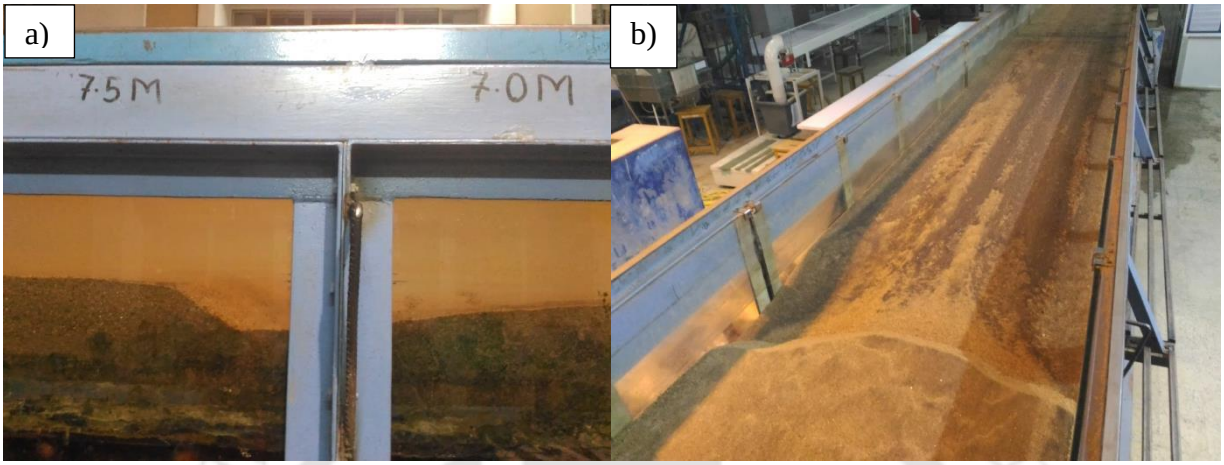

Figure 3.3 Snapshot of bed profile (a) side view (b) top view

It may so happen due to the higher values of shear stress at downstream of the pit than the upstream. Shear stress is calculated by using reach average shear stress method, which is based on force balance approach.

$$\tau_o = \gamma R S_f \tag{3.1}$$

where τ_o is the bed shear stress in N/m^2, γ is the specific weight of water (N/m^3), R is the hydraulic radius. If ratio of channel width to the flow depth (aspect ratio) is greater than 4, in place of hydraulic radius (R) flow depth can be used (Prasad, 1991), and S_f is friction slope. Friction slope can be calculated by using the following formulation given by Rao et al. (2011).

$$S_f = S_w(1 - F_r^2) + S_b F_r^2 \tag{3.2}$$

where F_r is Froude number, S_b is bed slope which is constant for all the experiments, and S_w is the water surface slope. Water surface slope for V8 and V10 is plotted in Figure 3.4. Water surface in the test section shows two distinctly different slopes and the slopes are higher at the downstream of the pit than at the upstream. It results in a higher value of downstream shear stress than the upstream.

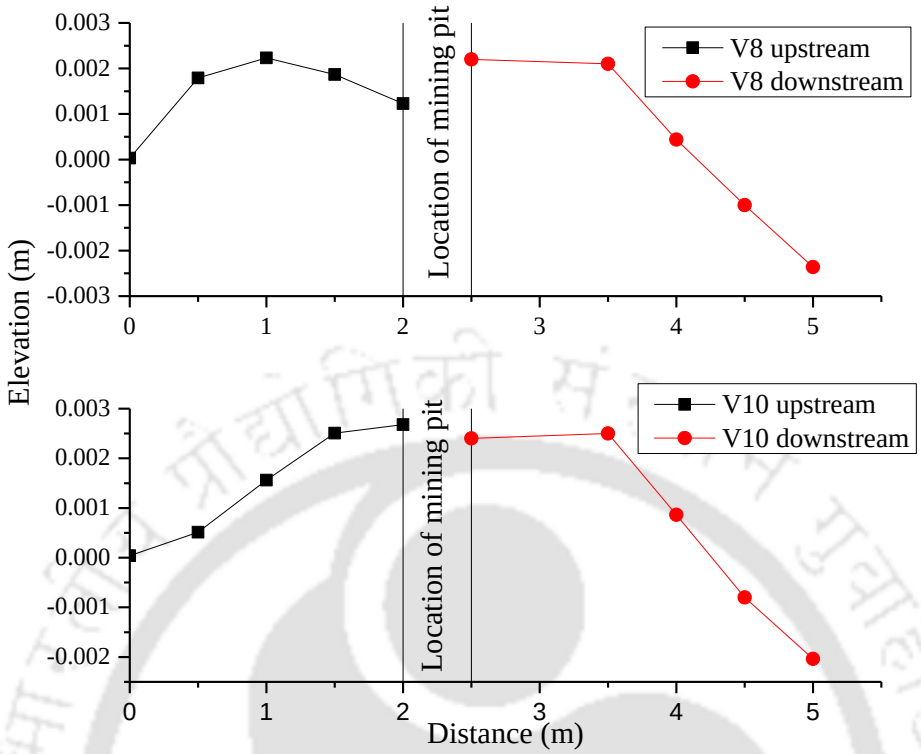

Figure 3.4 Water surface profiles along the centerline of the channel at 4 hours

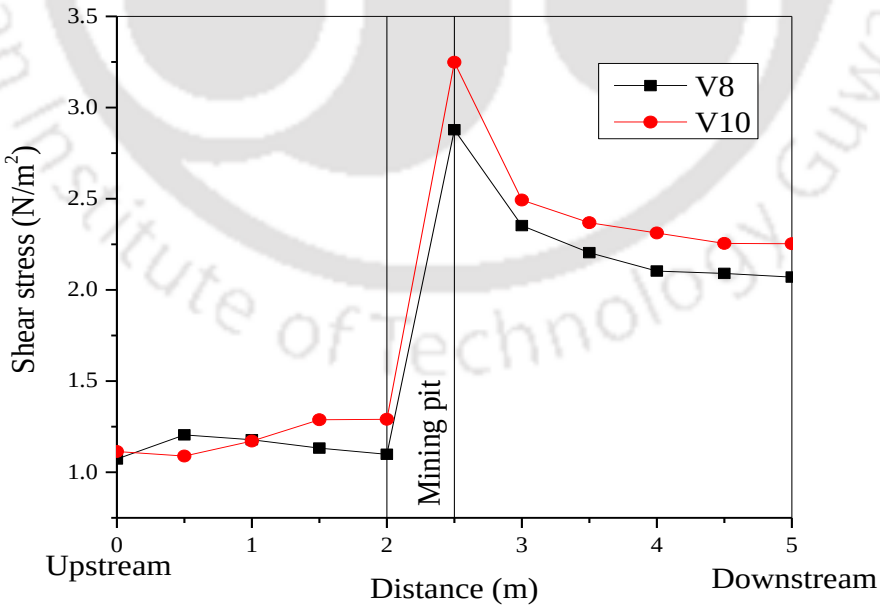

Figure 3.5 Variation of shear stress along the test section at 4 hours

Average shear stress along the center line of the channel is shown in Figure 3.5. Shear stress increases from the upstream to the downstream and highest value is observed at downstream edge of the pit. From downstream edge, it again starts to decrease for further downstream, but not less than the upstream shear stress values.

3.3 Morphological Characteristics of Trapezoidal Mining Pit (Shape-II)

Morphological changes of channel bed occur due to the presence of the mining pit. Experimental and field study revealed morphological changes in terms of bed and bank erosion due to the presence of in-stream mining. Longitudinal profiles after 4 hours along the center line of the channel for Shape-II of Set-I and Set-II are presented in Figure 3.6 and similar trend has been observed as obtained in previous section and also by the previous researchers for the rectangular pit (Lee et al., 1993; Neyshabouri et al., 2002).

A)

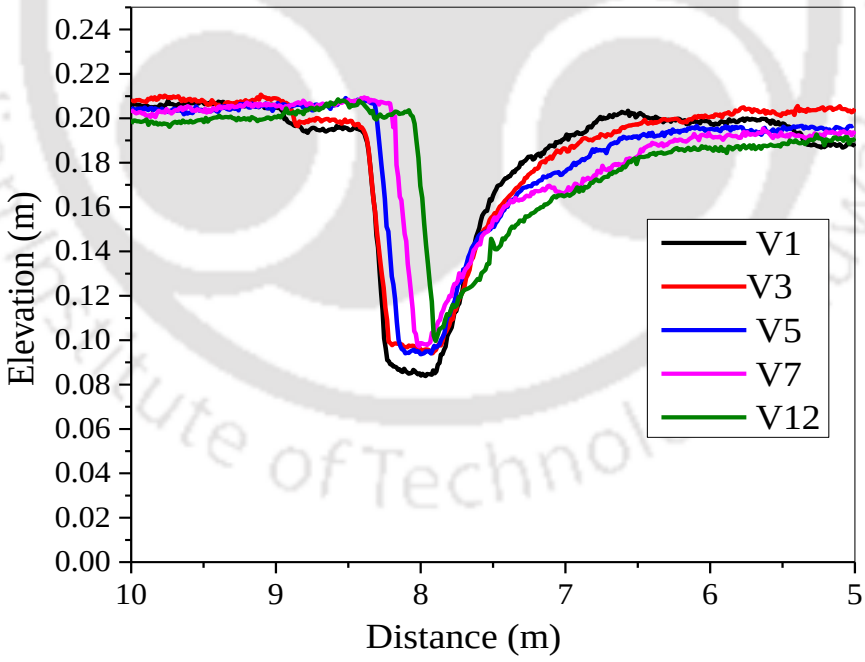

B)

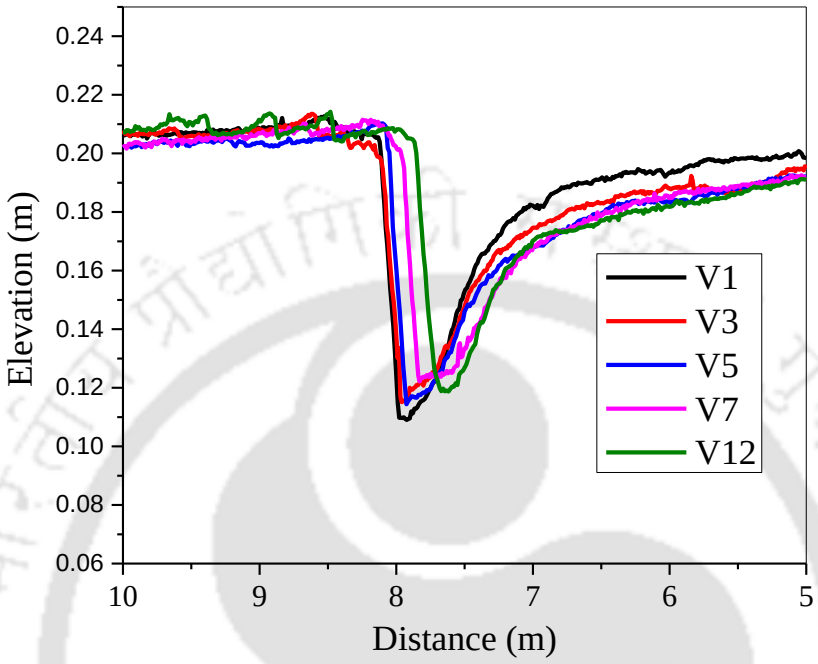

Figure 3.6 Longitudinal profiles along the center line of the channel for Shape-II of A) Set-I, B) Set-II after 4 hours

In Figure 3.6, bed elevations along the centerline of the channel have been plotted for five different average velocities at a particular time for the trapezoidal shaped mining pit. Sediment transport increases with increase in discharge and transported sediment from the upstream gets deposited at the pit. The deposition occurs along the upstream edge of the pit and the edge moves forward towards downstream. Erosion occurs at downstream of the pit and it is also observed that the downstream edge of the pit starts to flatten with time. The similar trend of results for longitudinal profile along the centerline has been observed for all other sets of experiment including all shapes. We have also observed more downstream erosion with the passage of time, which is represented by the cross-sectional profiles at downstream of the pit. The time variation of bed profile at the different cross-section of the trapezoidal mining pit is presented in Figure 3.7.

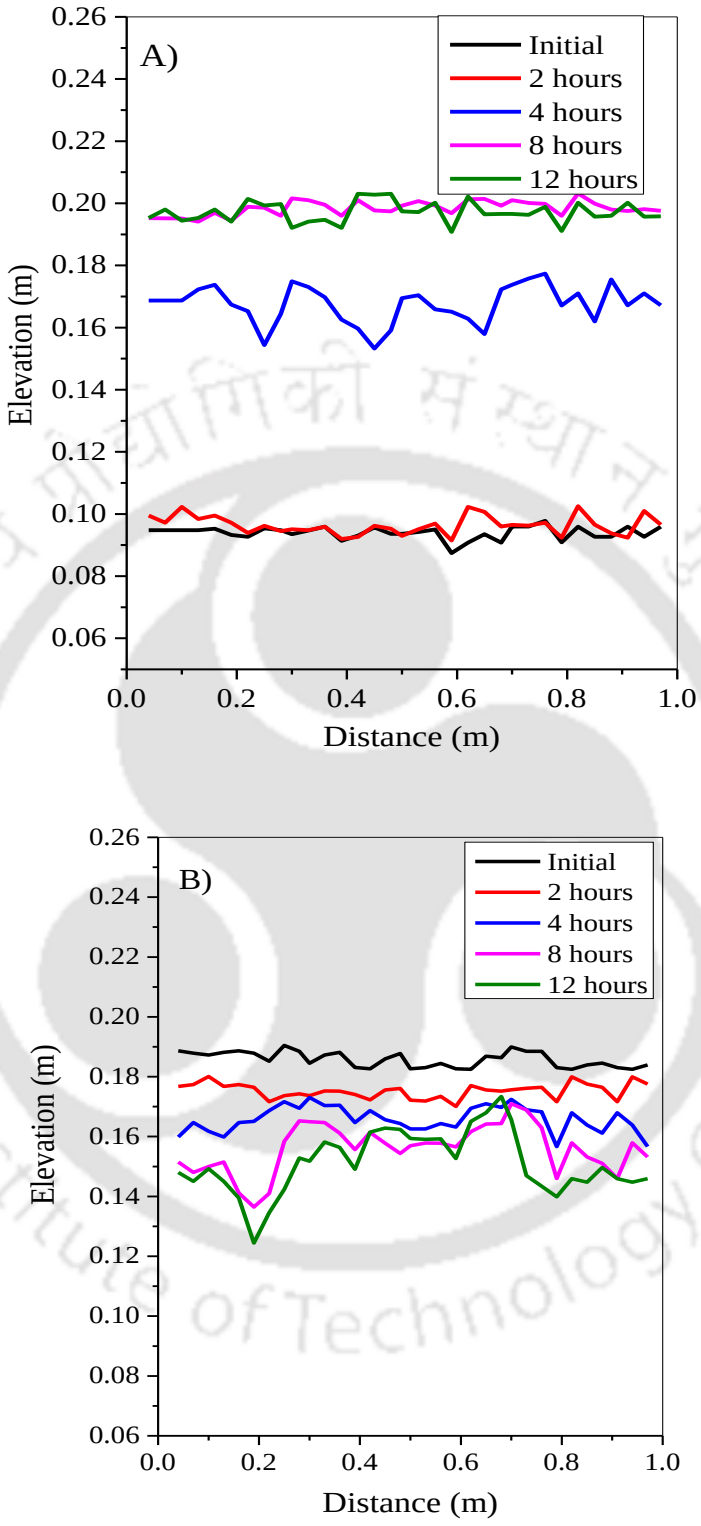

Figure 3.7 Cross-sectional profiles A) at 7.9 m (center of the pit), B) at 7 m (0.5 m from downstream edge of the pit) for Set-I of velocity V12

Cross-sectional profile at the center of the pit (7.9 m) shows filling up of the pit with time, that is, the depth of the pit decreases with the increase in time. Cross-sectional profile at downstream of the pit (7 m) shows the degradation of channel bed with time. The average rate of channel bed degradation at downstream of the pit is 10.5% for 0-4 hour interval, 6% for 4-8 hour interval and 3% for 8-12 hour interval. Both longitudinal and cross-sectional profile shows that the initial depth of the pit decreases with time, which denies the statement as proposed by Lee et al. (1993), that maximum scour depth occurs when the upstream edge reaches the downstream edge of the pit.

The surface plot of initial bed profile, 4 hours and 8 hours bed profile of trapezoidal pit (Shape-II) after the application of discharge is presented in Figure 3.8. The surface plot of the test section reveals that initial bed profile gets distorted due to the application of high discharge and the downstream edge starts to get flattened with the passage of time.

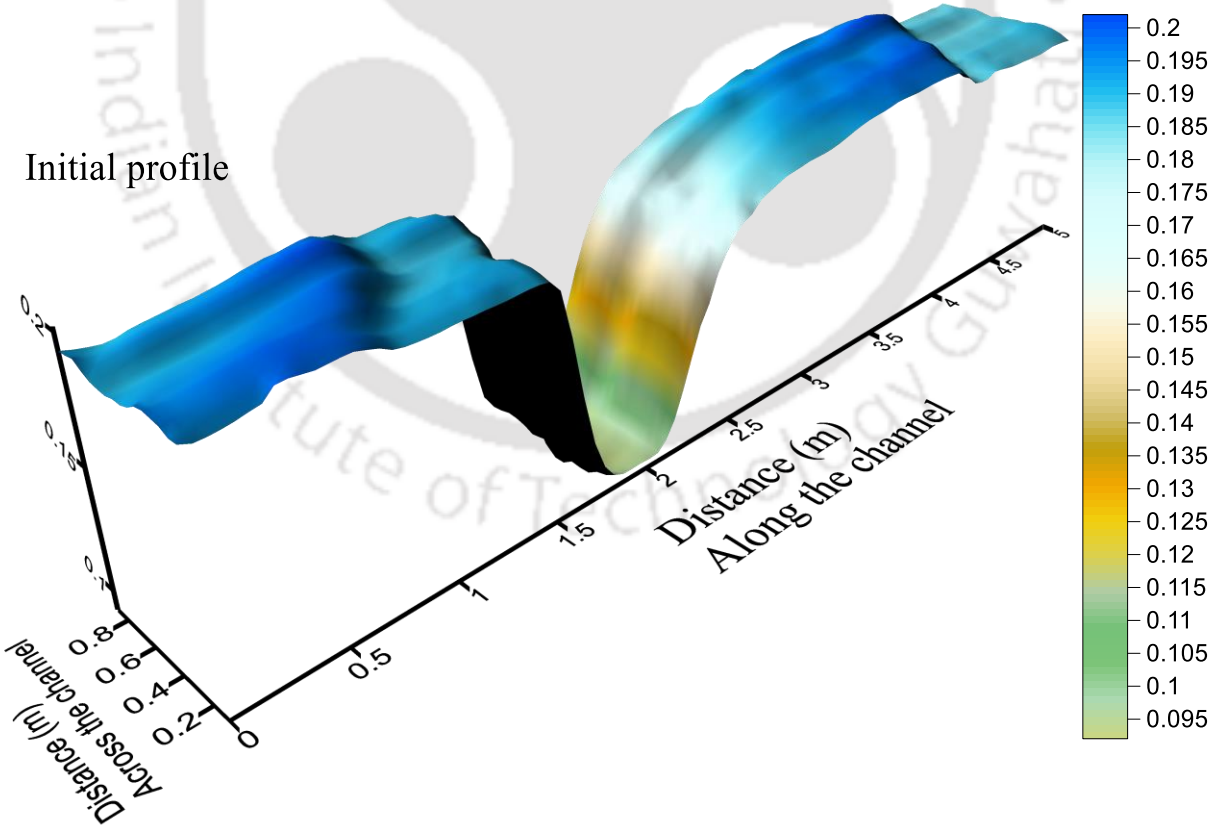

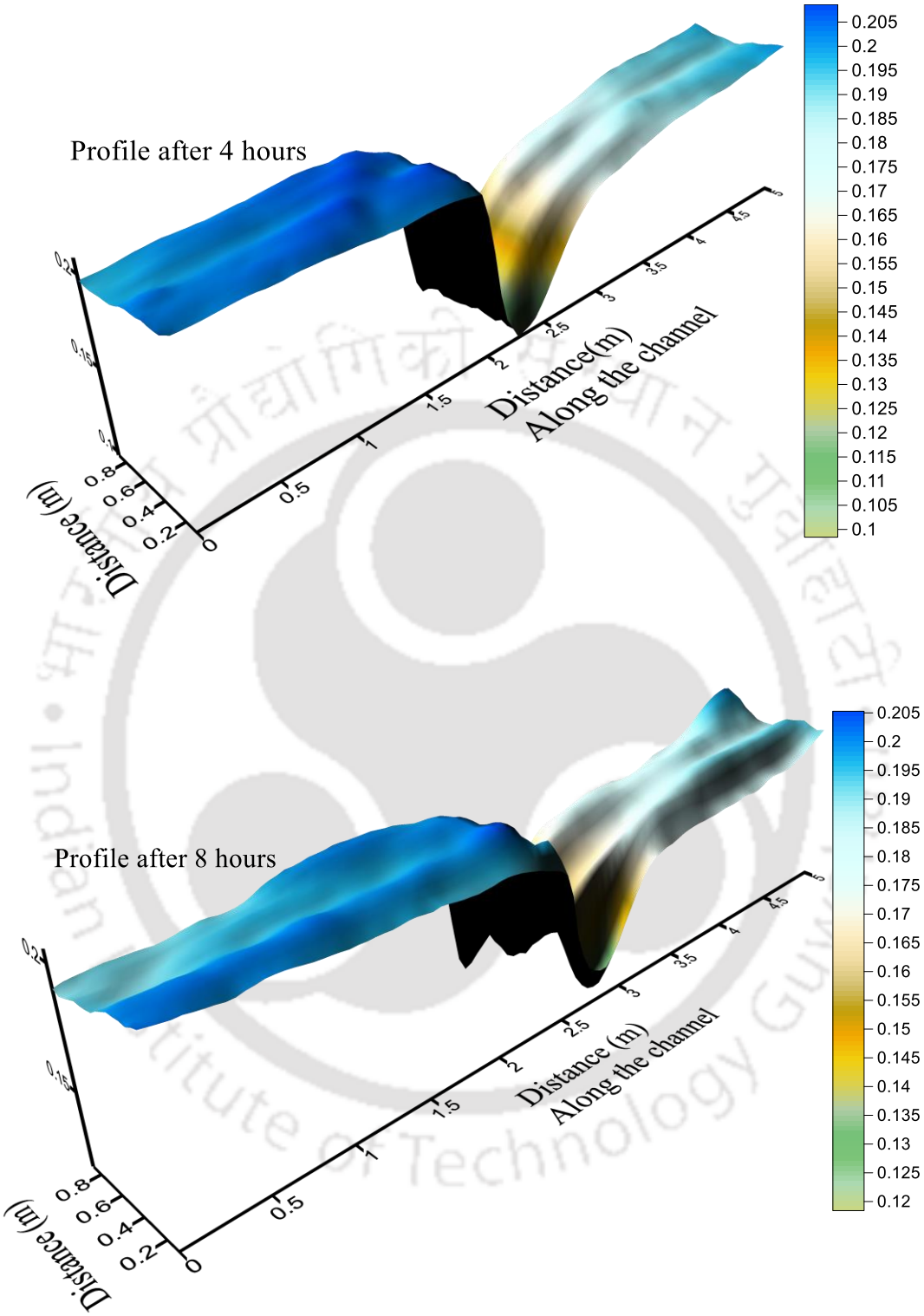

Figure 3.8 Bed surface plot for Shape-II of velocity V12 after Initial, 4 hours and 8 hours of flow (Set-I).

3.4 Morphological Characteristics of Shape-III, Shape-IV and Shape-V

In the case of the rectangular and trapezoidal pit (Shape-I and Shape-II), the pit was constructed along the whole width of the channel but in the case of Shape-III to Shape-V, the pit was constructed with a bank on both sides. Figure 3.9 and Figure 3.10 shows cross-sectional profile at the center of the pit and at 0.5 m from downstream edge of the pit for Shape-III with velocity V12. Figure 3.10 shows erosion at downstream of the pit, which leads to the degradation of channel bed. The cross-sectional profile of the pit in Figure 3.9 shows erosion of bank and decrease in scour depth with time. The initial dry bed slope of the bank line was distorted and the eroded material got deposited on the adjacent section of the pit. A higher depth of water decreases the flow velocity in the pit region. Bed material transported from the upstream of the pit and the bank of the pit starts to deposit at the bottom of the pit.

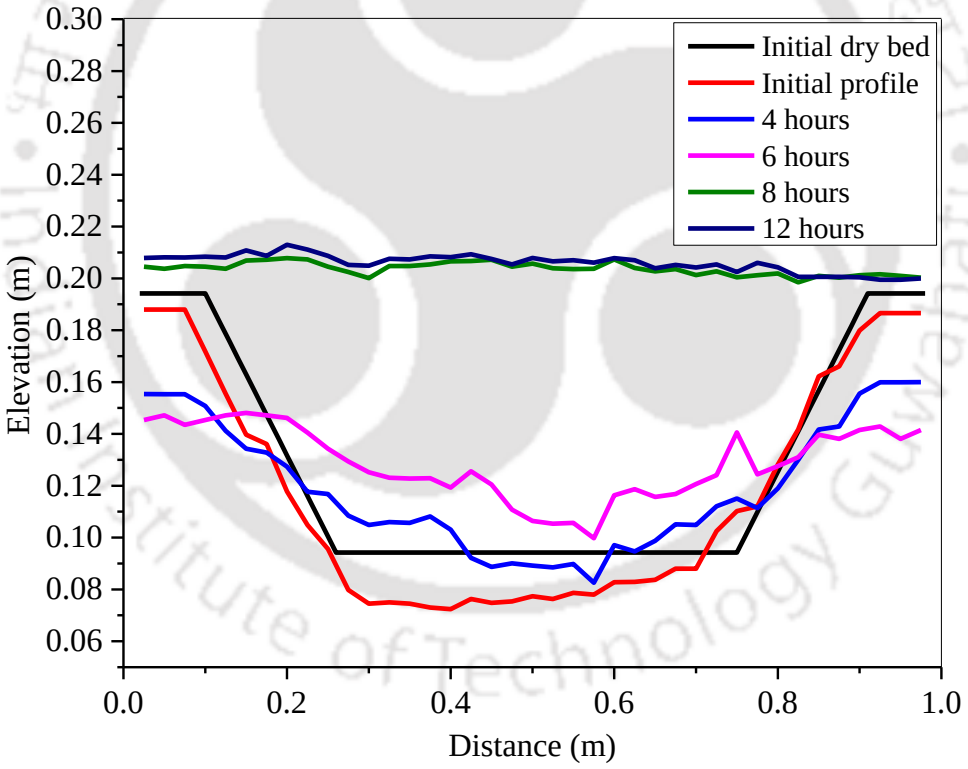

Figure 3.9 Cross-sectional profiles at the center of the pit (7.9 m) for Shape-III of velocity V12 (Set-I)

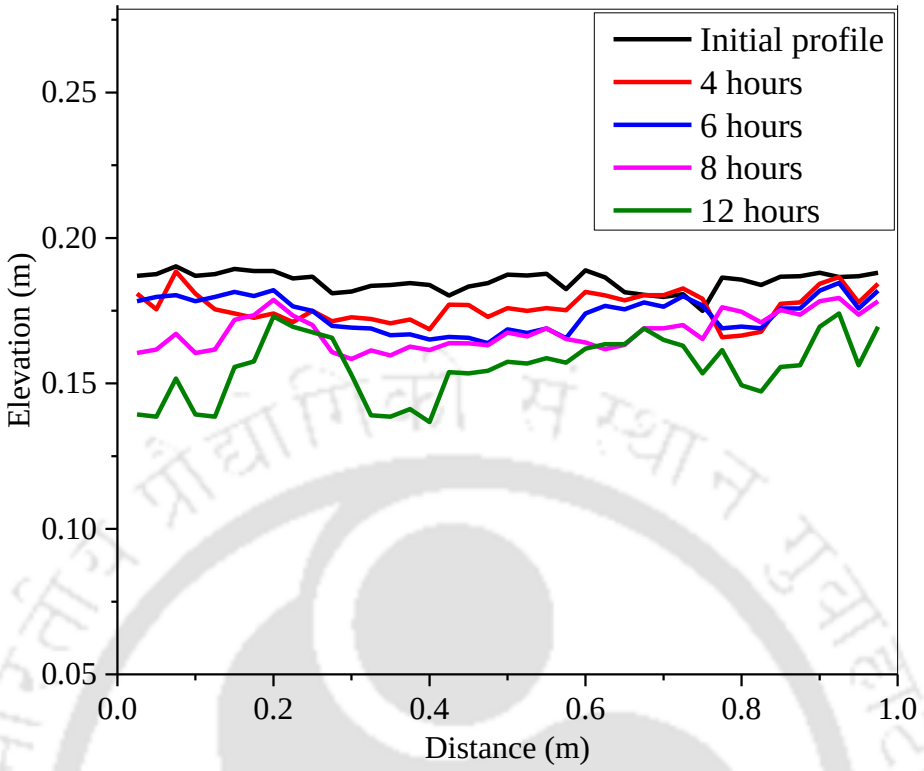

Figure 3.10: Cross-sectional profile at 7 m (0.5 m from downstream edge of the pit) for Shape-III of velocity V12 (Set-I)

Fredsoe (1978) also observed flattening of the cross-sectional slope of a river navigation channel with time. Here, the bank of the pit completely vanishes and the upstream edge of the pit moves forward by water along the channel. Erosion at the downstream of the pit also spread to the whole width of the channel by completely destroying the downstream edge of the pit. It can be observed from the two dimensional profile of channel bed as shown in Figure 3.11. Initial bed surface profile after the application of velocity V12 shows the presence of the bank in the mining region, but it is completely destroyed by the flow with time. In Figure 3.11, the bed surface profiles for Shape-III are presented. It shows total destruction of the initial bank profile and expansion of erosion towards downstream.

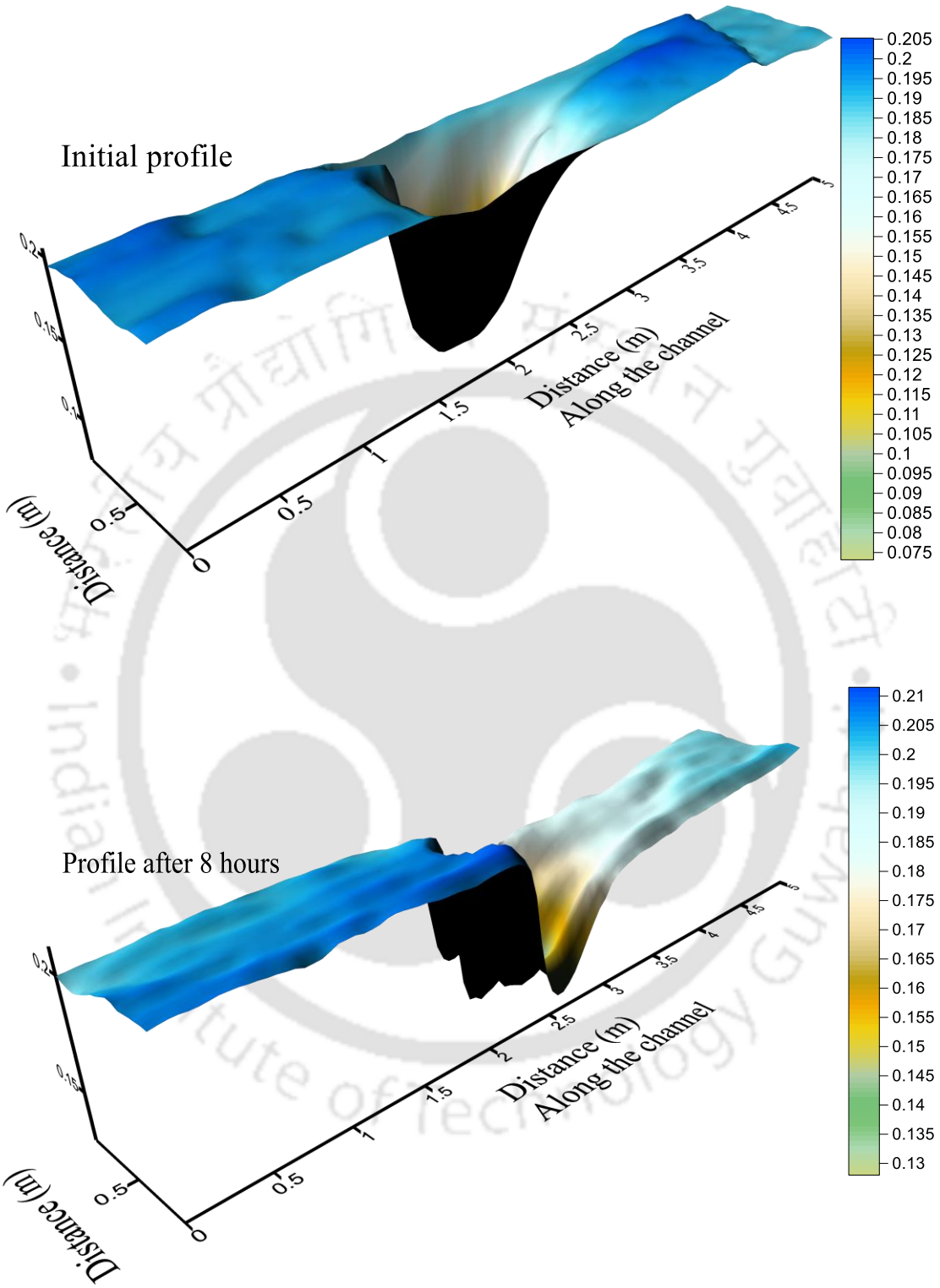

Figure 3.11 Initial and distorted bed surface plot for Shape-III of velocity V12

For Shape-III the bank sides were constructed with an angle as shown in Figure 2.15. However, for Shape-IV and Shape-V sides were vertical (Figure 2.16 and Figure 2.17). Figure 3.12 (B and C) shows the cross-sectional profile for Shape-IV at 8.5 m an 8 m from the downstream of the flume. The location of the profile is shown in Figure 3.12 (A).

A)

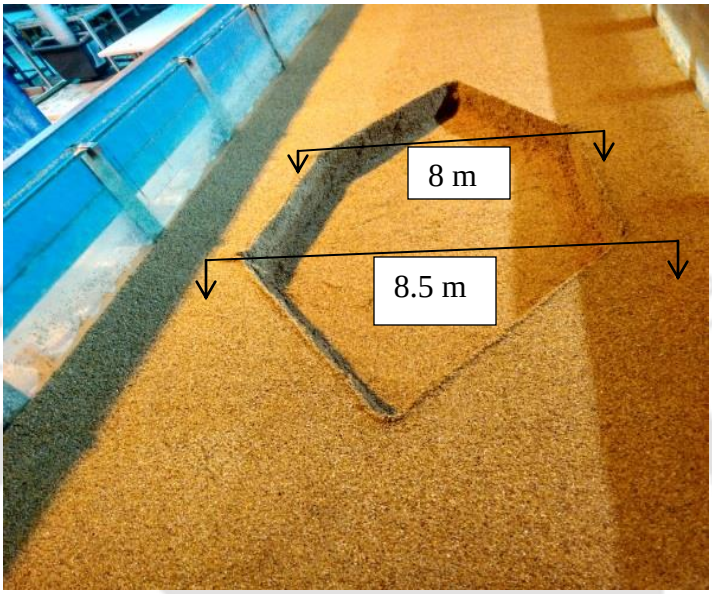

B)

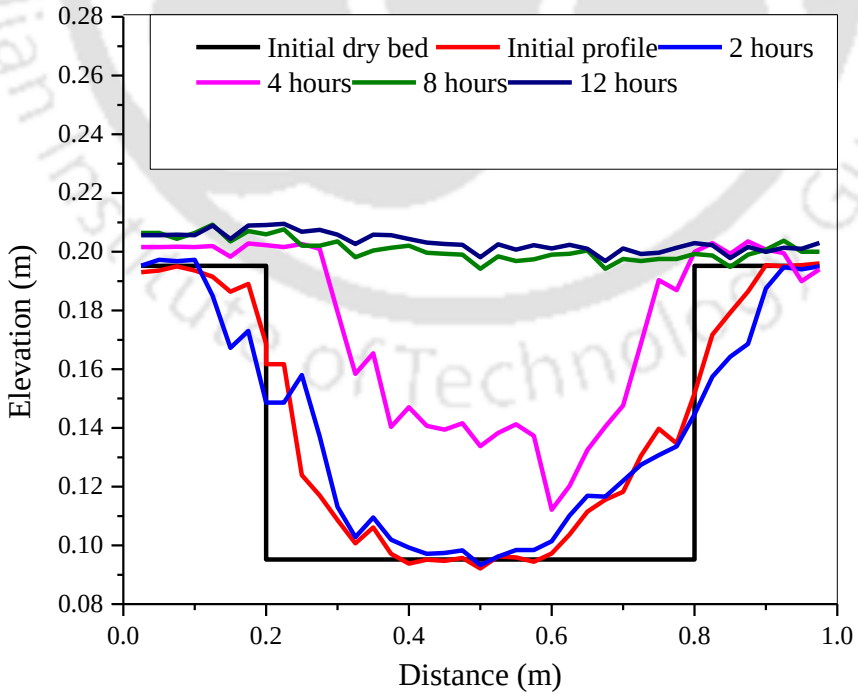

C)

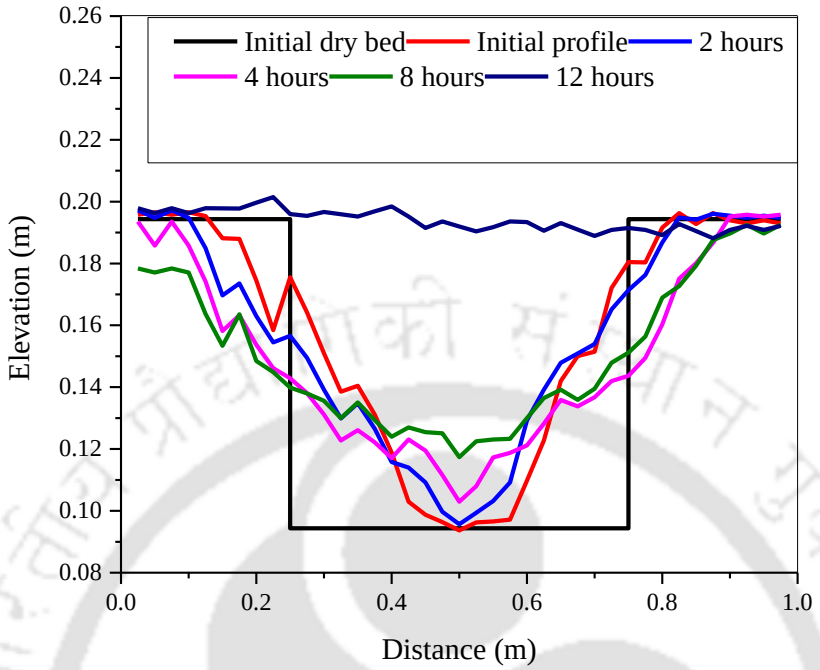

Figure 3.12 A) Location of cross-sectional profile, B) Cross-sectional profiles at 8.5m and (C) Cross-sectional profiles at 8m from downstream for Shape-IV of velocity V12 (Set-I)

The cross-sectional profile shows erosion of the bank of the pit just after application of the discharge. The slopes get flattened with increase in time and the pit filled up due to the movement of the upstream edge in the flow direction. The width of the pit was varying in this case but the erosion expanded to the whole width of the channel. Surface plot of bed profile in this case shows the downstream erosion very clearly. The surface plot of Shape-IV for initial and after 8 hours of flow is presented in Figure 3.13 and destruction of the bank of the pit is observed. Similar type of profile is also observed from circular pit (Shape-V) and the surface plot for the bed profile with this shape is presented in Figure 3.14. Figure 3.15 shows snapshots of channel for Shape-III, Shape-IV and Shape-V after distortion of bank profile

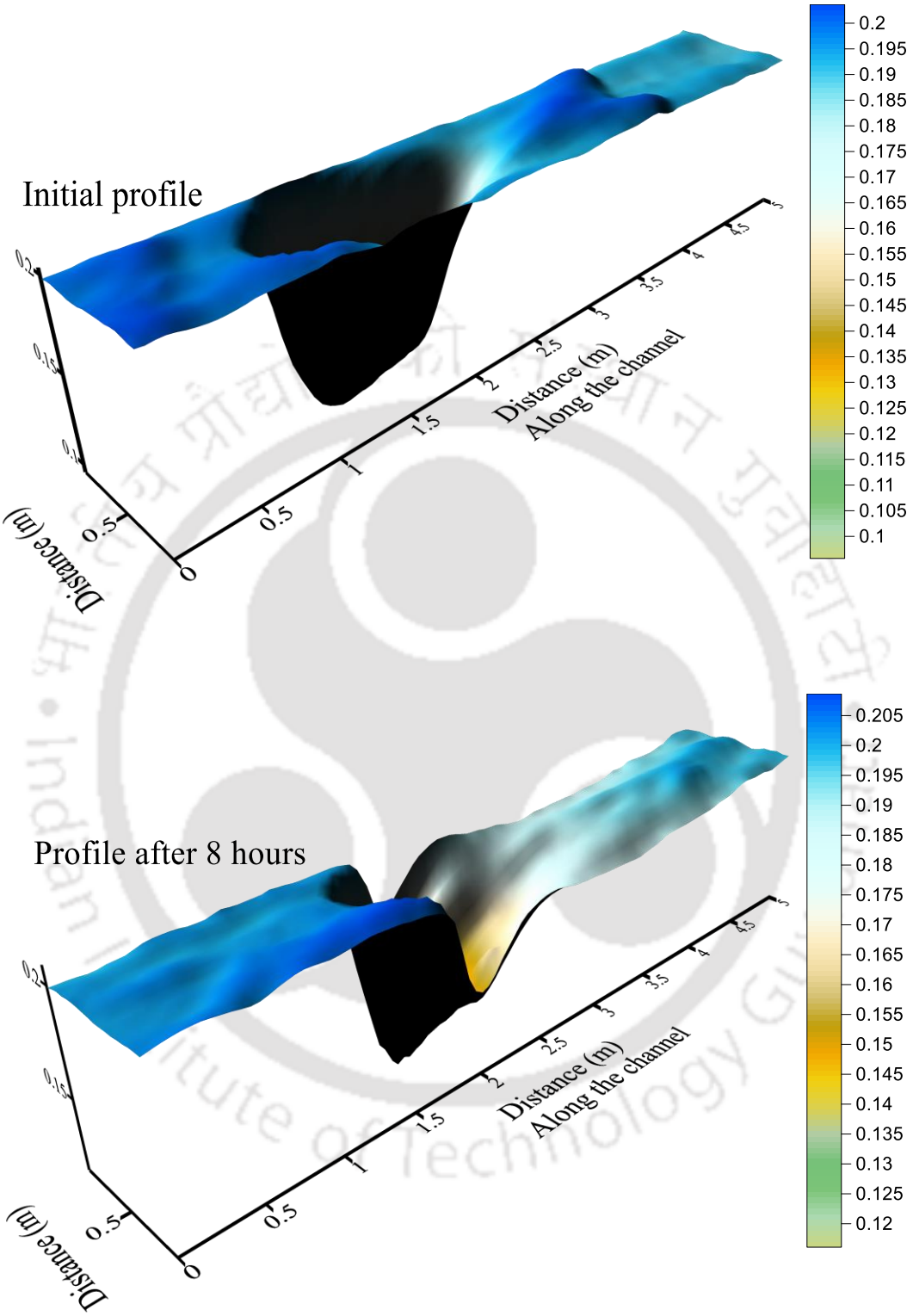

Figure 3.13 Initial and distorted bed surface plot for Shape-IV of velocity V12

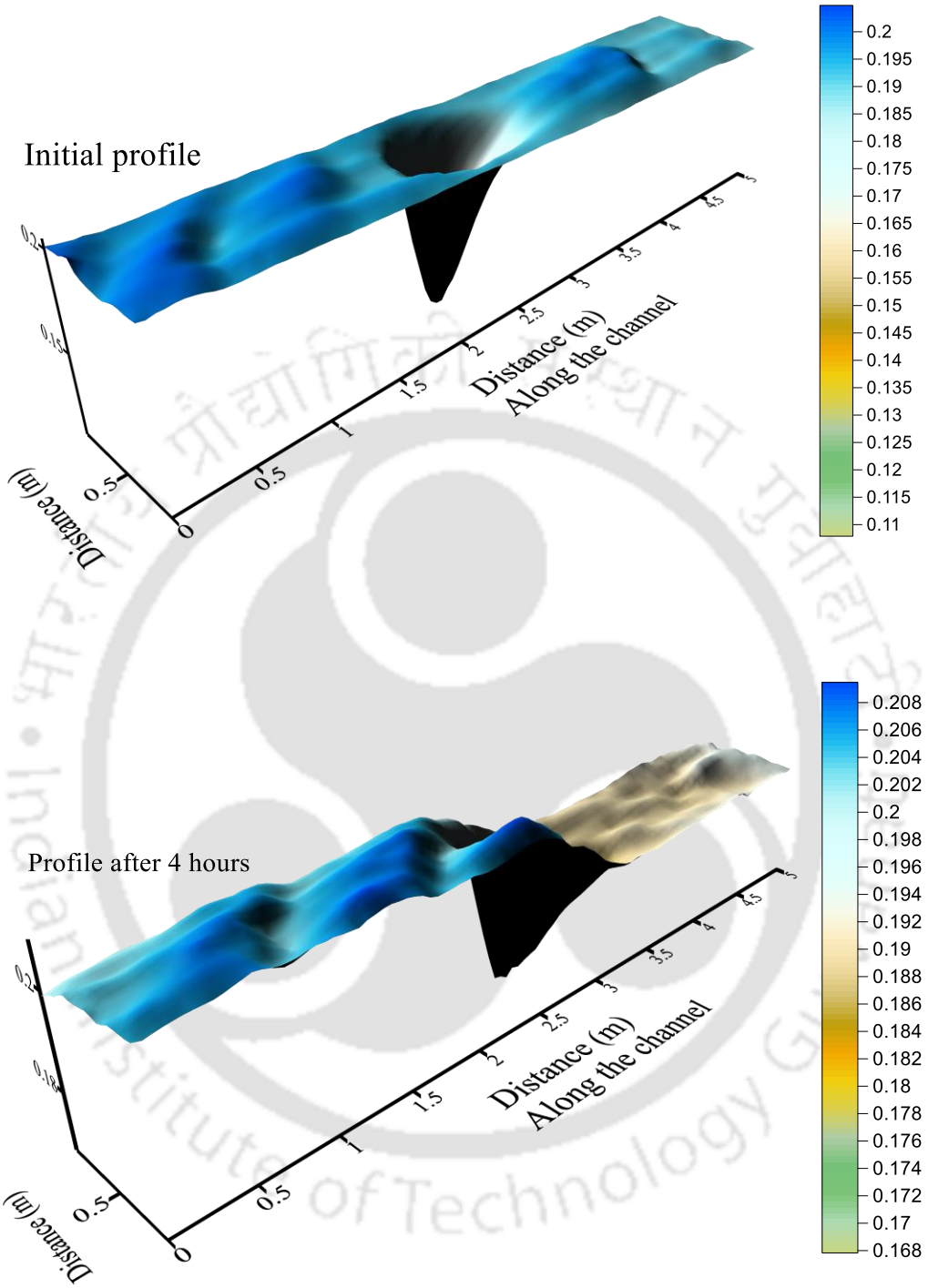

Figure 3.14 Initial and distorted bed surface plot for Shape-V of velocity V12

A)

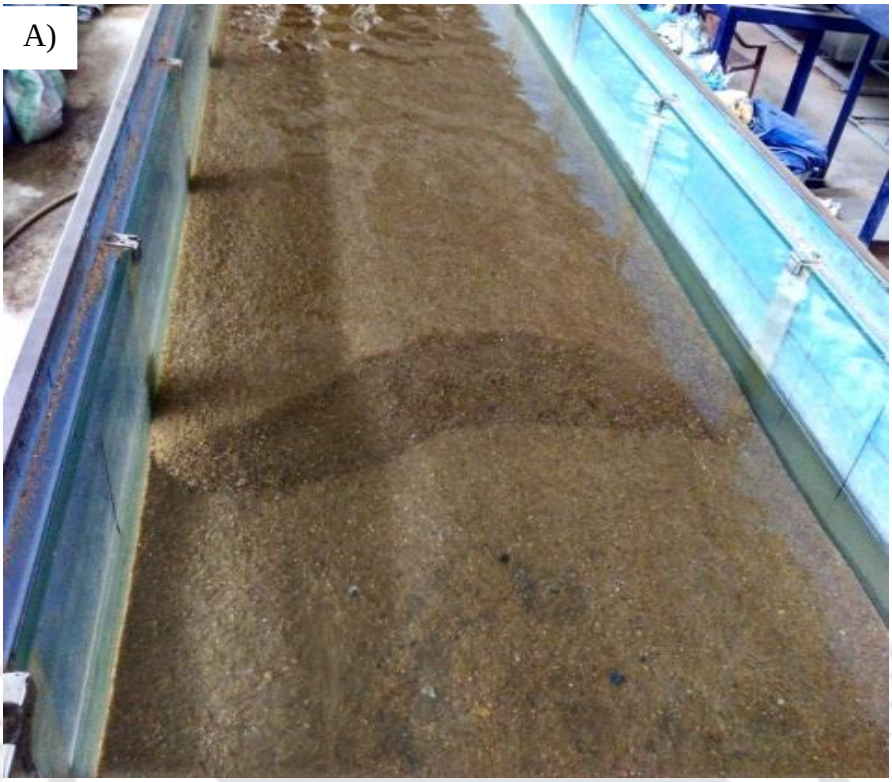

B)

Figure 3.15 Snapshot of channel for A) Shape-III, B) Shape-IV and C) Shape-V after distortion of bank profile.

Distortion of the cross-sectional shape of the pit and its influence on downstream can adversely affect the waterway at mining region as well as downstream of it. Channel degradation has a direct influence on the erosion of foundation level of the bridge pier or any other hydraulic structure, exposure of underground pipeline crossing and many others. The change in morphology due to mining activity directly disturbs the habitat and biota. The actual sand mining problem is very complicated due to the haphazard nature of mining activities. The results obtained in this study can be implemented to describe the extent of erosion in the mining pit region, and deposition in the pit. However, a scaled model is needed to verify the results and implement in a real field condition.

3.5 Conclusions

Experiments were conducted to study the impact of mining pit on morphological changes of channel bed. Reach average shear stress shows increase in shear stress from upstream to the

downstream of the pit. Experimental observations are discussed on the longitudinal and cross-sectional variation of channel bed deformation from upstream of the mining pit to the downstream of it. Morphology of channel bed with five different shaped mining pits has been discussed. Morphological profile shows the propagation of erosion towards the downstream of the pit for all five shaped mining pit. The upstream face of the mining pit maintains an angle nearly equal to the angle of repose of the bed material while migrating towards the downstream. In case of the pit with bank (Shape-III, Shape-IV and Shape-V) the cross-sectional profile indicates collapse of the bank of the pit and flattening of bank with time. For the Shape-III, Shape-IV and Shape-V the erosion is not constraint within the pit excavation region but expanded to the whole width of the channel at the downstream.

4 Turbulent Flow Structure and Bed Load Transport Characteristics in a Mining Affected Alluvial Channel

4.1 Introductions

The literature study of various field investigations showed erosion of bed and bank of the river due to mining activities. Experimental study on sand mining also shows severe downstream erosion and the partial filling of the mining pit. Erosion of sand bed occurs due to the detachment of sand particles from channel bed and basically depends on the hydrodynamic characteristics of flow and its interaction with channel bed material. Therefore, to understand the process of erosion in a mined channel we need to investigate the nature of the turbulent structure in the mined region. Alfrink and van Rijn (1983) developed two-equation turbulence model for flow over a trench and described the phenomenon of recirculating flow by using turbulence model closure. A fix trench with a layer of gravel of 0.006 m and a Laser Doppler Velocity meter for instantaneous velocity measurement were used by Alfrink and van Rijn (1983) for experimental verification of their numerical model, and observed reversal flow at the center of the pit bottom from both experimental and numerical results. In case of a mining pit on a sandy channel, the bed material acts as a mobile boundary over which the flow occurs. Sediment transport in fluvial system governs the morphodynamic changes and the transport mechanism is highly influenced by the turbulent nature of the flow. Turbulent flow transfers its momentum to the bed particles and starts to accelerate the motion of the particles, while bed resists the process and dissipation of fluid energy occurs. Previous study by various researchers mainly concentrated on the morphological changes due to the presence of the mining pit. Detailed appraisal of the turbulent parameters in the region of the mining pit for sandy channel has not been done so far. Thus, the primary aim of this chapter is to investigate the turbulent characteristics in a mining pit region and to understand the relation between the turbulent structure of flow and morphological changes in that region. Based on the experimental investigation we have also formulated an empirical bed load transport equation for the mining affected channel.

Various turbulent parameters of flow, such as Reynolds shear stress, velocity distribution, von Karman constant, turbulent intensity, anisotropy and conditional Reynolds shear stress have been

investigated from these experiments. The change in flow parameters due to the presence of mining pit is also discussed in this chapter.

4.2 Turbulent Characteristics

Understanding of turbulent structure of flow is essential for the assessment of morphological changes due to the presence of mining pit. The linkage between the instantaneous flow and sediment transport characteristics in the mining region can give us detail insight of fluvial mechanism. Time-averaged velocity distribution, Reynolds shear stress, turbulent intensities, anisotropy, conditional Reynolds shear stress are calculated in four different sections. The position of sections of ADV data collection for trapezoidal pit is shown in Figure 4.1. Results for turbulent characteristics are presented for of Shape-II of Set-I with discharge Q1.

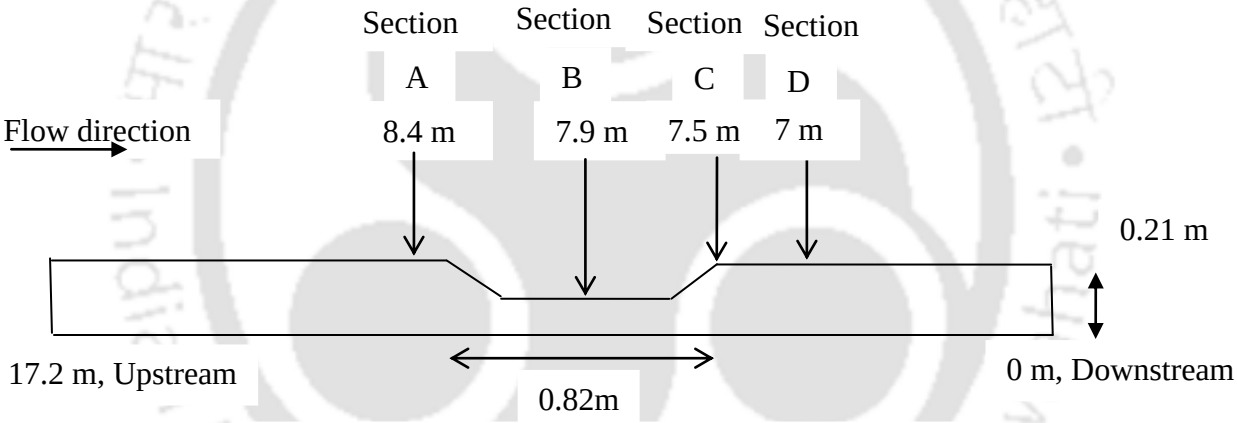

Figure 4.1 Different sections of velocity measurement.

4.2.1 Reynolds shear stress distribution (RSS)

The momentum diffusion mechanism can be described from the vertical distribution of Reynolds shear stress. The Reynolds shear stress distribution is nonlinear for channel flows and the linearity occurs only for flow depth above the peak as stress decays from its maximum near the boundary to the free surface (Nepf and Vivoni, 2000; Emadzadeh et al., 2010; Afzalimehr et al., 2011). RSS is calculated by using Equation 2.6 at each vertical section.

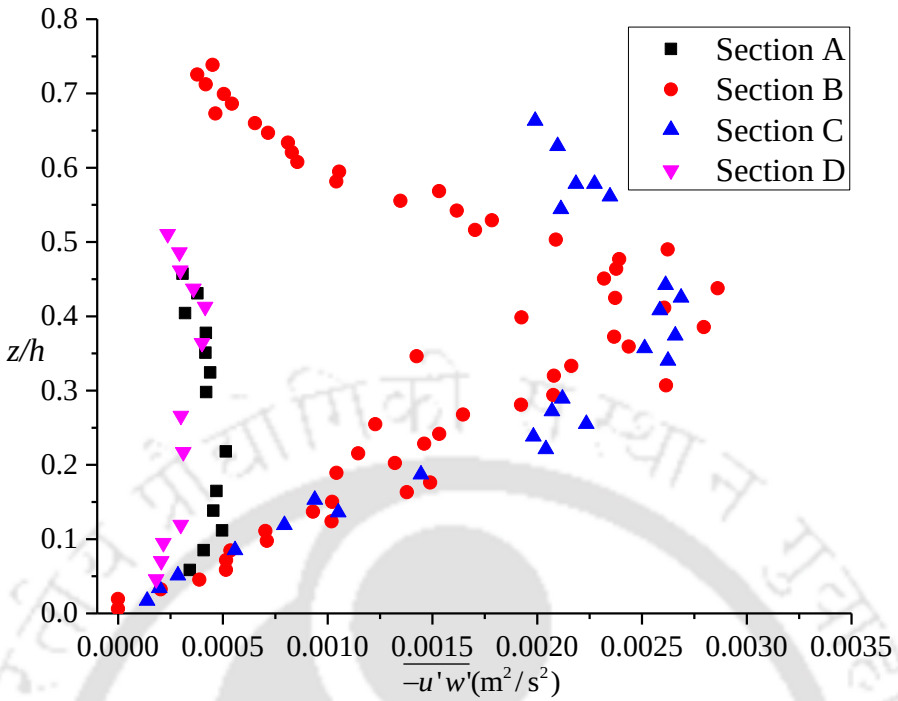

Figure 4.2 Vertical distribution of Reynolds shear stress

Figure 4.2 shows vertical distribution of RSS for four different sections. From the figure it is observed that maximum values of RSS increases for Section B and C as compared to Section A.

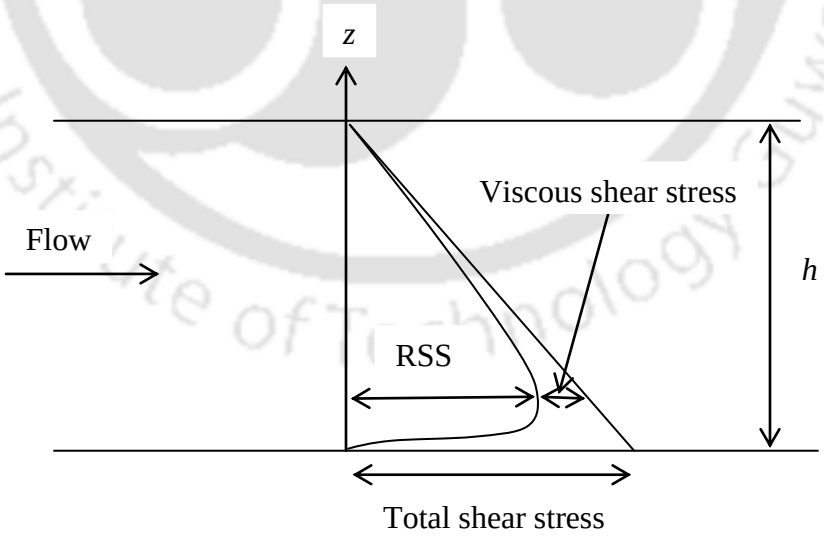

Figure 4.3 Distribution of shear stress in an open channel flow for steady uniform flow

Total shear stress increases linearly from zero at the free surface to maximum at the channel bottom in case of steady uniform flow in an open channel. The total shear stress is the sum of Reynolds shear stress and viscous shear stress.

$$\tau = \left(1 - \frac{z}{h}\right)\tau_0 \tag{4.1}$$

τ is the total shear stress and τ_0 is the shear stress at the bottom of the channel. We assumed that RSS follows linear law having total shear stress zero at the free surface. Using linear projection of RSS profile, the total shear velocity on channel bed has been calculated from $U_* = \left(\overline{-u'w'}\right)^{0.5}$ at z=0 (Nezu, 1977) for all four sections. Figure 4.4 shows vertical distribution of normalized Reynolds stress ($\overline{u'w'}^{+} = \overline{-u'w'}/U_*^2$) at Section A, B, C, and D with respect to non-dimensional flow depth (h^+=z/h). Here, z is the vertical location of measurement from bed surface and h is the total flow depth at a particular section.

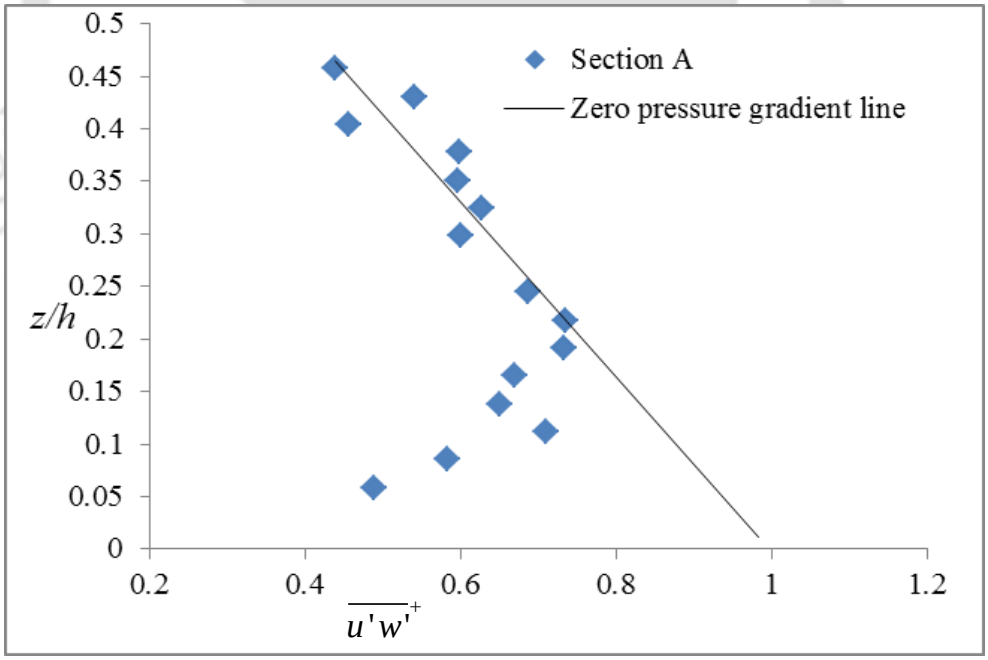

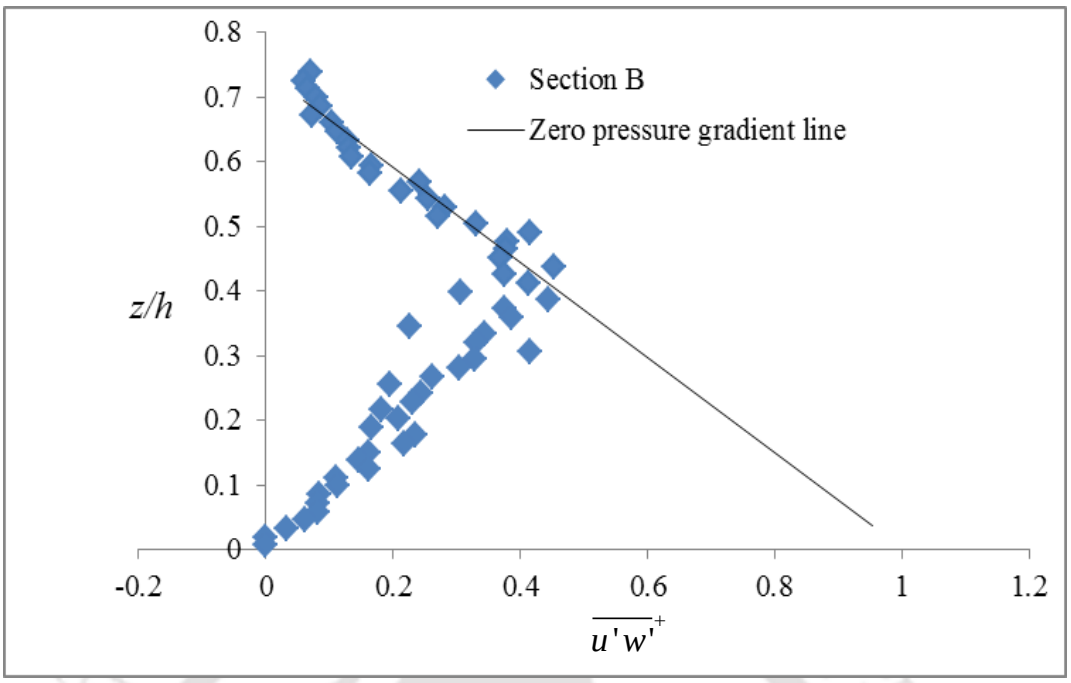

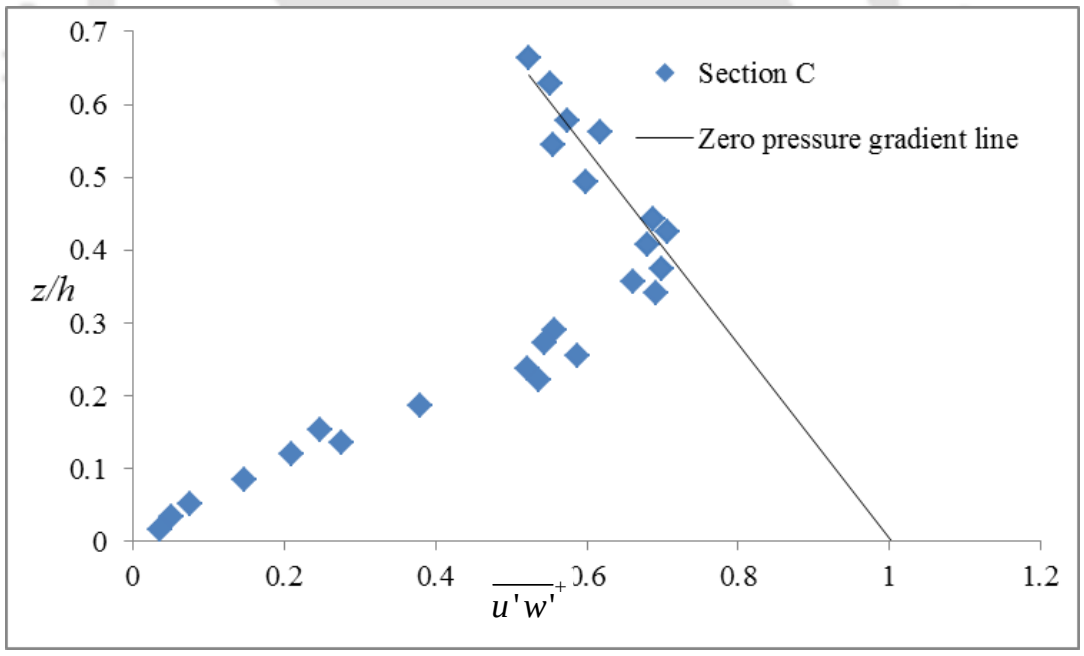

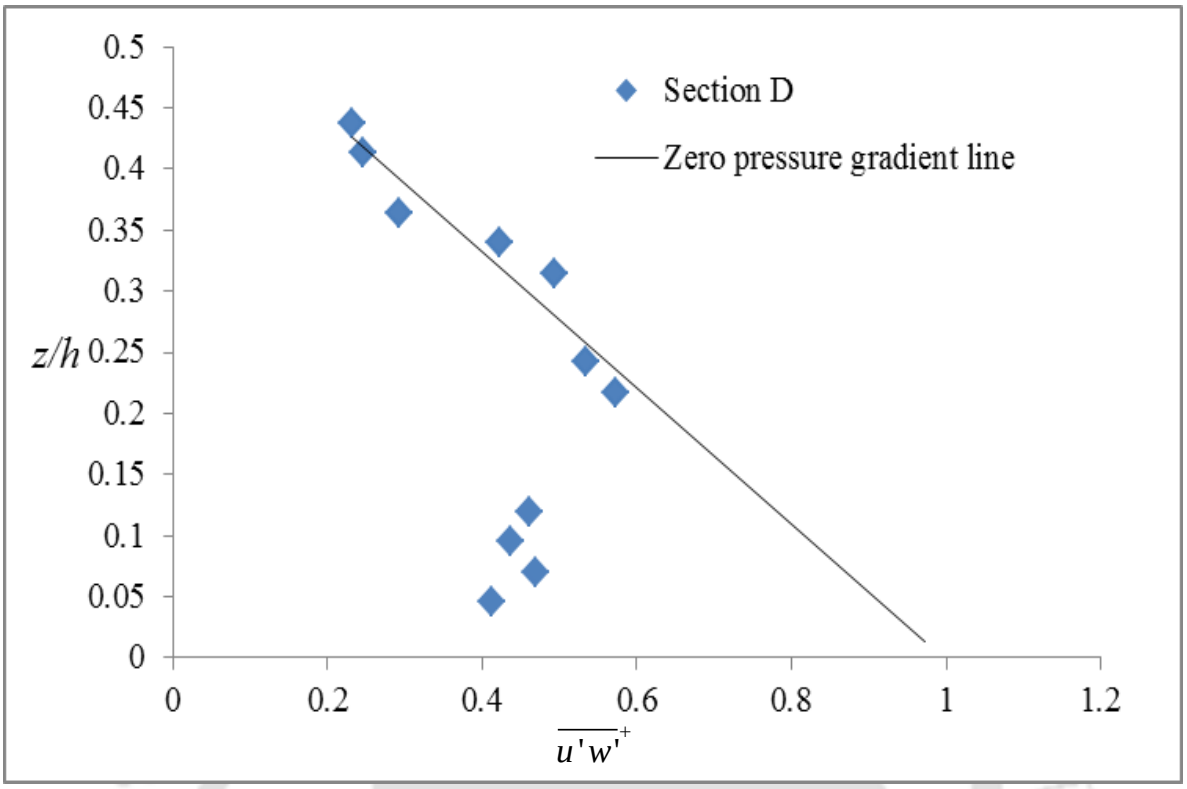

Figure 4.4 Vertical distribution of normalized RSS ($\overline{u'w'}^{+}$) and zero pressure gradient at four different sections.

From Figure 4.4 normalized RSS is observed to be consistent with the linear law of RSS with zero pressure gradient at free surface ($\overline{u'w'}^{+} = -\overline{u'w'}/U_*^2 = 1 - z/h$). However, near the boundary region damping of $\overline{u'w'}^{+}$ distribution is observed from the deviation of data points from the linear law. This damping is more prominent in case of mobile bed as compared to the clear water, which is caused due to the fact that the mobile bed particle reduces the flow velocity with respect to the particle velocity to drag those (Zrostlík *et al.*, 2016). Characteristics of RSS distribution at all four sections are observed to be similar but magnitudes are different in each section. The distance of occurrence of maximum RSS from the bed surface increases in the pit as well as in the downstream of the pit. At upstream of the pit (Section A) RSS attains its maximum value at about $z/h \sim 0.2$, but in the pit region (Section B and C) and downstream of the pit (Section D) maximum value observed is between $0.35 \geq z/h \geq 0.45$. The increase in the distance of occurrence of maximum RSS at the above-mentioned sections attributes to the fact that more

turbulence is created due to the oscillation on the top of the pit, which further increases the occurrence of momentum exchange and results in more RSS at those sections. Shear velocity (U_*) from the linear projection of RSS for all four sections are tabulated in table 4.1

Table 4.1 Shear velocity (U_*) from the linear projection of RSS

	Section A	Section B	Section C	Section D
Shear velocity (U_*) in m/s	0.0272	0.0794	0.0617	0.0312

The shear velocity are observed to be higher than the critical shear velocity u_{*c} = 0.0262 m/s. Two to three-fold increase in shear velocity is observed at Section B and C as compared to Section A, which indicates high amount of sediment transport in the mining pit region. At the downstream of the mining pit (Section D), shear velocity is 14.5 % more than the upstream shear velocity (Section A), which also indicates more sediment transport at the downstream of the mining pit.

4.2.2 Time-averaged flow velocity

Time-averaged flow velocities were calculated from the instantaneous velocity data at different vertical distances from the channel bed. Vertical distribution of time-averaged stream wise flow velocity $\overline{U}$ with respect to normalized vertical distance ($h^+ = z/h$) at four different sections is presented in Figure 4.5. At the center of the pit (section B), stream wise velocity is observed to be negative, indicating the presence of reversal flow at the bottom of the pit (Alfrink and van Rijn, 1983). In other three sections positive stream-wise velocity was observed. Sudden increase in flow depth in the pit reduces the flow velocity and deposition of sediment occurs.

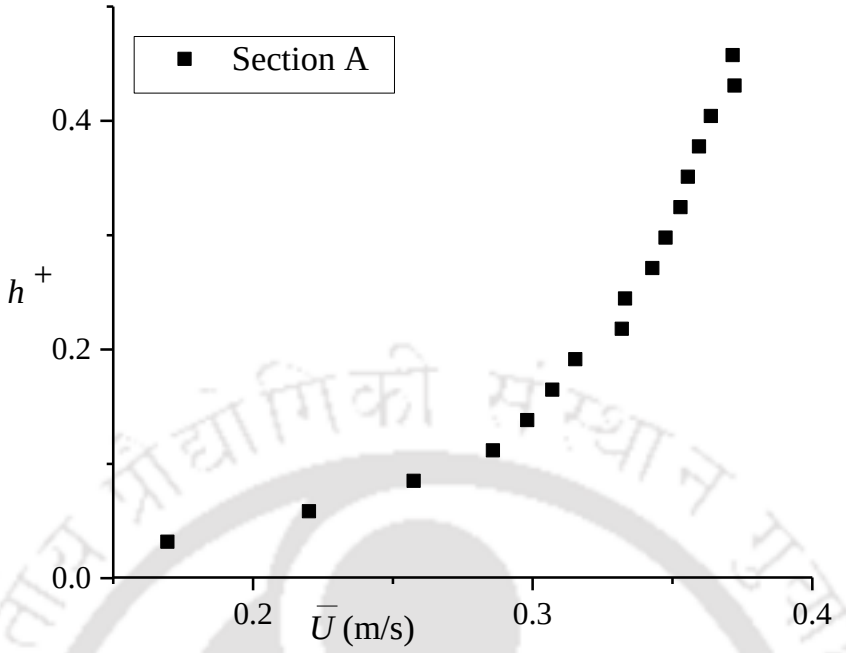

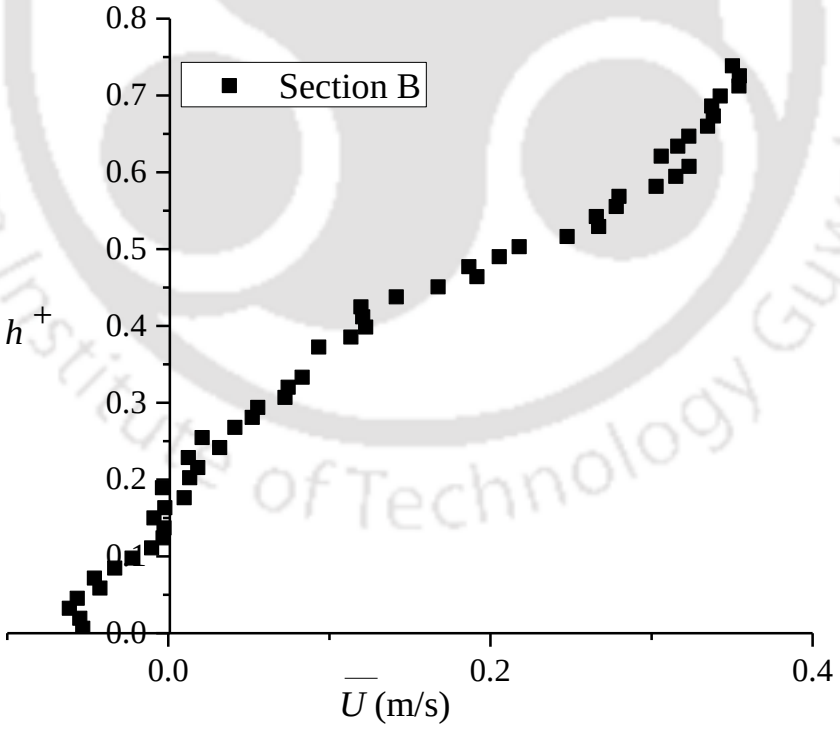

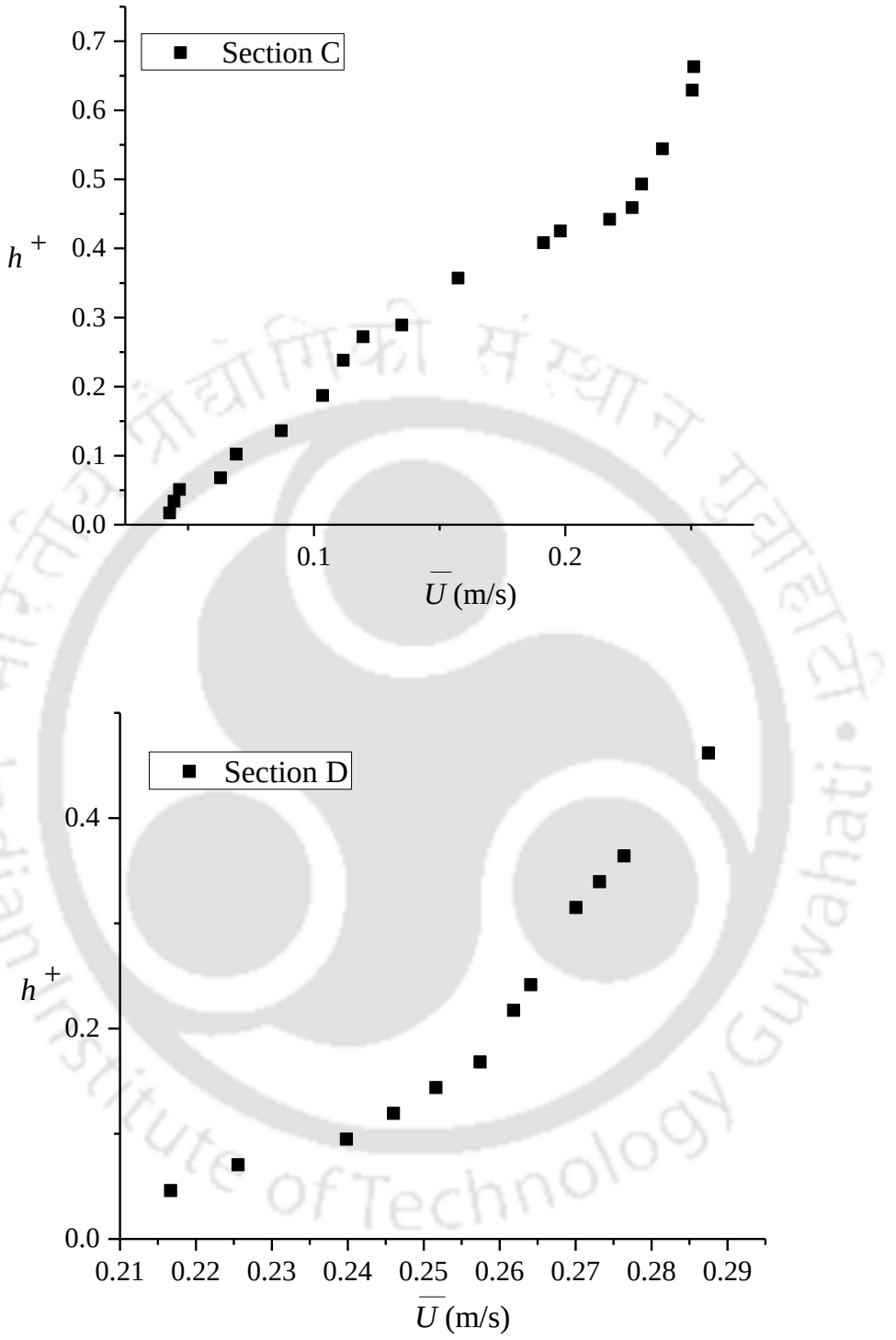

Figure 4.5 Time-averaged vertical distribution of flow velocity in stream wise direction at different sections.

Velocity profile data has been fitted to the modified logarithmic law in the inner layer (z/h = 0.2) as discussed by Despande and Kumar (2016) for Section A and D. Logarithmic law is expressed in the non-dimensional form as follows:

$$\frac{\overline{U}}{U_*} = \frac{1}{k}\ln\left(z^+ + \Delta z^+\right) - \frac{1}{k}\varepsilon^+ \qquad (4.2)$$

Here, $z^+ = z/d_{50}$, $\Delta z^+ = \Delta z/d_{50}$ (Δz represent the virtual bed level), $\varepsilon^+ = z_0/d_{50}$, z_0 = zero velocity level, k = von Karman constant. It is observed from Figure 4.6 that modified log law further modifies into two different logarithmic laws with k value 0.34 and 0.39 respectively at section A and section D, which shows strong momentum exchange between the flows and bed material. k values for both the section are lower than its universal constant (k=0.41), indicating mobile bed condition (Despande and Kumar, 2016).

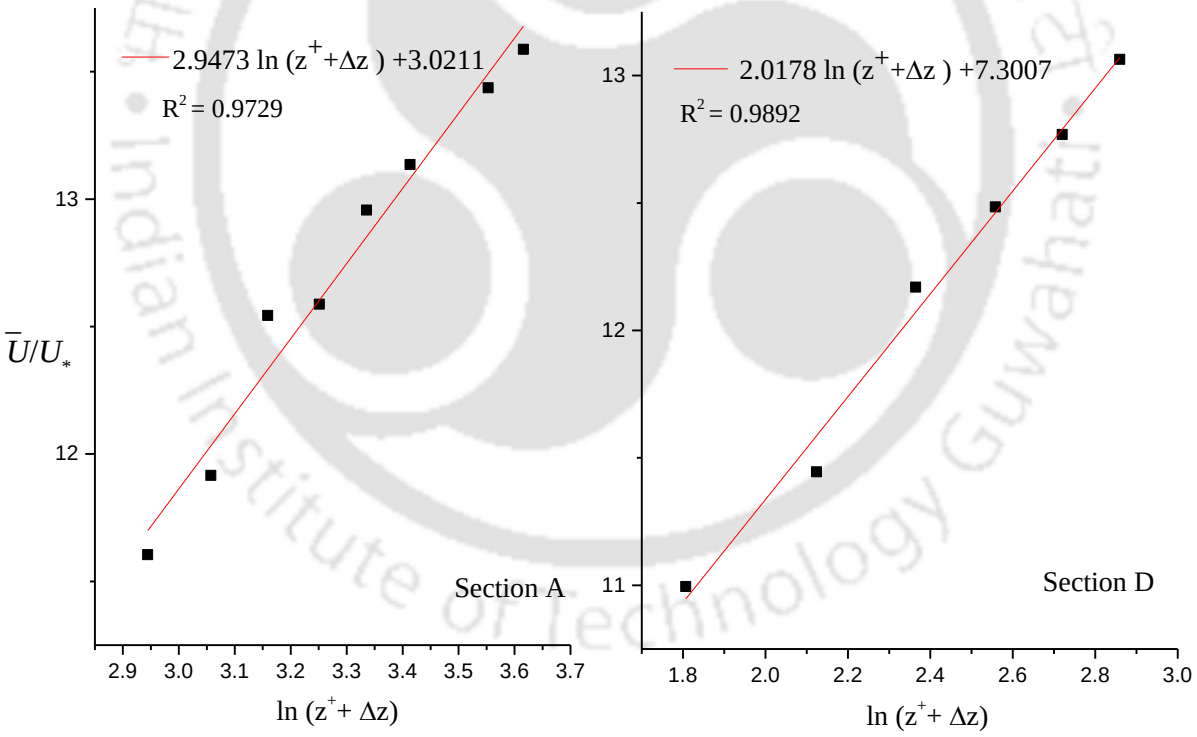

Figure 4.6 Profile of velocity logarithmic law

Regression equation of logarithmic law shows virtual bed level and zero velocity level at 5.4 mm and 0.395 mm respectively for Section A; 5 mm and 0.133 mm respectively for Section D.

Higher value of virtual bed level and zero velocity level at the upstream of the mining pit (Section A) than the downstream (Section D) suggests a higher exposure of upstream sediment particles with increased velocity as compared to downstream sediment particles, which are also in transport condition. At section B and C, it is observed that flow in the inner zone does not follow the logarithmic law. Negative stream wise velocity at section B shows the presence of recirculation zone at the bottom of the pit (Alfrink and van Rijn, 1983). Flow with high velocity from the upstream enters into the pit, and with the increase in flow depth flow velocity reduces in the pit region, which influences the sediment particles carried by the flow to be deposited at the bottom of the pit. Negative bottom velocity recovers at section C but vertical distribution of velocity shows tapering of the velocity profile for $z/h < 0.4$ and does not follow the logarithmic law for the inner zone. The logarithmic velocity profile is restored at Section D as shown in Figure 4.6.

4.2.3 Reynolds normal stress distribution (RNS)

Reynolds normal stress is also called turbulence intensities of velocity. It can be calculated from the equations as mentioned below:

$$\left.\begin{aligned}\sigma_u &= \sqrt{\overline{u'u'}} \\ \overline{u'u'} &= \frac{1}{m}\sum_{i=1}^{m}\left(u_i-\overline{U}\right)\left(u_i-\overline{U}\right)\end{aligned}\right\} \tag{4.3}$$

$$\left.\begin{aligned}\sigma_w &= \sqrt{\overline{w'w'}} \\ \overline{w'w'} &= \frac{1}{m}\sum_{i=1}^{m}\left(w_i-\overline{W}\right)\left(w_i-\overline{W}\right)\end{aligned}\right\} \tag{4.4}$$

Turbulence intensity in the flow direction σ_u and vertical to the flow direction σ_w have been made non-dimensional by using shear velocity (U_*) such that $\sigma_u^+ = \sigma_u / U_*$ and $\sigma_w^+ = \sigma_w / U_*$. It is observed from Figure 4.7(a) and 4.7(c) that turbulent intensities are higher in section B, C, and D in comparison with section A, whereas non- dimensional turbulent intensities are lowest for section B (Figure 4.7(b) and4.7(d)). The decrease in non-dimensional turbulent intensities may be due to the contribution of high shear velocity (U_*) at the center of the pit (section B).

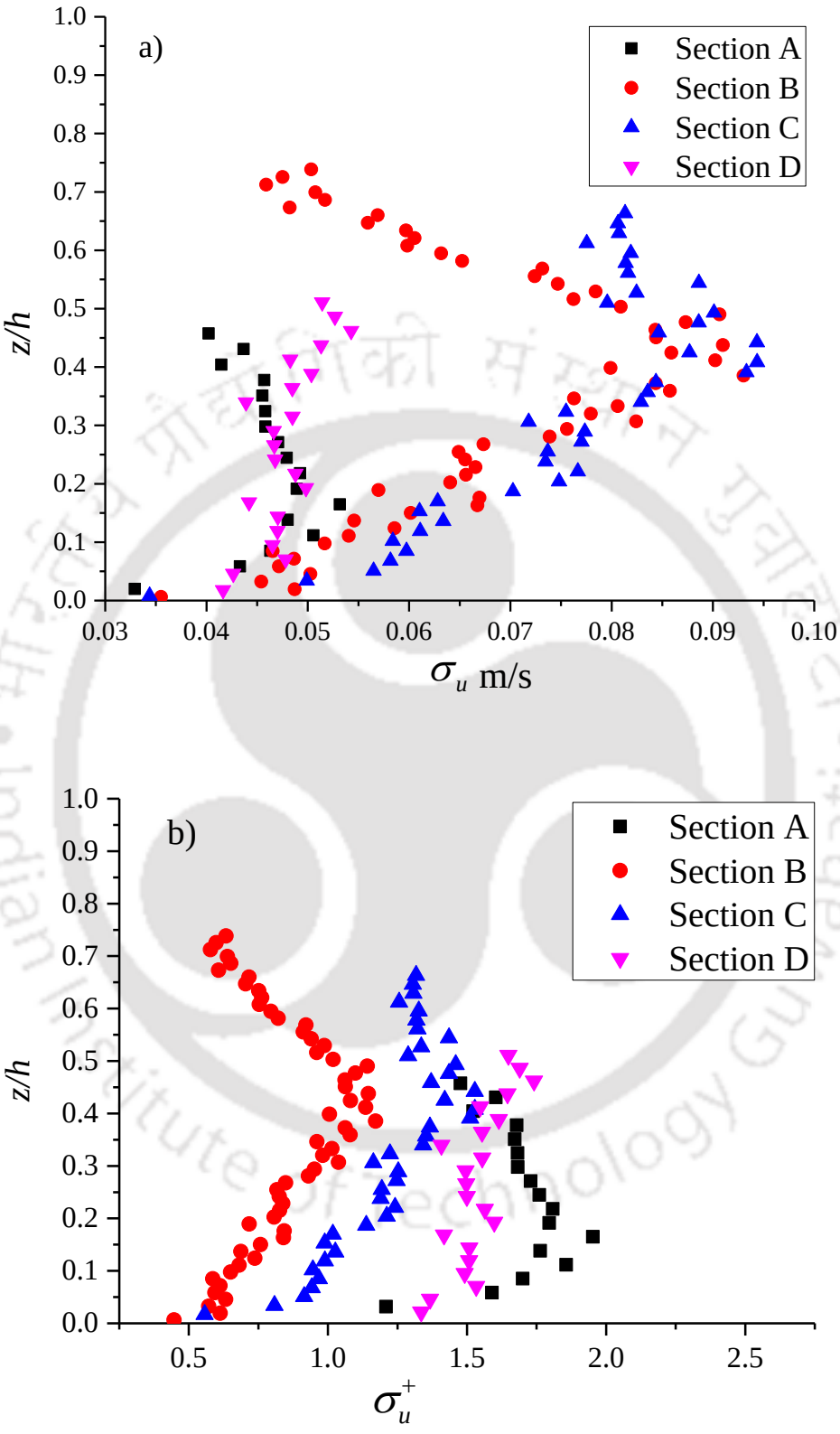

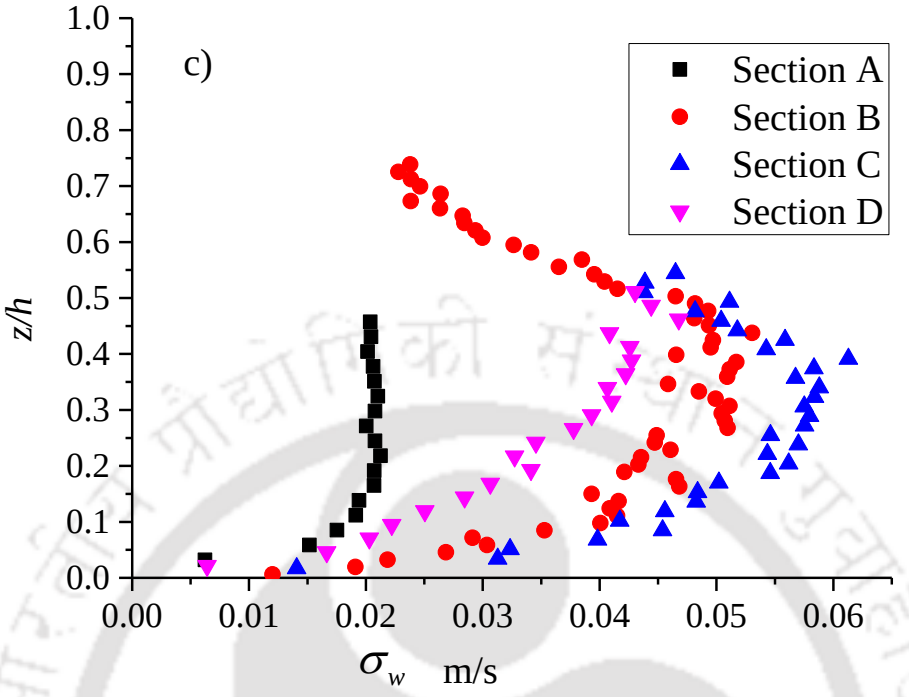

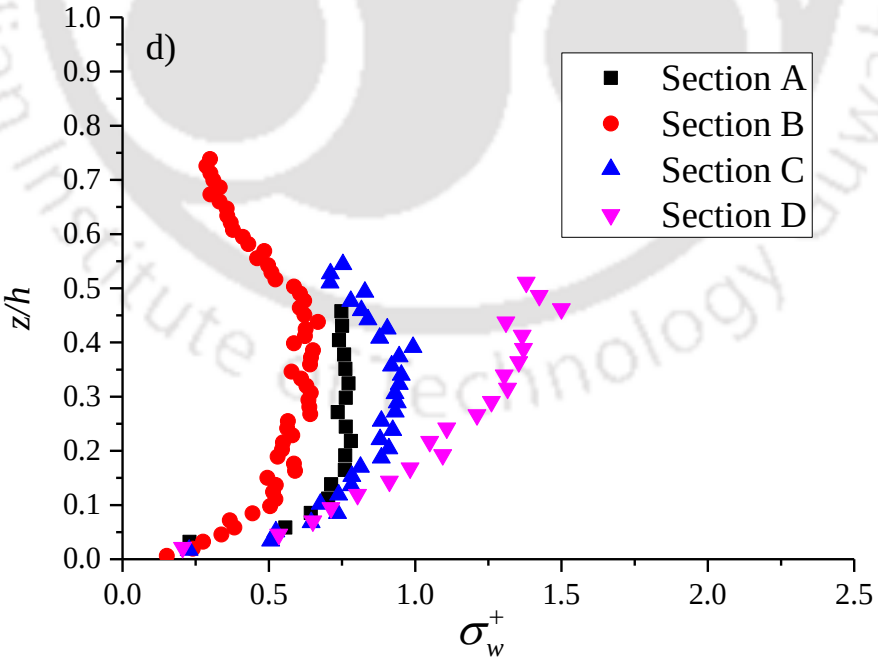

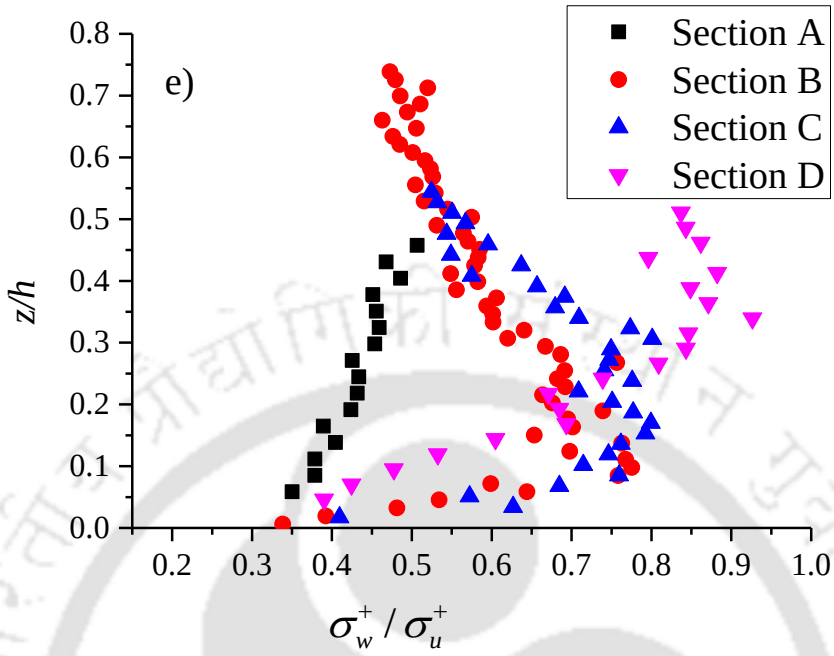

Figure 4.7: a) Vertical distribution of turbulent intensities in flow direction, b) vertical distribution of non-dimensional turbulent intensities in flow direction, c) turbulent intensities in vertical direction, d) non-dimensional turbulent intensities in vertical direction, e) flow anisotropy profile.

It is noticed that presence of mining pit increases near-bed stream wise and vertical turbulent intensities at section B, C, and D than the upstream section A. Table 4.2 shows the percentage increase in turbulent intensities of other section with respect to upstream section A at $z/h \sim 0.03$

. Table 4.2 Comparison of turbulent intensities in near-bed region ($z/h \sim 0.03$)

	Section B	Section C	Section D
σ_u	7.85%	4.44%	26.49%
σ_w	92.78%	125.87%	2.76%

Vertical distribution of the degree of anisotropy (σ_w^+ / σ_u^+) in Figure 4.7 (e) shows highly anisotropic nature of flow as $\sigma_w^+ / \sigma_u^+ < 1$. Nezu and Nakagawa (1993) predicted the ratio as a constant of 0.55 throughout the depth for a smooth boundary. In this present study, we observed that the ratio is varying with respect to flow depth at different sections. Near the boundary, ratio is approximately as 0.35, 0.34, 0.41, and o.39 at section A, B, C, and D respectively and varies linearly with flow depth. It is also noted that in the mining region and at the downstream of it, the ratio starts to decrease towards the free surface from $z/h \sim 0.2$ to 0.3.

4.2.4 Conditional statistics of Reynolds shear stress distribution

Detachment or movement of sediment particles due to turbulent flow can be explained by the occurrence of different bursting events. The sum of all bursting events at any point defines the total Reynolds shear stress at that point. Based on the relative sign of fluctuating component of instantaneous velocity u' and w', four different quadrants such as outward interaction $(i=1, u'>0, w'>0)$, ejections $(i=2, u'<0, w'>0)$, inward interaction $(i=3, u'<0, w'<0)$, and sweeps $(i=1, u'>0, w'<0)$ can be defined for understanding the different phenomenon of bursting events. Thus the various form of momentum transfer contributes to the total Reynolds shear stress and this contribution at any point can be calculated as:

$$\langle u'w' \rangle_{i,H} = \lim_{T \to \infty} \frac{1}{T} \int_0^T u'(t) w'(t) I_{i,H} \left[u'(t) w'(t) \right] dt \tag{4.5}$$

where T is the total sampling time, t is time and $I_{i,H}$ is the indicator function. Indicator function can be defined as:

$$I_{i,H} \left[u'(t) w'(t) \right] = \begin{cases} 1, \text{ if } (u'w') \text{ is in quadranti and if} \\ |u'w'| \geq H \left(\overline{u'^2} \right)^{0.5} \left(\overline{w'^2} \right)^{0.5} \\ 0, \text{ otherwise} \end{cases} \tag{4.6}$$

Here, parameter H is the hyperbolic hole region, which allows differentiating the larger contribution to total Reynolds shear stress by neglecting the smaller events. The hole region H can be determined by the curve $|u'w'| = H\left(\overline{u'^2}\right)^{0.5}\left(\overline{w'^2}\right)^{0.5}$ (Nezu and Nakagawa, 1993).

The stress function or the fractional contribution of the different bursting event to the total Reynolds stress can be defined as:

$$S_{i,H} = \frac{\langle u'w' \rangle_{i,H}}{\overline{u'w'}} \quad \text{and} \quad \sum_{i=1 \text{ to } 4} S_{i,H} = 1 \tag{4.7}$$

For outward and inward interaction $S_{i,H} < 0$, for ejection and sweep $S_{i,H} > 0$. Vertical distribution of $S_{i,H}$ considering all events at H=0 is shown in Figure 4.8 for four different sections.

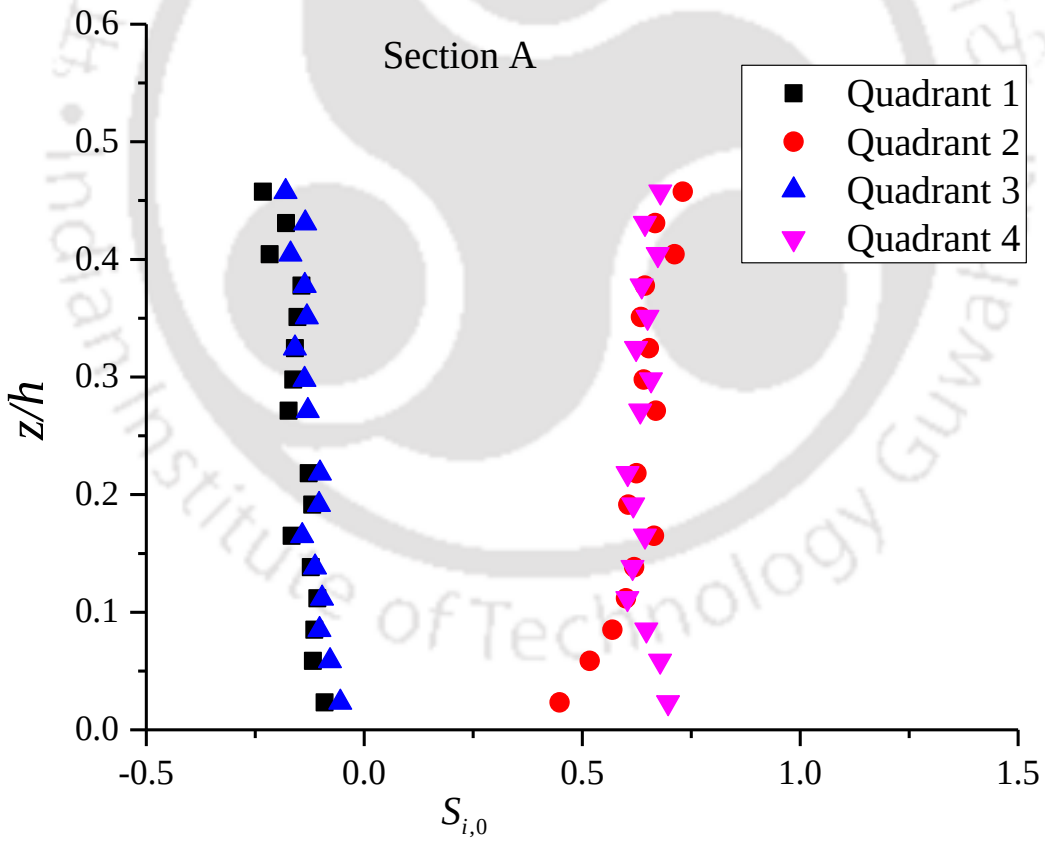

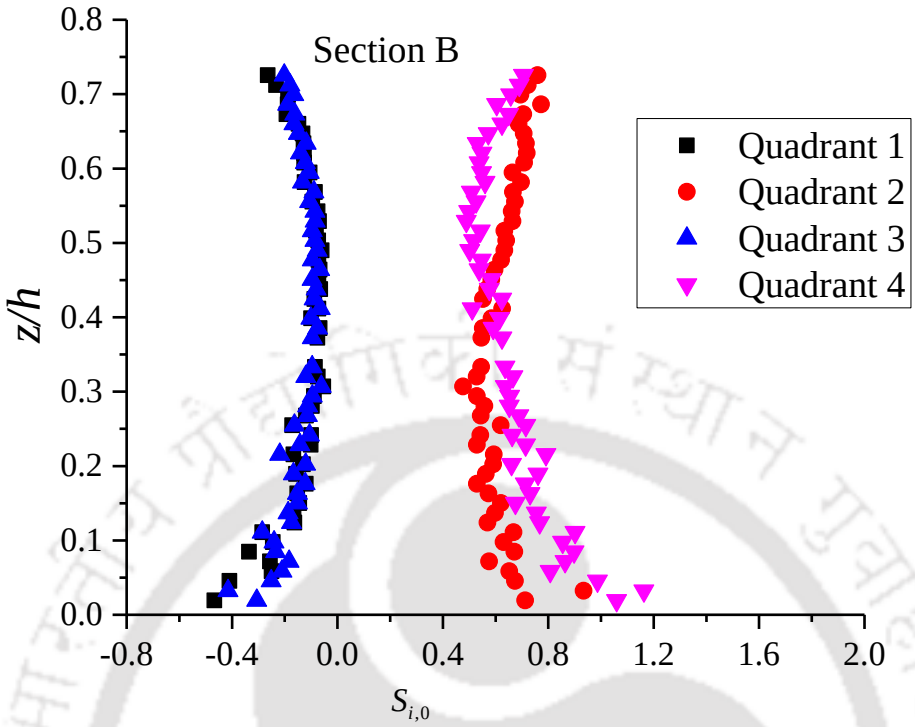

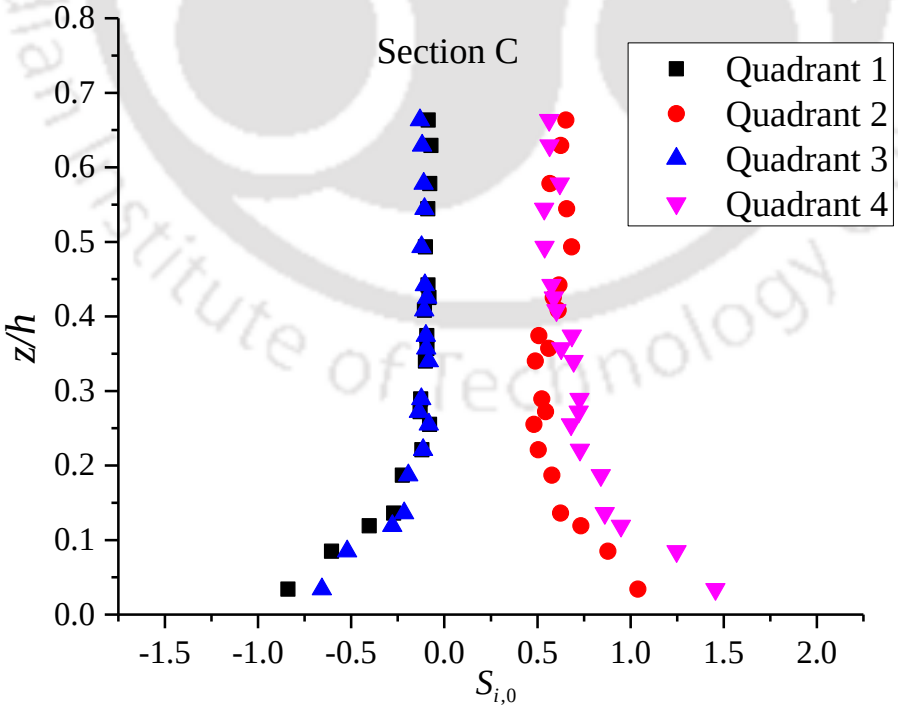

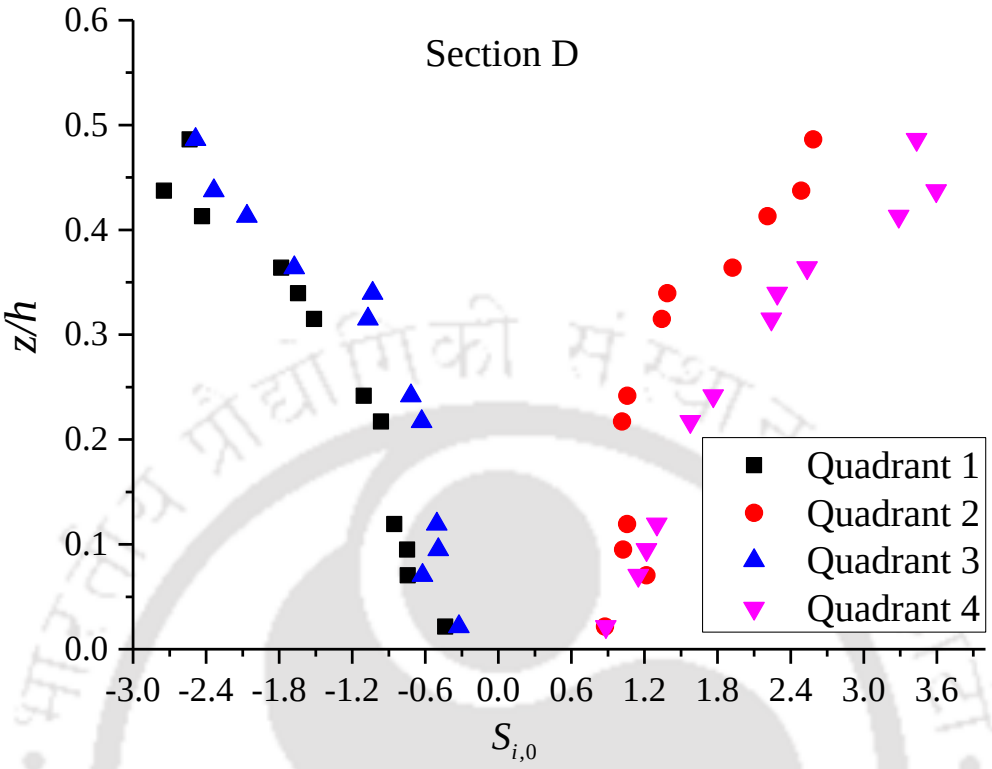

Figure 4.8: Vertical distribution of conditional Reynolds stress $S_{i,0}$ at H=0 for Section A, B, C, and D.

Stress function profile from Figure 4.8 shows that ejection and sweep events give maximum contribution to the total Reynolds stress rather than the outward and inward contribution at all four sections. At the upstream of the pit (section A) in the upper flow region, the contribution of ejection and sweep events are almost equal but in the near-bed region sweep event dominates the sediment transport mechanism over ejection till $z/h \sim 0.1$. The contribution of sweep and ejection in the near-bed region is about 69.7% and 45% respectively. In the mining pit region, contribution of sweep event is more prominent till $z/h \sim 0.4$ from the bed surface, and above that ejection dominates the flow. At the downstream of the pit (Section D), domination of sweep event over ejection is observed throughout the flow depth. The percentage contribution of all the events to the total Reynolds stress in the near-bed region ($z/h \sim 0.03$) of all the sections is tabulated in table 4.3. Contribution of sweep and ejection is positive, whereas outward and

inward interaction is negative. The total percentage contribution of all positive and negative events should be equal to 100 percent.

Table 4.3 Percentage contribution of all the events to the total Reynolds shear stress at near-bed region ($z/h \sim 0.03$)

Types of Events	Section A	Section B	Section C	Section D
Sweep (positive contribution)	69.7%	106%	145.5%	88.33%
Ejection (positive contribution)	45%	71%	104%	87.35%
Outward interaction (negative contribution)	9.08%	46.6%	83.9%	43.5%
Inward interaction (negative contribution)	5.5%	30.6%	65.7%	32.45%

Further analysis of these results shows that dominance of sweep event is maximum in the mining region (Section B and C) followed by the downstream section (Section D). The thickness of sweep dominance zone increases from $z/h \sim 0.1$ in section A to $z/h \sim 0.4$ in section B, C and further for the entire z/h in section D. The increase in contribution of sweep event and also the thickening of sweep dominant zone due to the presence of mining pit indicates increase in momentum exchange from the flow to the bed sediment particles, which subsequently increases the sediment transport at the downstream of the pit than the upstream.

The probability of occurrence of bursting events can be determined as follows (Cellino and Lemmin, 2004):

$$P_{i,H} = \frac{\int_{t=0}^{T} I_{i,H}\, dt}{\int_{t=0}^{T} \left[I_{1,H} + I_{2,H} + I_{3,H} + I_{4,H} \right] dt} \tag{4.8}$$

$I_{i,H}$ represents the indicator function as mentioned in Equation 4.6. Figure 4.9 shows the vertical profile of probability of occurrence of bursting events at Section A, B, C, and D, bearing all small events (H=0).

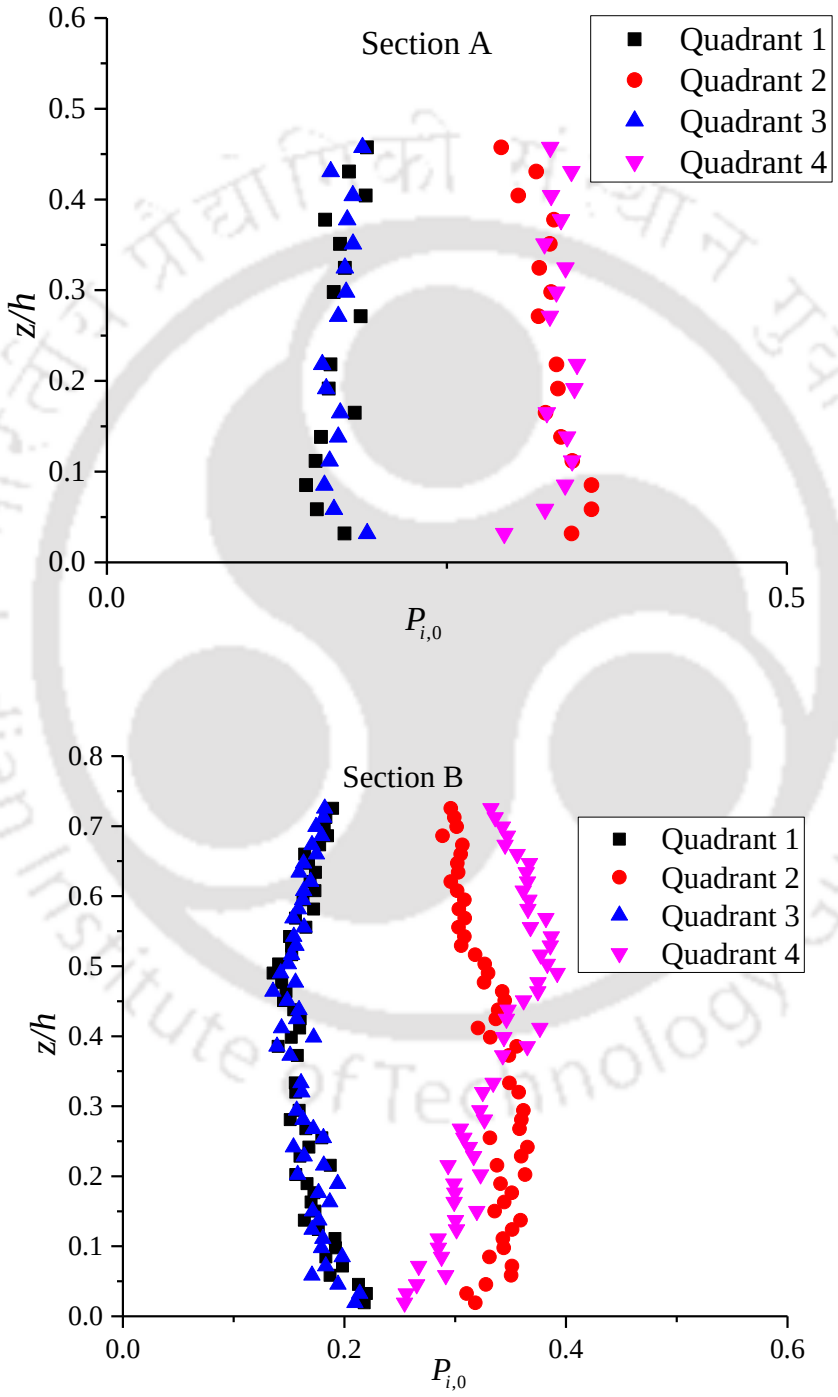

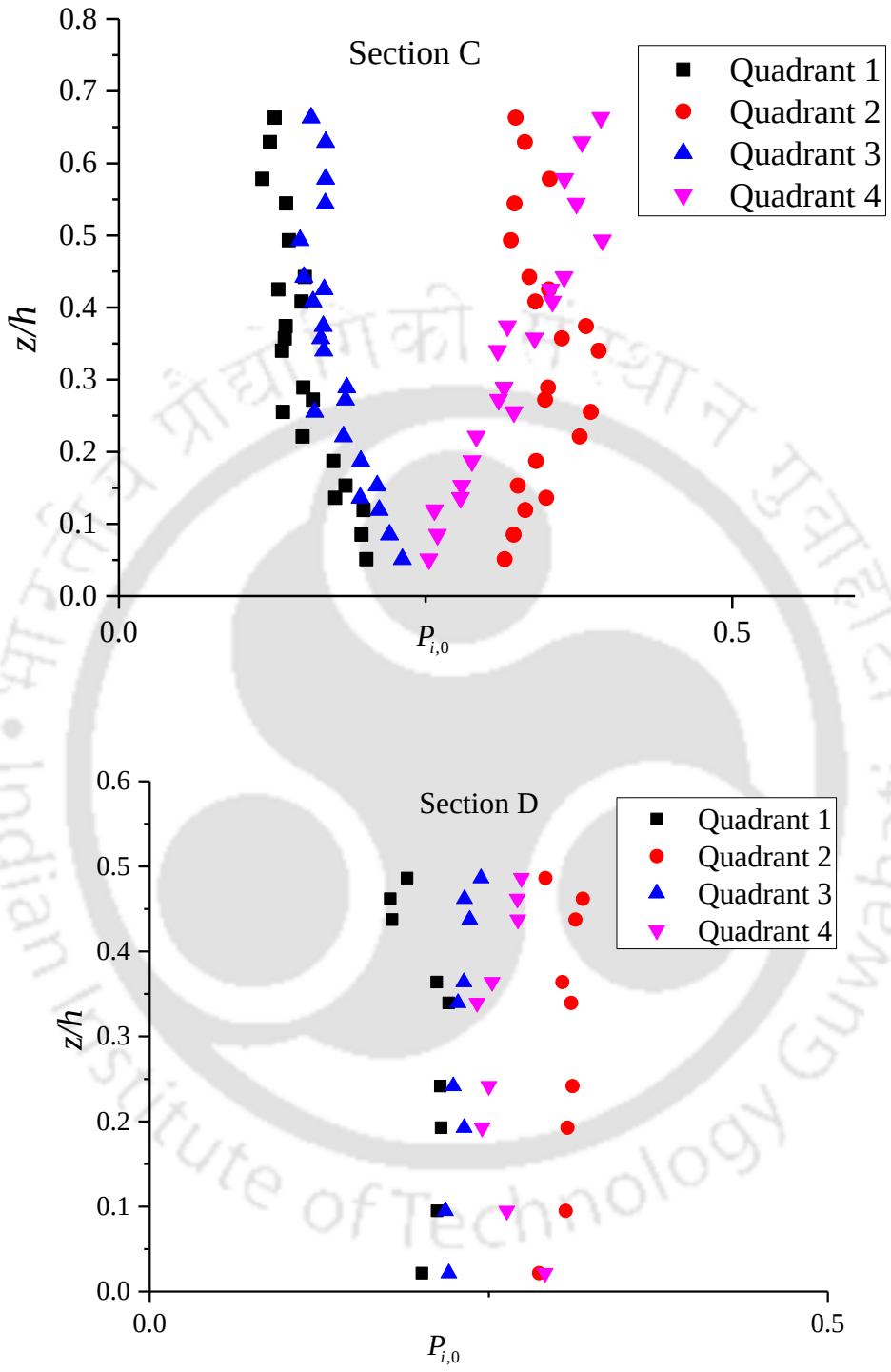

Figure 4.9: Vertical distribution of $P_{i,H}$ in flow at four different sections

Probabilities of outward and inward interaction are observed to be less than the ejection and sweep events in all the sections. It is also noticed from Figure 4.9 that probability of occurrence of ejection dominate over sweep in the near-bed region, while the contribution of sweep event to the total Reynolds shear stress is observed to be more significant in the near-bed region (Figure 4.8). It indicates that ejection event is more frequent, while sweep event is the strongest one.

4.3 Empirical Prediction of Bed Load Transport Rate in a Mined Alluvial Channel

Prediction of bed load in a channel with mining pit is important since mining pit acts as a sediment entrapper to the most of the sediment load coming from the upstream of the pit. This phenomenon leads to the passing of hungry water to the downstream and thus increases the sediment transport capacity at the downstream of the pit (Kondolf, 1997). Lee et al. (1993) formulated sediment supply rate from the upstream of the pit as a function of critical shear velocity and upstream shear velocity of the flow. An experimental study by Neyshabouri et al. (2002) also showed similar investigation as Lee et al. (1993). Prediction of bed load in a mining affected channel has not been done till date to the best of authors knowledge. Thus we have attempted to acquire an empirical fit for bed load transport rate by using hydraulic characteristics q, h, g; water and sediment properties $\rho, \rho_s, \nu, d_{50}$ as an independent variable. Here, q = flow discharge per unit width of the channel, h = average depth of flow, g = acceleration due to gravity, ρ and ρ_s are the density of water and bed material, d_{50} is the median particle diameter of bed material. Bed load discharge data for uniform sand with five different shape of pit are used to develop the equation. However, bed load discharge was not considered as a function of pit geometry. So we have obtained

$$Q_b = f\left(q, d_{50}, \rho, \rho_s, \nu\right) \tag{4.9}$$

where Q_b is the bed load discharge rate in kg/s. By making bed load discharge and flow rate dimensionless, we have

$$q_b = f\left(\frac{V - u_{*c}}{u_{*c}}\right) \tag{4.10}$$

where $q_b = \frac{Q_b}{(\rho_s - \rho) v d_{50}}$ is the dimensionless bed load transport rate, $V = q/h$ = average flow velocity, u_{*c} is the critical shear velocity of bed material. The final form of the equation from this analysis is as follows:

$$q_b = 1.873 e^{0.237 \frac{V - u_{*c}}{u_{*c}}} \tag{4.11}$$

Figure 4.10 shows the predicted bed load transport rate by Equation 4.11 with respect to the corresponding experimental values.

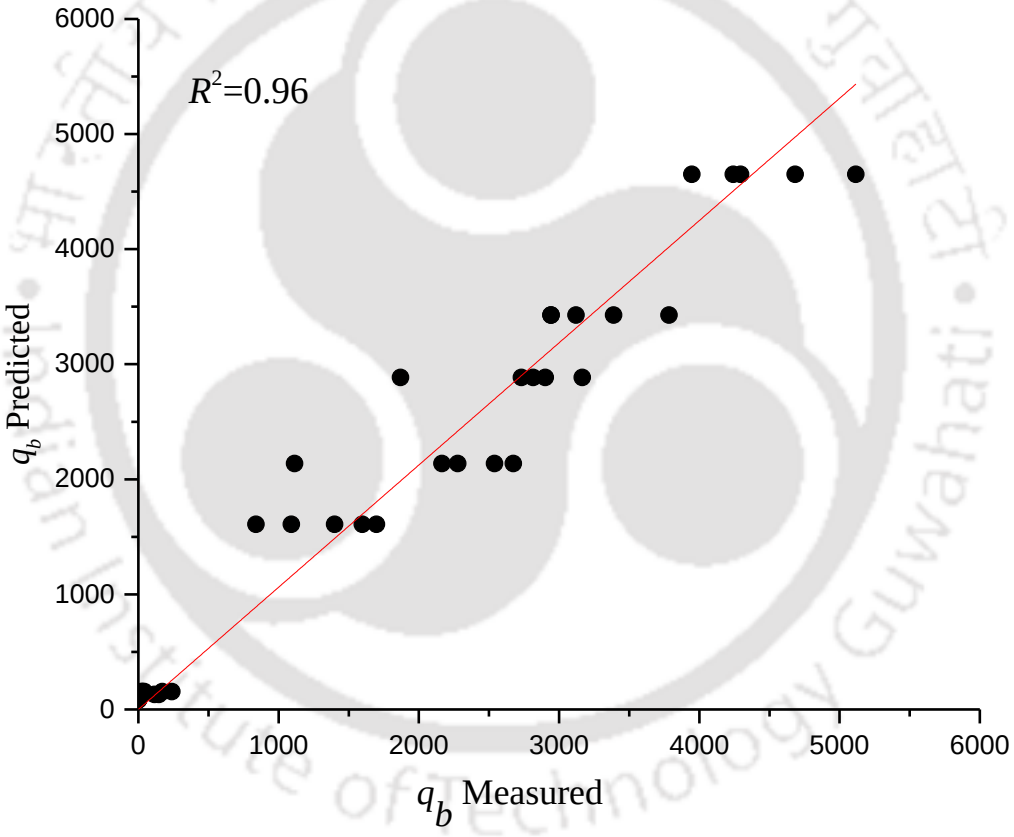

Figure 4.10: Predicted bed load transport rate

However, caution must be taken during the application of present derived bed load equation to the field. The inherent assumptions while developing the equation are: bed particles composed of

uniform sizes and sediment mining pits are regular. Here, more observations on field and flume are required to generalize the presently developed equation.

4.4 Comparison of the Non-Dimensional Sediment Transport Parameter between Channel having Mining Pit and Plain Bed Channel

The erosion of channel bed is caused by the intense sediment transport. It is also found in previous sections that change in flow characteristics in the pit region lead to the inflation of shear stress in the pit and downstream of it. Therefore, the sediment transport rate may be different for the channel with mining pit as compared to the plain bed. Here, we have compared the non-dimensional sediment transport rate for the channel having mining pit with the plain bed experiment for the same discharge. The bar chart showing the non-dimensional sediment transport parameter for channel having five different shape of mining pit with five different discharges is presented in Figure 4.11.

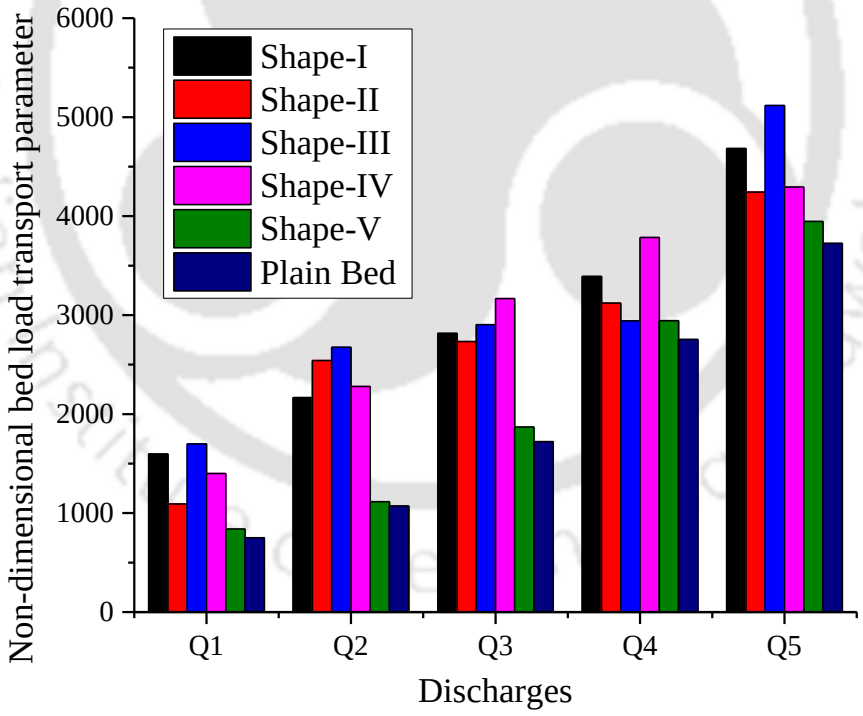

Figure 4.11 Comparison of the non-dimensional sediment transport parameter for channel having pit with the plain bed channel (Set-II)

From Figure 4.11 it is observed that non-dimensional sediment transport parameter is higher for all experiments as compared to the plain bed experiment, which indicates a higher rate of sediment transport due to the presence of in-stream mining pit.

Increased erosion in the upstream of mining pit can affect the river environment at the downstream as the increased sediment load propagates downstream through the river network. In-stream mining directly alters the channel geometry and bed elevation as shown in the present experimental work. It has been observed that turbulence plays an important role in sediment transport and significantly affects the processes, which governs morphological changes in terms of erosion and deposition of sediment particles. Present work gives insights of such processes and put forth an empirical model for assessing bed load in the mining affected channel. Understanding sediment transport in different scenarios finds many real applications such as prediction of the effects of land use or flow regime change and channel restoration efforts (Wilcock, 2001). The relationship between discharge and bed load transport rate in a mined channel is critical to assess the morphological effect on different protection and restoration efforts. However, bed load transport is not simple to measure or predict owing to its variability on both spatially and temporally. Presently developed bed load transport equation is very nascent in nature, which can be strengthened by employing more field and flume observations.

4.5 Conclusions

The geomorphic behaviour of channel bed under the influence of mining has been explained by using various turbulent structures, such as vertical distribution of velocity profile, von Karman constant, virtual bed level, zero velocity level, Reynolds shear stress, turbulence intensity, anisotropy and conditional Reynolds shear stress or different bursting events of the flow. Velocity profile at the center of the mining pit shows negative velocity layer at the bottom of the pit. At the upstream and downstream of mining pit, velocity profile follows the logarithmic law in the inner zone of flow. The flow velocity starts to drop once it reaches the higher depth region of the mining pit and recirculation zone at the centre of the pit occurs. Velocity profile at the downstream edge of the pit also does not follow the logarithmic law in the inner zone of the flow, which may be due to the higher flow depth and adverse slope at the immediate upstream of the section. The reduction of velocity in the mining region leads to the formation of shear layer along the depth of the mining pit.

The occurrence of maximum Reynolds shear stress is observed at $0.35 \geq z/h \geq 0.45$ in the mining region, rather than $z/h \sim 0.2$ at upstream. Also, the location of maximum RSS increases from $z/h \sim 0.2$ at the upstream to $z/h \sim 0.4$ at the downstream of the pit. Maximum value of RSS is observed at the centre of the pit, which is about 2.9 times of upstream RSS followed by 2.3 times at the downstream edge of the pit. Presence of mining pit also increases the RSS by 14.5 % from upstream of the pit (Section A) to the downstream of it (Section D). Turbulent intensities are also calculated for each section and observed an increase in near-bed turbulent intensities in the mining pit and downstream of it as compared to the upstream. The percentage increase in near-bed stream wise and vertical turbulent intensities at section B, C, and D as compared to the upstream section A are 7.85%, 4.44%, 26.49% and 92.78%, 125.87%, 2.76% respectively. The degree of anisotropy also shows highly anisotropic flow in all the four sections, which is approximately 0.35, 0.34, 0.41, and 0.39 at section A, B, C and D respectively.

The turbulent bursting phenomenon or the contribution of velocity fluctuation to the total Reynolds shear stress is studied by quadrant analysis. Dominance of sweep in the near-bed region is evident in all the sections. An increase in dominance of sweep event in the near-bed region is observed in Section B, C, and D than the upstream of the pit. This high speed fluid parcel is sufficient to increase the sediment transport in the downstream of the pit. This result on turbulent parameters gives us a deep insight of the change in flow characteristics in the mining and downstream of the mining zone. It shows deposition of sediment particles transported from the upstream along the upstream edge of the pit due to the sudden decrease in velocity in the pit region and thus migration of upstream edge occurs. Again increase in momentum transfer between flow and bed sediment in the mining pit and downstream of it increases the erosion, which leads to the lowering of downstream bed elevation. The proposed equation for bed load transport is purely empirical in nature based on two different size of uniform sand. In-stream mining pit also causes change in the sediment transport properties of the channel. The changes in bed load transport characteristics for channel having pit has been compared with the plain bed experiment for the same hydraulic conditions. We have observed minimum 4% to maximum 50% increase in non- dimensional bed load transport parameter for the channel having mining pit as compared to that of plain bed experiments.

5 Migration of Mining Pit and Multi-Scale Characterization of Migration Speed

5.1 Introduction

Sediment transport leads to the change in morphology of the alluvial channel. The disturbance caused by the mining pit modifies the flow pattern in the pit region and causes increase in shear stress in the pit and the downstream of it. The increased shear stress dislodges the bed material and causes scouring of the bed at the downstream. The sediment transported from the upstream of the pit region gets deposited along the upstream edge of the pit due to the sudden increase in flow depth and the reversal velocity at the bottom of the pit, and thus the migration of the pit occurs (Alfrink and van Rijn, 1983). Migration of pit is one major concern in case of sand mining. It can damage the downstream structure by scouring the bed level. Lee et al. (1993) investigated migration of rectangular mining pit from experimental data. They conducted experiments by constructing a rectangular pit across the whole width of the channel on uniform sand bed. Various functional relationships and regression equation to determine the scour depth and the shape of channel bed profile were developed by Lee et al. (1993) in their study. Gill (1994) developed mathematical model to simulate mining pit migration. Partial filling and downstream propagation of the pit was observed by Gill (1994) from his model. Neyshabouri et al. (2002) conducted experimental investigation to study mining pit migration of rectangular pit. These authors used different length by width ratio of rectangular pit for a constant discharge and observed that width was more influencing than the length. Neyshabouri et al. (2002) also postulated empirical formulation to determine migration speed of the pit with respect to different length by width ratio.

Sediment mining is observed to be an external disturbance to a stable section of a river, which changes the hydrodynamic and sediment transport conditions throughout the channel. A stable section is generally assumed to be in equilibrium. As per Lane's hypothesis $Q_s d_{50} \sim QS_b$, where Q_s is the quantity of sediment, d_{50} is the sediment size in terms of diameter, Q is the discharge of water, and S_b is the bed slope (Lane, 1955). Disturbance to the any one of these parameters causes changes to the others and equilibrium condition gets disturbed. Bed load is the major portion of sediment load in most of the river. So, if bed material is extracted and sediment supply

is less than the extraction of sediment in the river, sediment movement will occur and the morphological features of alluvial river will get affected (Yue et al., 2014). Sediment mining also creates an active zone for sediment transport by disturbing the bed and also increases the interaction between the flow and channel bed (Cao and Pender, 2004). Since mining from channel bed enhances the interaction between flow and sediment, and increases sediment transport of the channel, there is a need to study the sediment transport characteristics of mining induced alluvial channel.

Determination of spatial and temporal variation of mining pit is important to regulate the in-stream mining operation. The migration speed of mining pit or the speed at which the original dry bed pit filled up can become an important measure for quantitative analysis of sustainable mining operation. The dynamic nature of scouring process signifies the scale dependent celerity of mining pit. Singh et al. (2011) did thorough investigation of the dynamics of bed form celerity by using multi-scale statistical analysis. The scouring of channel bed and migration of pit shows significant variability over the range of various time and length scale. This phenomenon can be captured by using multi-scale statistical analysis. Hence, the primary aim of this chapter is to investigate the characteristics of mining pit migration or celerity from both physical and statistical analysis. In this research, the characteristic of migration speed of the upstream edge of the pit until it reaches the initial downstream edge has been investigated in terms of scale dependent celerity of mining pit. Based on the experimental data we have also formulated an empirical function to find the mining pit migration speed. Earlier experimental studies conducted by Lee et al. (1993), Neyshabouri et al. (2002) was based on rectangular mining pit; however the pit geometry won't be rectangular in actual situation. The pit formed on the river bed can have various irregular shapes. In this research we have performed our analysis for the trapezoidal shaped mining pit with a side slope of approximately equal to the dry angle of repose of bed materials and for an irregular pattered pit with vertical sides (Shape-II, Shape-III, and Shape-IV). In the later part of the chapter analysis has been done for rectangular mining pit (Shape-I).

5.2 Theoretical Backgrounds

Celerity or migration speed of mining pit can be analyzed by using multi-scale statistical approach. For statistical analysis of mining pit celerity, wavelet based two points cross

correlation method has been implemented. The theoretical backgrounds for calculating scale dependent celerity are explained in the following sections.

5.2.1 Spectral analysis

The power spectral density (PSD) of a signal $x(t)$ can be hypothesized based on Fourier transformation. The characteristics of *x* over the time *t* can be visualized from the PSD of signal $x(t)$. The PSD can be defined as the average of the Fourier transform magnitude squared, over a large time interval:

$$S_x(f) = \lim_{T\to\infty} E\left\{\frac{1}{2T}\left|\int_{-T}^{T} x(t)e^{-j2\pi ft}dt\right|^2\right\} \quad (5.1)$$

It can also be termed as the Fourier transform of the auto-correlation function.

$$S_x(f) = \int_{-T}^{T} R_x(\tau)e^{-j2\pi ft}dt \quad (5.2)$$

Where, τ and $R_x(\tau)$ are the time lag and the auto-correlation function respectively. Auto-correlation function can be defined as:

$$R_x(\tau) = E\{x(t)x^*(t+\tau)\} \quad (5.3)$$

Signal $x(t)$ in Equation 5.1 is a function of time. $x(t)$ can also be explained for the spatial data series. In that case the frequency will be replaced by the wave number. The wave number ω can be written as:

$$\omega = \frac{2\pi K}{N\Delta x} \quad (5.4)$$

where N represent the total number of samples in the data series, $\Delta x = 1.2$ cm is the sampling interval and *K* is an index.

5.2.2 Wavelet transformation

A signal with greater variability and frequency that changes with time is preferable to analyze by using wavelet transformation.

If $f(t)$ is a signal, then wavelet transformation of the signal is the integral transform with a series of functions $\psi_{a,b}(t)$, that is,

$$W_f(a,b) = \int_{-\infty}^{+\infty} \psi_{a,b}(t) f(t)\, dt \tag{5.5}$$

Here, the function $\psi_{a,b}(t)$ is the wavelets. A mother wavelet $\psi(t)$ by can be used to obtain $\psi_{a,b}(t)$ by scaling and translation.

$$\psi_{a,b}(t) = \frac{1}{\sqrt{a}} \psi\left(\frac{t-b}{a}\right) \tag{5.6}$$

where a, b and $1/\sqrt{a}$ are the scaling parameter, location parameter and normalizing factor respectively (Kumar and Foufoula-Georgiou, 1997; Mallat, 1998). For invertible wavelet transformation, the area under the curve should be zero, that is,

$$\int_{-\infty}^{+\infty} \psi(t)\, dt = \psi(0) = 0 \tag{5.7}$$

Equation 5.8 shows the wavelet with higher order vanishing moments.

$$\int_{-\infty}^{+\infty} t^k \psi(t)\, dt = \psi(0) = 0 \tag{5.8}$$

Where k=0, 1, 2, ….., (M-1),… ∞

Polynomial trends of a signal can be removed by using wavelets with higher order vanishing moments. A wavelet with M vanishing moments can eliminate a polynomial trend of order (M-1). Linear trend can be removed by using second order differencing filter. A mother wavelet is basically a family of Gaussian based wavelets. It can be defined by the M^{th} order derivative of a Gaussian function $g_0(t)$, that is, $g_M(t) = \left(d^M / dt^M\right) g_0(t)$, ($M$=1,2,….), where M is the order of the derivative. In present study we have used Mexican hat wavelet, which is a second order differencing filter. It removes the linear trend from the bed elevation series. The Mexican wavelet gives improved estimate of the variance pertaining to smaller events for given frequency

compared to other approaches (Singh et al., 2011). Mexican hat wavelet $g_2(t)$ can be represented as

$$g_2(t) = (2/\sqrt{3})(\pi)^{-1/4}(1-t^2)e^{-(t^2/2)} \tag{5.9}$$

In this present study we have a spatial dataset. So the spatial data set has to be discretized into a range of length scales. The wavelet coefficients for data series $f(x)$ at a location b and scale a can be written as:

$$WC_f(a,b) = \frac{1}{\sqrt{a}}\int_R g_2\left(\frac{x-b}{a}\right) f(x)\,dx \tag{5.10}$$

5.2.3 Length scale dependent celerity

The scale dependent celerity can be quantified by decomposing the original signal into the wavelet coefficients. The wavelet cross covariance between these two signals, namely $f_1(x)$ and $f_2(x)$ can be calculated as

$$WCC_{f_1 f_2}(a,\Delta x) = \int_{-\infty}^{+\infty} W_{f1}(a,b)W_{f2}(a,b+\Delta x)\,db \tag{5.11}$$

where $W_{f1}(a,b)$ and $W_{f2}(a,b+\Delta x)$ are the wavelet coefficients of $f_1(x)$ and $f_2(x)$ respectively at scale a and two adjacent locations b and $b+\Delta x$ respectively. To determine celerity at each particular scale, we have to compute the lag corresponding to the maximum correlation coefficient between the two wavelet coefficients of the bed elevation series. Subsequently, the length scale dependent celerity can be obtained by dividing the lag by the time interval between the two consecutive data series.

5.3 Analysis for Shape-II, Shape-III and Shape-IV

The celerity or the migration speed of mining pit for Shape-II, Shape-III, and Shape-IV for Set-III has been investigated by using both physical characteristics and multi-scale statistical approach.

5.3.1 Physical characteristics of mining pit migration

Morphological changes were tracked by using the URS and shifting of upstream edge was recorded at every 30 minutes. Longitudinal displacement of upstream boundary till the filled up of the pit with respect to time has been plotted for each shape of mining pit for V1 and V5 as shown in Figure 5.1. It shows similar trend for each set and the slope of the line increases from Shape-II to Shape-IV, that is, migration speed of upstream edge increases with increase in bank value. Experimental results from Neyshabouri et al. (2002) showed increase in pit migration with increase in length by width ratio of mining pit. By comparing the trapezoidal pit (Shape-II and Shape-III) with length by width ratio 0.82 and 1.025 respectively, we have observed the similar trend as that of Neyshabouri et al. (2002). Mining pit with irregular geometry has variable width as shown in Figure 2.16 and we observed maximum migration speed in this case. While comparing the migration speed with volume of extraction, it is observed that migration speed is more sensitive to the pit geometry than the volume of extraction.

A)

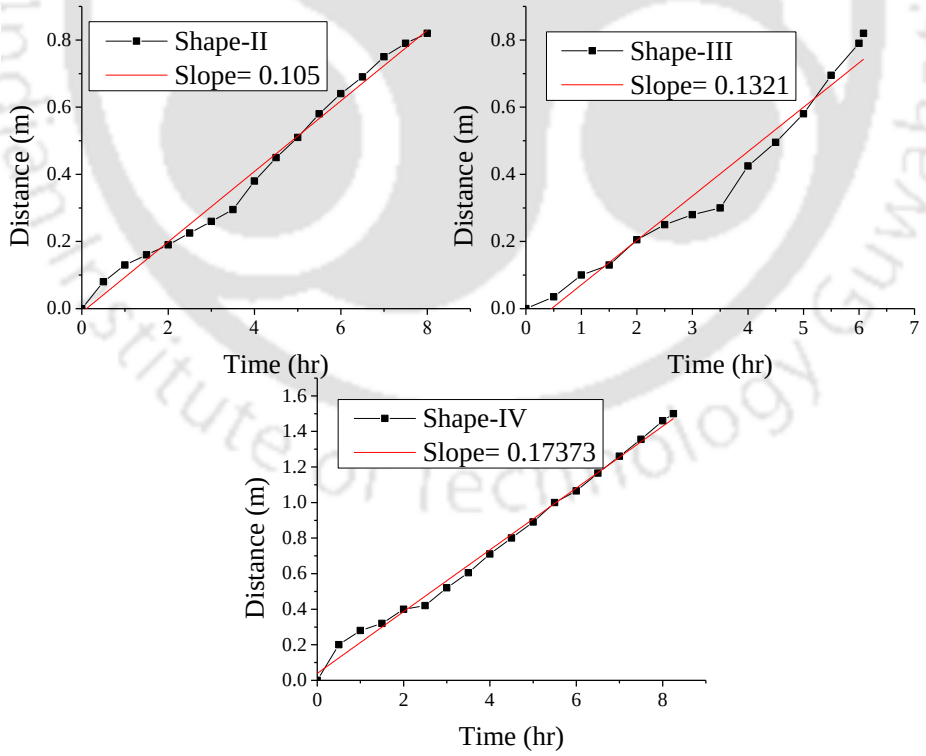

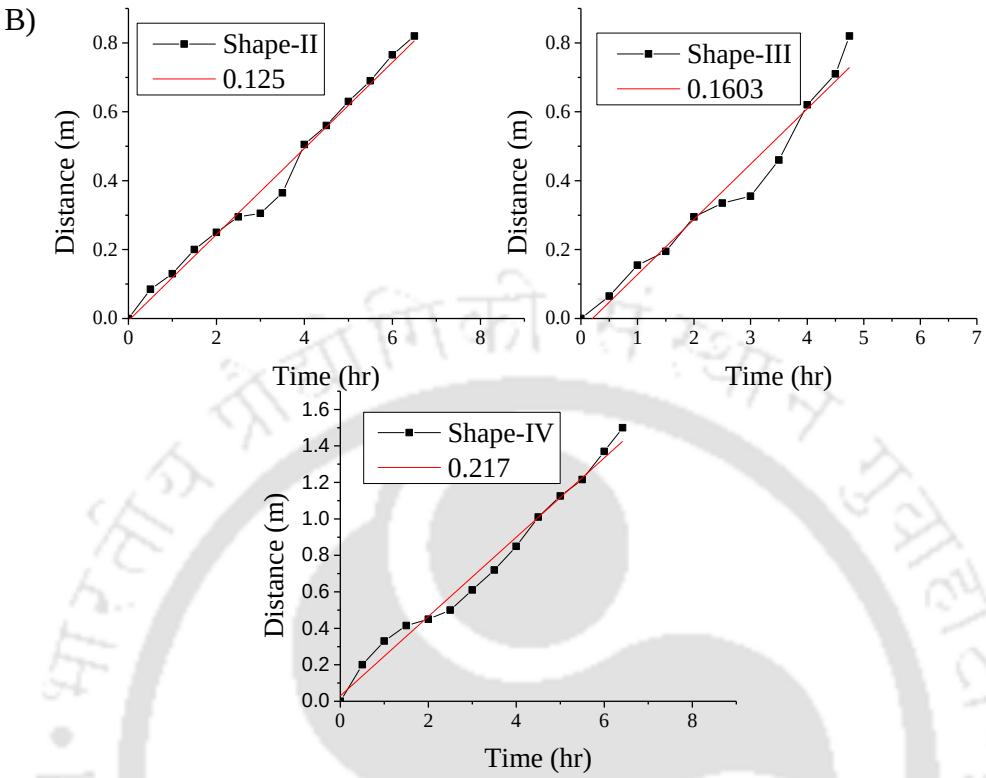

Figure 5.1 Longitudinal displacement of upstream boundary with respect to time for A) V1 and B) V5

Shape-II is having highest volume of extraction and the lowest migration speed as compare to the other two sets. While comparing Shape-III and Shape-IV, higher migration speed is observed in Shape-IV with higher value of volume of extraction. This higher value of migration speed in Shape-IV may be due to the irregular pit geometry with length by width ratio almost 2.44 times of the L/B ratio of Shape-III. Mining pit also leads to the erosion of the bank and the greater bank value for Shape-IV allows the bank particle to get deposited in the pit, thus filing up the pit in a faster rate. The average migration speed of upstream edge at various discharges is plotted for three Shapes as shown in Figure 5.2. An increase in migration speed with increase in length by width ratio is observed for each discharge. It indicates the influence of length by width ratio of mining pit on the migration speed. The empirical formulation developed by Neyshabouri et al. (2002) for migration of mining pit was based on only the length and width of the pit since they

had conducted the experiment for a constant discharge. However, migration of mining pit also depends on the flow characteristics.

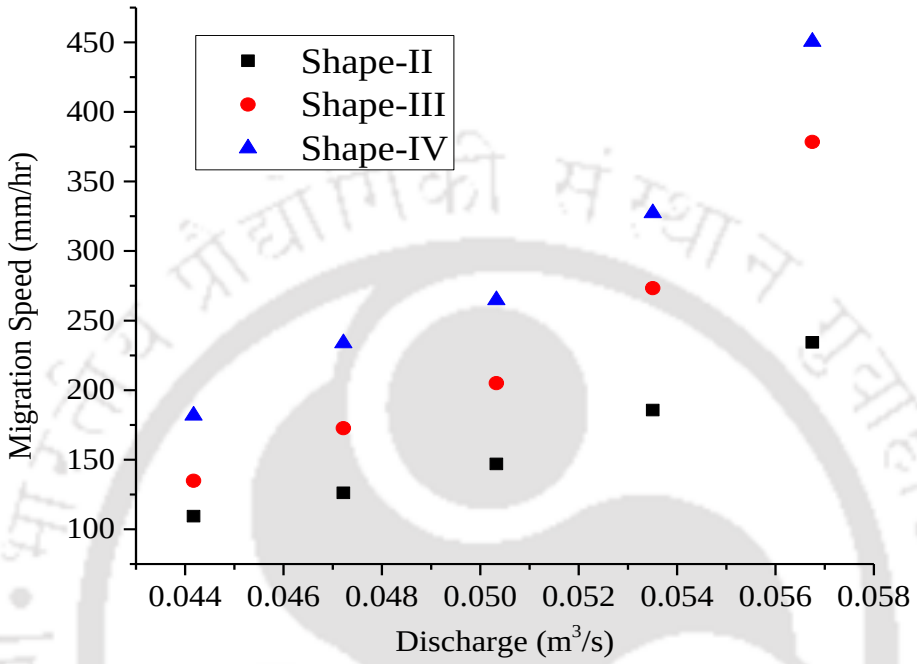

Figure 5.2 Average migration speed of upstream edge of the pit at each discharge for all three shapes

An empirical formulation has been developed to determine the migration speed of the upstream edge till the downstream. The functional form of the pit migration speed U_p can be assumed as follows:

$$U_p = f\left(\text{pit properties, flow properties, fluid properties, sediment properties}\right) \quad (5.12)$$

where pit properties includes length (L), maximum width (B) and depth of the mining pit (y); flow properties includes the average cross-sectional flow velocity $V = q/h$, q is the discharge per unit width of the channel and h is the depth of flow; fluid and sediment characteristics are the density of water (ρ), density of bed material (ρ_s), kinematic viscosity of water (υ), median

grain diameter (d_{50}), geometric standard deviation of bed material (σ_g). The grain parameter is combined in terms of critical shear velocity (u_{*c}) for representative grain diameter d_{50} of the bed material by neglecting the standard deviation σ_g (Mohtar et al., 2016). ρ, ρ_s, υ are kept constant during the experiment; hence these parameters can be neglected. In present work we have considered different geometric shaped pit with constant depth of pit for various discharge and flow depth. Therefore, the depth of pit can be omitted from the equation. By using dimensionless analysis Equation 5.12 can be written as

$$\frac{U_p}{u_{*c}} = f\left(\frac{V}{u_{*c}}, \frac{L}{B}\right) \tag{5.13}$$

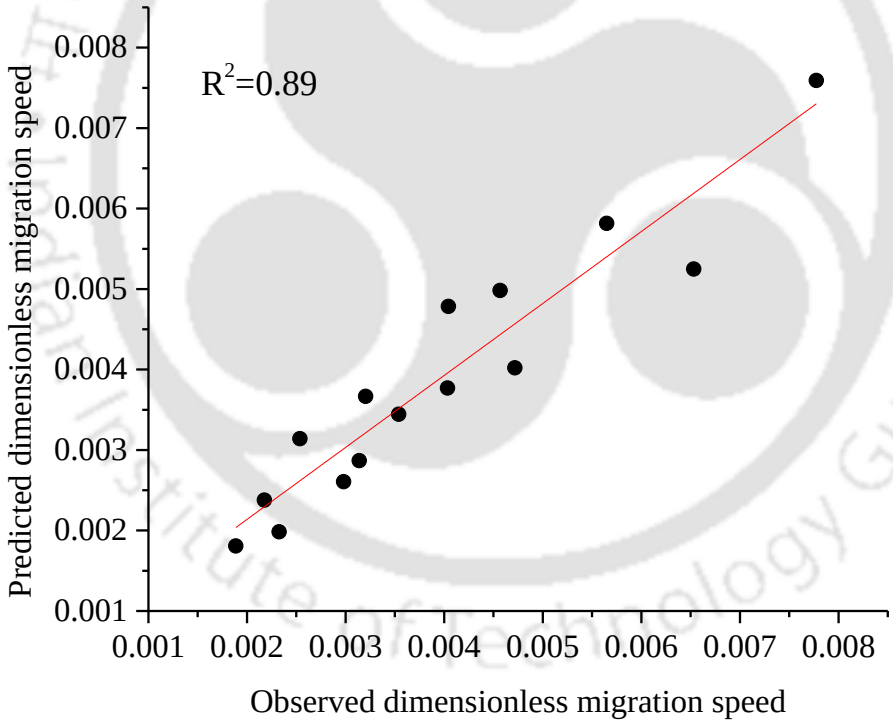

Figure 5.3 Predicted non-dimensional migration speed of mining pit

The final consolidated form of empirical formulation for the migration speed of mining pit is as follows:

$$\frac{U_p}{u_{*c}} = 0.22 \times 10^{-12} \left(\frac{V}{u_{*c}} \right)^{6.89} \left(\frac{L}{B} \right)^{0.414} \tag{5.14}$$

Predicted dimensionless migration speed and corresponding experimental values are plotted in Figure 5.3. This empirical formulation can be used to determine the migration of upstream edge of the pit and simultaneously to calculate the time required for complete filling up of the pit.

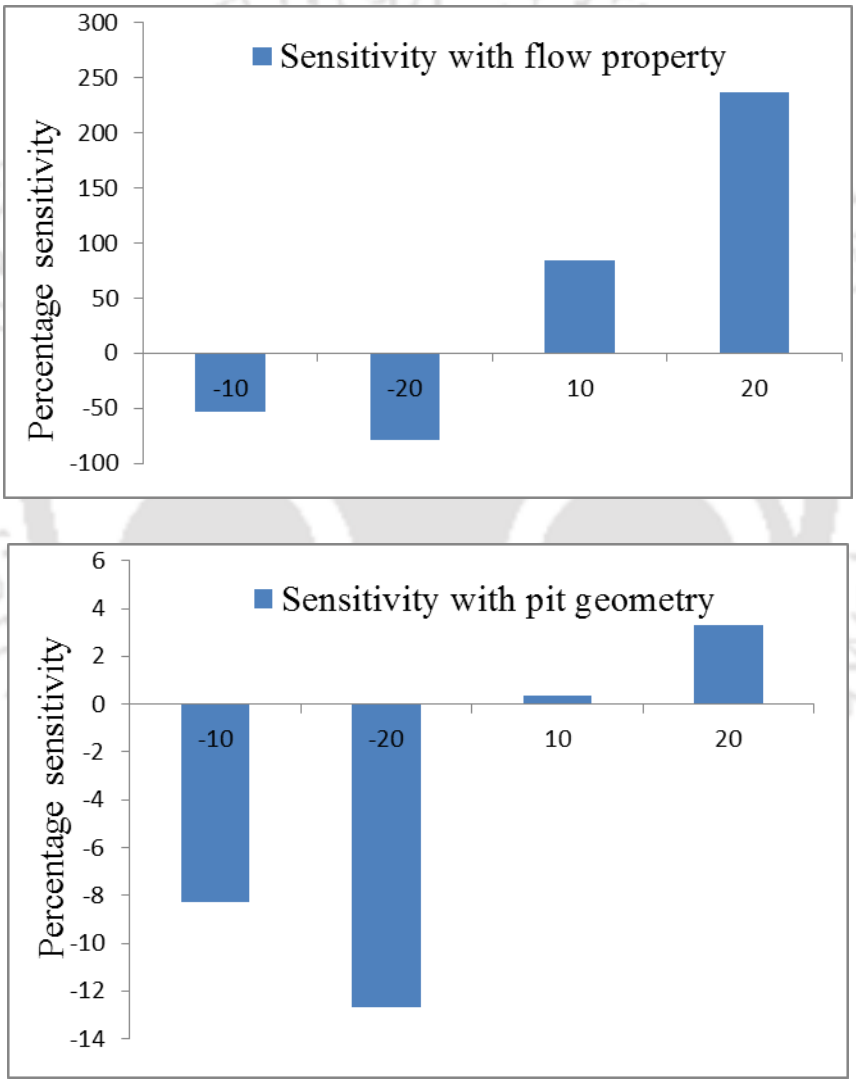

Figure 5.4 Sensitivity of pit migration with two independent parameters

From Equation 5.14, it is observed that flow properties (V/u_{*c}) and pit geometry (L/B) are two independent properties. The sensitivity of pit migration speed with respect to these two properties has been checked and presented in Figure 5.4. It is observed form the sensitivity analysis that pit migration speed is highly sensitive to the flow properties and less sensitive to the pit geometry.

The newly derived formula incorporates flow properties and pit geometry. Therefore, it can be applied for varying discharges as well as pit geometries. It also uses the pit geometry for the irregular-shaped pit by considering the maximum extents of the longitudinal and lateral disturbances, which gives a better justification for the application of the currently derived equation for a real problem, where finding the actual shape of the pit may not be possible. The transported sediment gets deposited along the upstream edge of the pit and causes filling of the original pit with time. Once the migration rate is calculated, the time required for filling of the pit can be determined using L/U_p with an assumption of a uniform infilling rate throughout the pit length. The knowledge of the infilling rate also will help in determining the potential mining site and the mining interval. However, more experimental and field observations are necessary for real field application of the equation.

5.3.2 Multi-scale statistical analysis of mining pit migration

Migration of mining pit occurs over the range of spatial and temporal time scale. The high resolution bed profile data collected from URS have enabled us to track the changes of mining pit along and across the channel with time. The transported sediment from upstream of the pit gets deposited at the pit along the upstream edge and the edge migrates towards the downstream. This migration phenomenon can be captured by using multi-scale statistical analysis in terms of celerity of mining pit. Here, we have calculated the celerity between the initial bed profile and the profile when upstream edge reaches the initial downstream edge of the pit. The bed profiles were considered along the centerline of the channel. The scale dependent celerity of mining pit is computed within the length scale of 150 mm to 300 mm. These scales are arbitrarily chosen from the scaling range of power spectral density as shown in Figure 5.5 (Singh et al., 2011). Figure 5.5 shows a scaling range (log-Log linearity) of approximately 25 mm to 330 mm for all three shapes with discharge Q1.

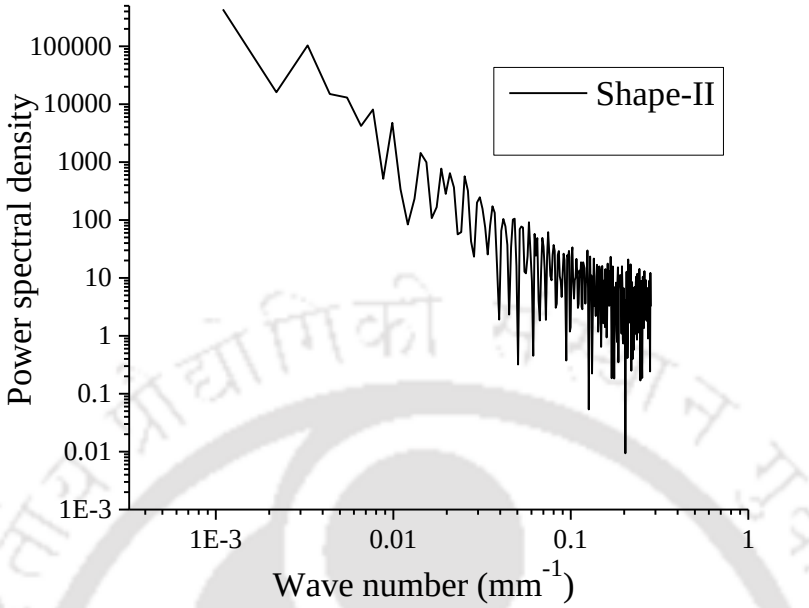

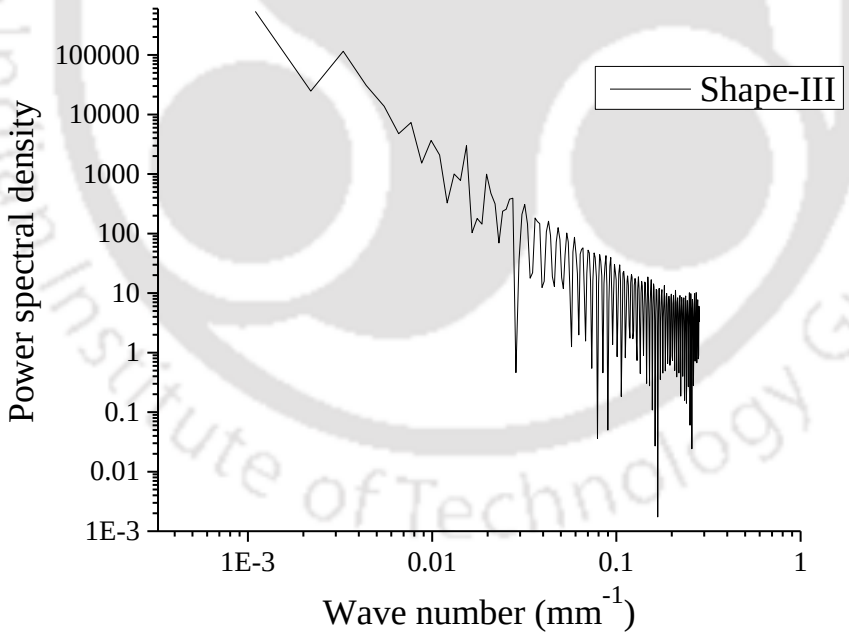

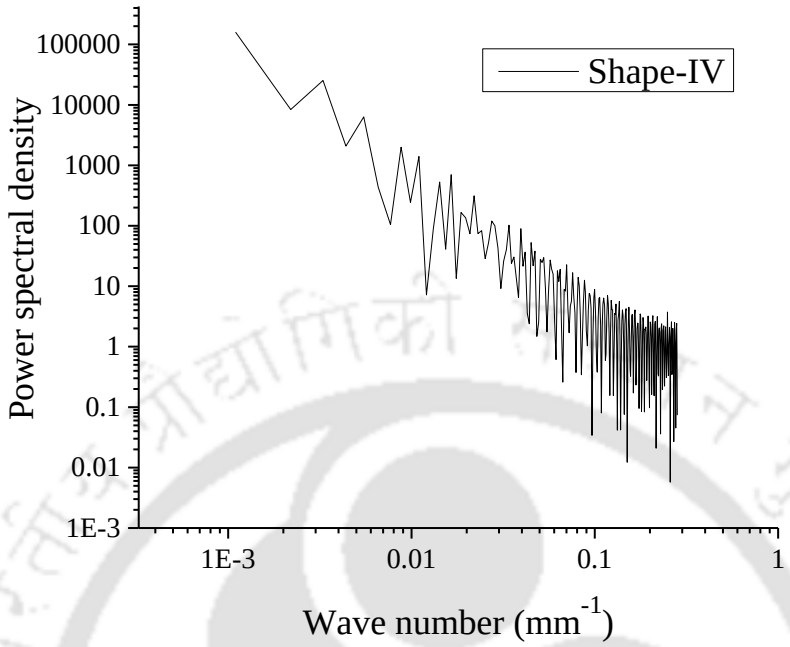

Figure 5.5 Power spectral density of initial bed elevation series along the center line

Figure 5.6 shows the maximum cross-correlation coefficient between initial and final bed elevation series. Maximum cross-correlation coefficient increases gradually with the increase in the scale. The celerity of mining pit with respect to different length scale has been presented in Figure 5.7. It is observed from the Figure 5.7 that there is a gradual decrease in celerity with increase in scale, which suggests that larger resistance is offered by large sized mining pit (Singh et al., 2011). There is an increase in celerity of mining pit with increase in discharge for each set of experiments, which suggests a higher migration speed at higher discharge. The similar trend of migration speed with various discharges is also observed in Figure 5.2 from physical characteristics.

The celerity at each scale for Shape-III is higher than that of Shape-II, and Shape-IV is higher than that of Shape-III. Table 5.1 shows the average celerity of mining pit for scale 150 mm to 300 mm with velocity V1 and V5.

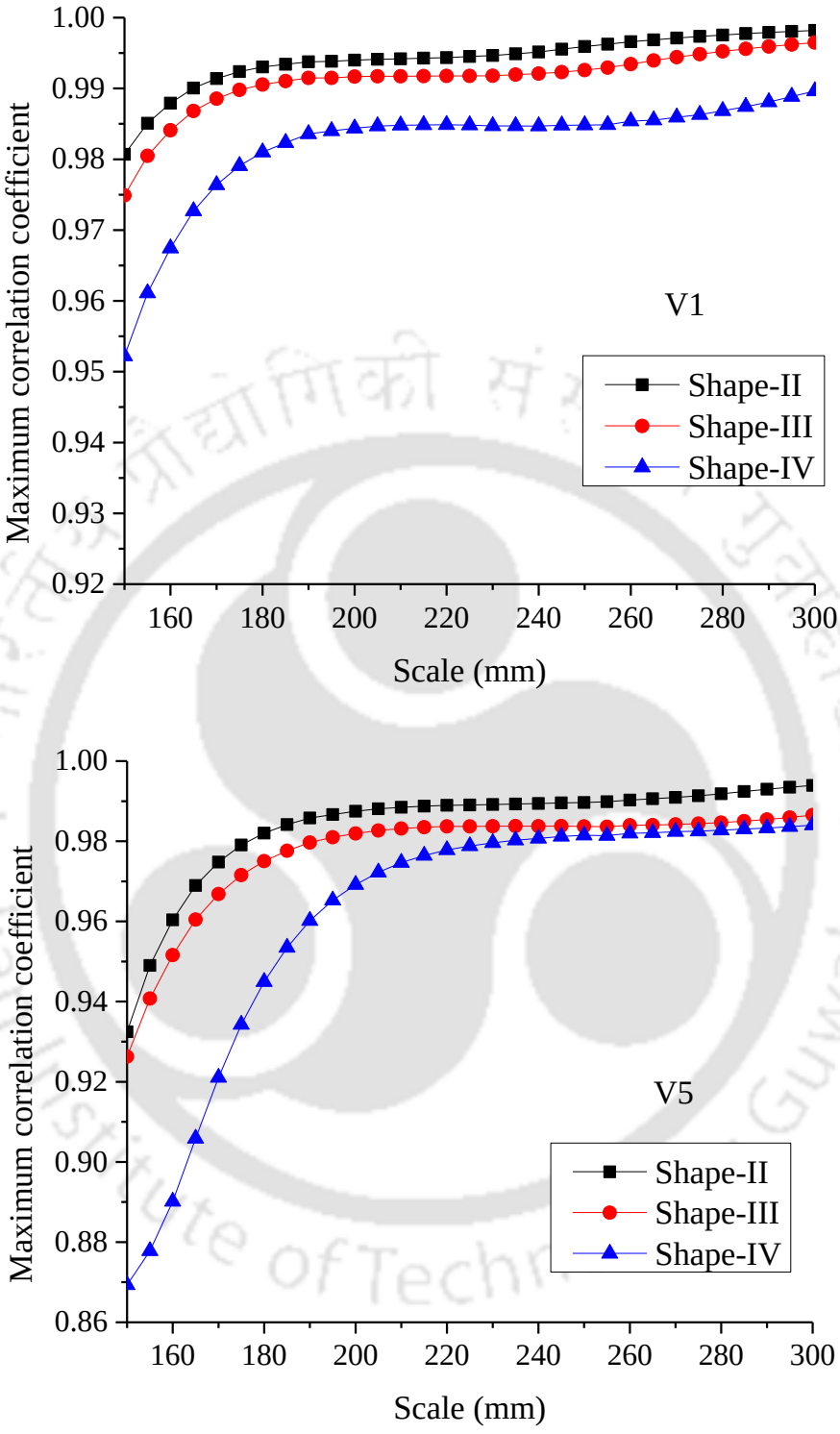

Figure 5.6 Maximum correlation coefficient between initial and final bed elevation series

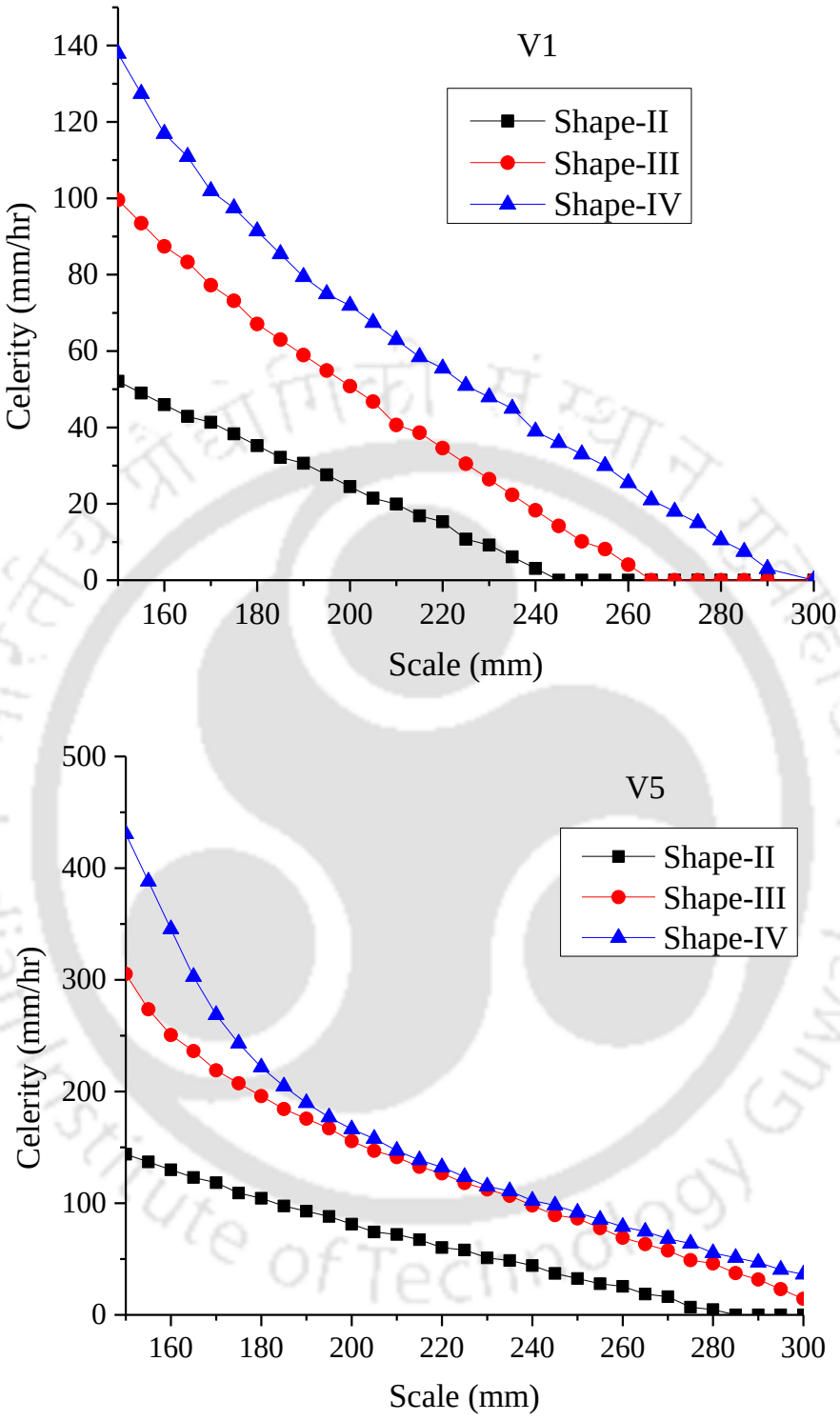

Figure 5.7 Scale dependent celerity of mining pit

Table 5.1 Average celerity of mining pit from multi-scale statistical analysis

	V1			V5		
	Shape-II	Shape-III	Shape -IV	Shape-II	Shape-III	Shape-IV
Avarage celerity (mm/hr)	29.98	52.76	65.89	81.73	128.95	174.1

The celerity of mining pit increases with the increase in length by width ratio of the pit. We have observed highest migration speed for Shape-IV in comparison with Shape-II and Shape-III. Similar trend of results is also observed from the physical characteristics in the previous section.

5.4 Analysis for Rectangular Mining Pit (Shape-I)

Power spectral density of bed elevation series for two different average velocities is as shown in Figure 5.8. The slope of power spectral density for average velocity of 0.445 m/s and 0.481 m/s is found to be -1.89 and -2.02 at high saturation zone. An increase in spectral slope with increase in average velocity is observed. From Figure 5.8 a clear scaling range of 15 mm to 125 mm is observed both for V8 and V10. Using a scale within this range length scale dependent celerity of mining pit at different time interval is obtained by applying aforementioned methodology.

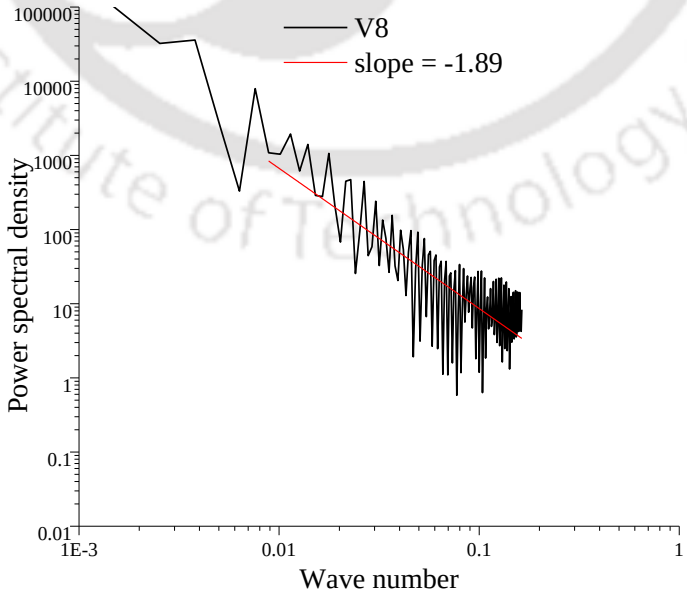

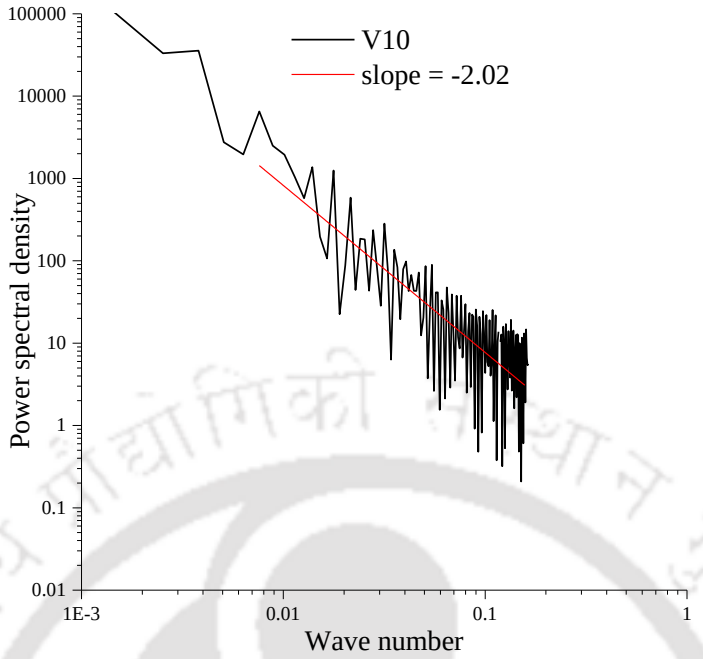

Figure 5.8 Power spectra of bed elevation series after 4 hours for V8 and V10.

Wavelet coefficient of bed elevation series at scale 51 mm and 55 mm using Mexican hat wavelet is shown in Figure 5.9. These scales are considered randomly from the scaling region obtained from power spectral density analysis. Mexican hat wavelet transformation of original signal forms the basis for the calculation of scale dependent cross correlation coefficient.

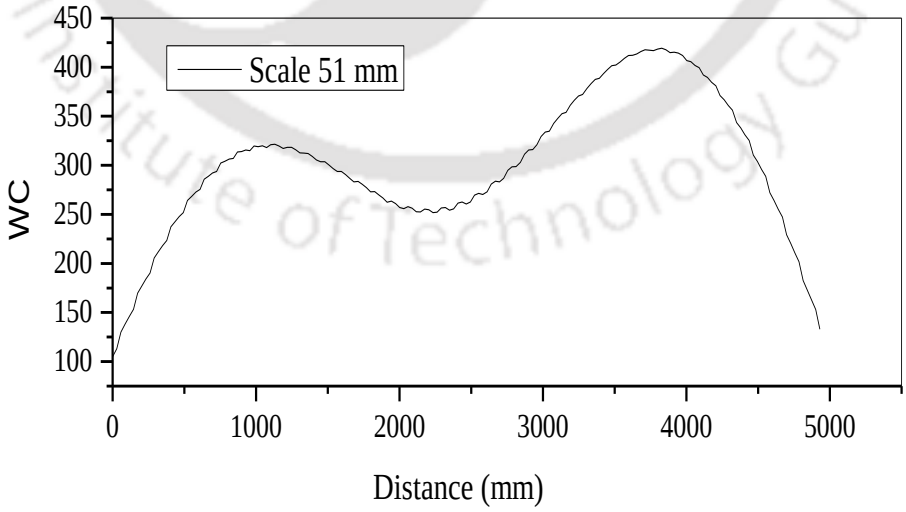

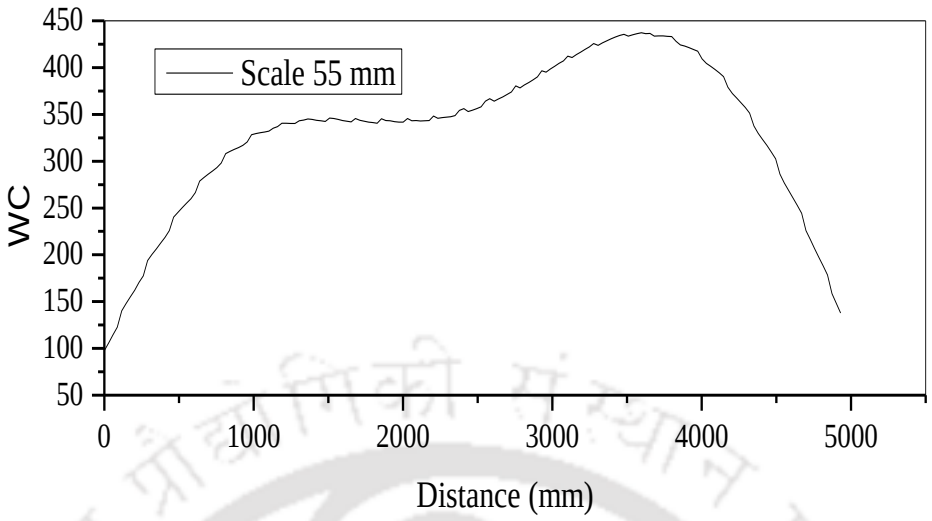

Figure 5.9 Wavelet coefficients of bed elevation series at 1 hour for V8 at two different scales

Celerity of the mining pit ranging from a length scale of 50 mm to 100 mm is calculated using wavelet cross correlation. Celerity of the mining pit for various length scales is shown in Figure 5.10. For V8 and V10, celerity of the mining pit is more in the time duration of (1-4) hour as compared to (4-7) hour, which demonstrate the results obtained in previous literature (Singh et al., 2011). It is also observed that migration/celerity of mining pit in sand mining channel increases with scale and attains the maximum value then decreases with increase in the length of scale. Here, it can be hypothesized that more resistance are being offered by scale structure of sand bed features, which retrogrades the celerity a lower value at high scale that is celerity become zero at scale above 90 mm. Figure 5.11 shows a comparison of celerity between V8 and V10 at 1-4 hours and 4-7 hours. During the initial time span (1-4 hours) celerity is increasing with increase in flow velocity but in a later time interval (4-7 hours) it is decreasing with increase in flow velocity. This may so happen that during the initial time span (1-4 hours), upstream bed material transport is increased with the increase in flow velocity due to which celerity of mining pit is increased with the increase of flow velocity. With the passage of time, sediment transport is decreased in both V8 and V10 and the decreased rate of sediment transport is higher in V10 as compared to V8 due to which channel becomes faster stable in V10 and celerity of mining pit is decreased in later time interval (4-7 hours) for V10. Decreased rate of

average celerity between the time interval (1-4 hours) and (4-7 hours) for V10 is 44 % whereas for V8 is 19%.

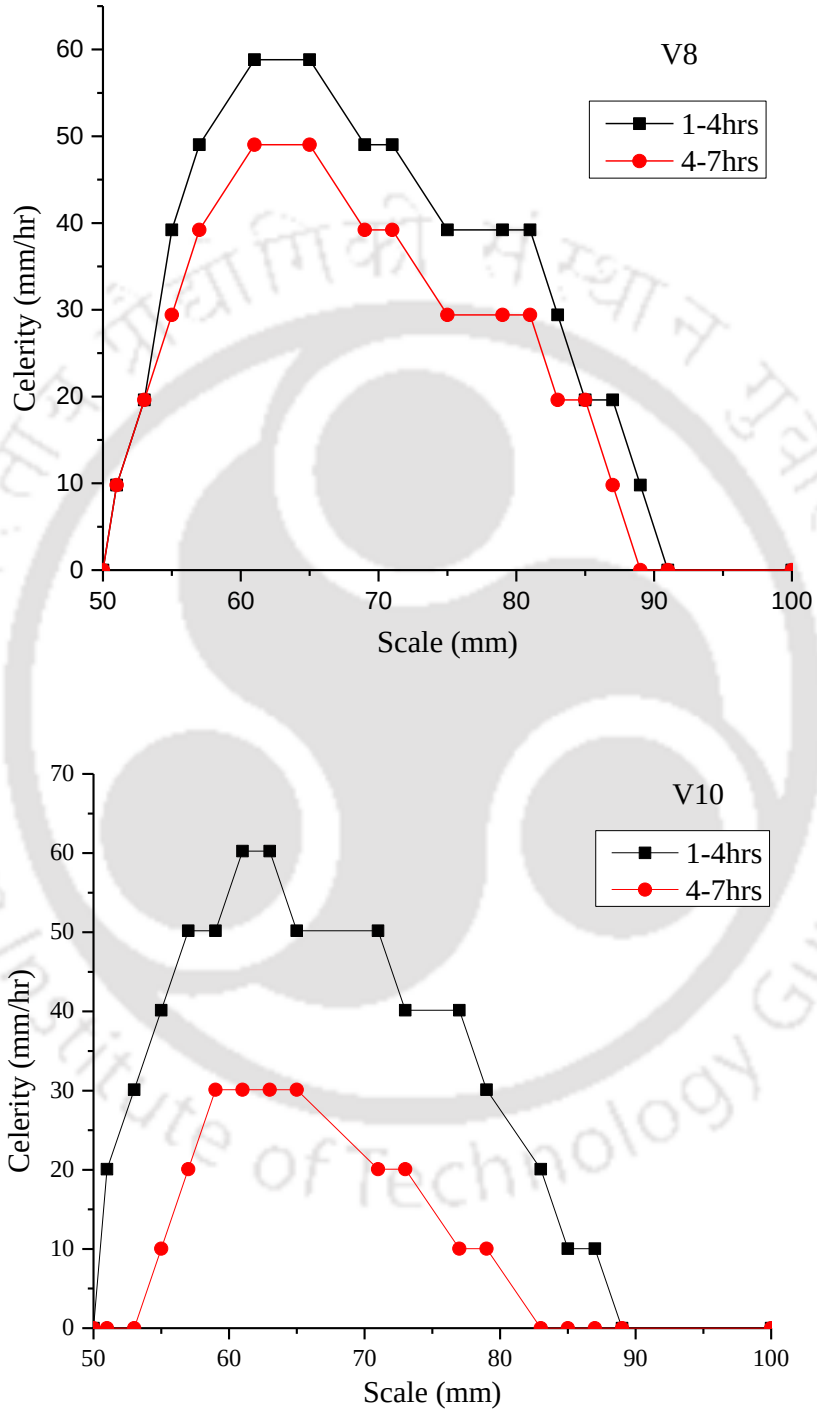

Figure 5.10 Celerity of mining pit for V8 and V10 at different time span

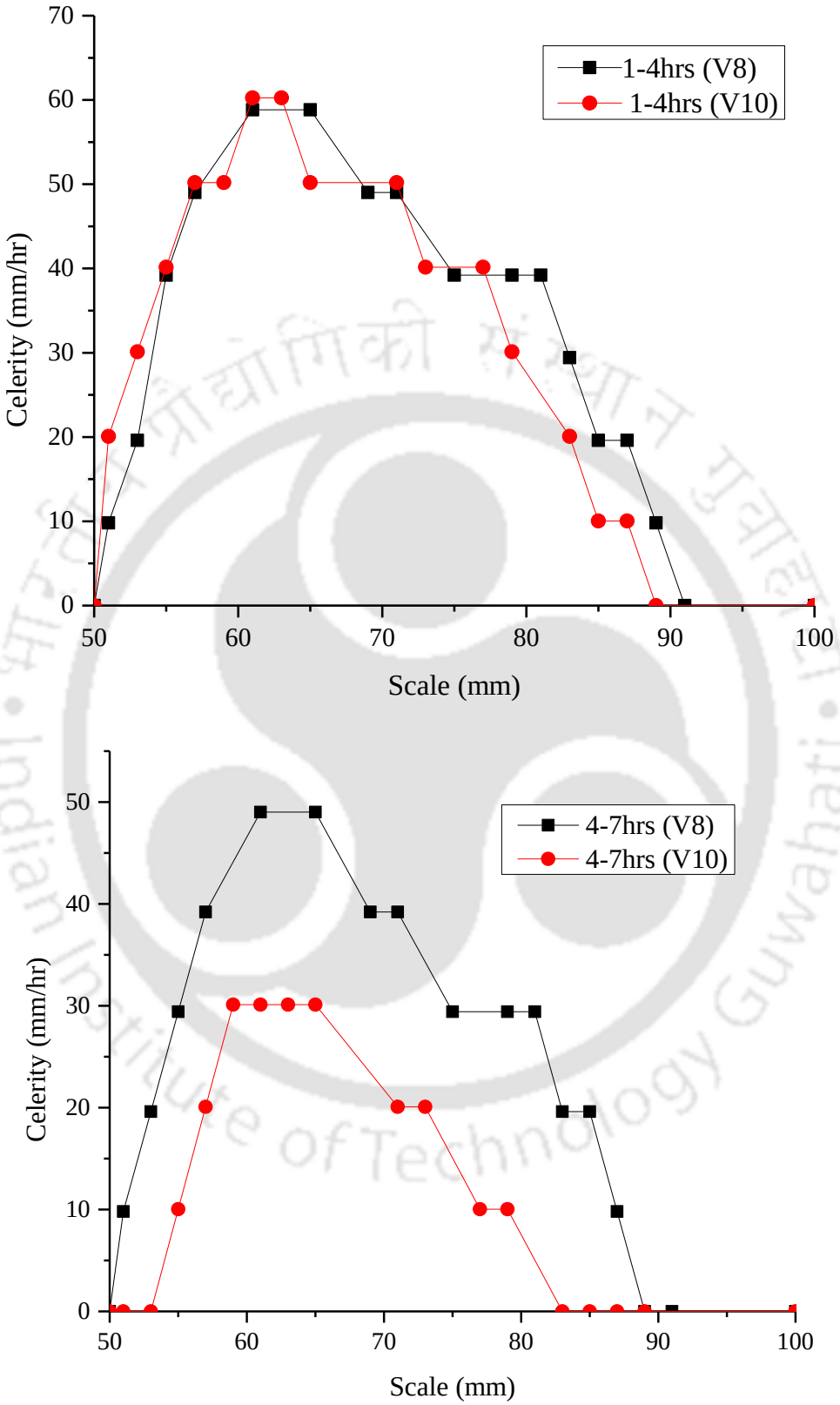

Figure 5.11 Comparison of celerity of mining pit between V8 and V10 at two different time span

5.4 Conclusions

Migration of mining pit has been studied by using experimental methodology. The celerity of the pit has been obtained from the both physical and multi-scale statistical characteristics of bed elevation series. The physical characteristics show increase in migration speed or celerity of the pit with increase in discharge and length by width ratio of the pit. The volume of extraction also plays an important role in the migration speed but the major influence is observed from the pit geometry. An empirical formulation for mining pit migration has been developed based on one non-uniform sand. The quantitative analysis of mining pit migration is necessary for sustainable development and management of sand mining activities. However, the mining activity is very random in nature, so the proposed equation for migration speed can be modified by using field observation data. The celerity of mining pit has also been explained by multi-scale statistical analysis. The scale dependent celerity of pit shows an increase in magnitude with an increase in discharge. The increase in celerity with an increase in discharge has also been observed from the physical characteristics. The celerity of pit also decreases with increase in scale, ensuring the increase in resistance with increase in scale. The average celerity and the celerity at each scale have been observed as maximum for Shape-IV followed by Shape-III and Shape-II. The trend of celerity of mining pit with respect to different length by width ratio has been observed to be similar to that of physical characteristics. The results obtained from both physical and multi-scale characteristics have shown that the celerity of mining pit is largely affected by the pit geometry. The present results may be implemented for quantitative understanding of pit celerity or migration speed; however, detailed field investigation is required since various other parameters such as grain size distribution of bed material, upstream sediment influx, river topography, and so forth, can highly influence the pit dynamics.

6 Scope of Applying Numerical Model for Simulating Pit Migration

6.1 Introduction

Sediment transport and morphological evolution of channel bed depends on the interaction of bed material with flow. For simulation of bed profile hydrodynamic equations can be incorporated with sediment continuity equations by using decoupled, semicoupled and coupled methodology. Coupled methodology is suitable for alluvial river with rapid bed evolution (Cao et al., 2002) whereas, semicoupled method is more flexible and appropriate for bedload dominant flow. For bed load dominant flow the time scale of flow and channel bed evolution processes may be different, therefore, fully coupling of flow and sediment transport may not be necessary (Wu, 2004). Determination of mining pit migration and extend of downstream erosion is important for sustainable development. So, here we have carried out a numerical investigation on mining induced channel bed erosion. We have developed a numerical model to predict mining pit migration by using different sediment transport capacity formula as model closure of the governing equations under equilibrium condition of sediment transport. Laboratory experiment data for rectangular mining pit have been used to validate of the numerical model. Semi coupled technique for simultaneous solution of hydrodynamic equations and sediment mass conservation equation of bed material have been used in this model. Since experiment were conducted under bed load transport condition, fully coupled model may not be necessary (Wu, 2004). Here, we are mainly discussing the applicability of numerical model in the context of mining pit migration by using different bed load transport formula as a model closure of the governing equation.

6.2 Theoretical Backgrounds

In this section the formulation of governing equations for one dimensional depth average model are presented. Mass and momentum equations of water as well as sediment mass conservation equations are used to describe the phenomenon of flow and channel bed evolution.

6.2.1 Governing equations for shallow water hydrodynamics

One dimensional shallow water equation can be expressed as

$$\frac{\delta U}{\delta t}+\frac{\delta F}{\delta x}=S \tag{6.1}$$

Where *t* is time and *x* is the longitudinal distance; *U* is representing the flow variable, *F* and *S* are the fluxes in *x*-direction and source term respectively. The matrix form of U, F, and S can be written as

$$U=\begin{bmatrix} h \\ hu \end{bmatrix}, \quad F=\begin{bmatrix} hu \\ hu^2+\frac{1}{2}gh^2 \end{bmatrix}, S=\begin{bmatrix} 0 \\ gh(S_b-S_f) \end{bmatrix} \tag{6.2 a, b, c}$$

where h, u are the depth of flow and depth average longitudinal velocity; S_b and S_f are channel bed slope and friction slope. The depth of water can be expressed as $h=h_z-z_b$ with h_z, z_b as water surface elevation and bed elevation above datum respectively. So Equation 6.2 can be rewritten as

$$U=\begin{bmatrix} h_z \\ hu \end{bmatrix}, \quad F=\begin{bmatrix} hu \\ hu^2+\frac{1}{2}g\left(h_z^{\,2}-2h_z z_b\right) \end{bmatrix}, S=\begin{bmatrix} \frac{\delta z_b}{\delta t} \\ gh_z S_b-ghS_f \end{bmatrix} \tag{6.3 a, b, c}$$

Here, bed elevation z_b is considered to be changed with time. Friction slope is calculated by using Manning's formulation $S_f=\frac{n^2u^2}{h^{4/3}}$, where *n* is Manning's constant.

6.2.2 Governing equation for bed elevation changes

Channel bed evolution can be represented by continuity equation of bed material. Governing equation for evolution of channel bed under equilibrium sediment transport of bed load dominant flow is as follows (Wu, 2007),

$$(1-p)\frac{\delta z_b}{\delta t}+\frac{\delta q_s}{\delta x}=0 \tag{6.4}$$

where q_s is the bed load transport rate per unit width of the channel, which can be determined by using various sediment transport formula. p is the porosity of bed material.

6.2.3 Sediment transport formula

Numbers of sediment transport formulations are available in various literature which are empirical and semi empirical in nature. Since sediment transport is assumed to occur as bed load transport for this study, different formulations for bed sediment transport are presented here and applied for the closure of the governing equation.

6.2.3.1 Shields approach

Sheilds (1936) obtained a semi empirical equation for bed load transport from incipient motion criterion (Yang, 1996).

$$q_s = \frac{10 q \gamma S_f (\tau - \tau_{0c})}{\gamma_s (\gamma_s - \gamma) d_{50}} \tag{6.5}$$

where q_s and q are bed load and water discharge per unit width of the channel respectively, $\tau = \gamma h s_f$, τ_{0c} is the critical shear stress, γ, γ_s are specific weight of water and sediment respectively, and d_{50} is median diameter of sediment particle.

6.2.3.2 Meyer-Peter and Muller (MPM) approach

Meyer-Peter and Muller (1948) formulation for bed load transport is based on energy slope approach (Yang, 1996).

$$q_s = 8\sqrt{g(s-1){d_{50}}^3}\left(\theta - \theta_{cr}\right)^{3/2} \tag{6.6}$$

here, g is the acceleration due to gravity, s is the specific gravity of sediment, d_{50} is the median diameter of sediment, θ is the Shields parameter, and θ_{cr} is critical Shields parameter.

6.2.3.3 Grass formula

Grass (1981) provided a sediment transport formulation based on power law of flow velocity.

$$q_s = A u \left| u^2 \right| \tag{6.7}$$

here, A is a coefficient which depends on interaction between flow and sediment particles, range between (0-1) with increase in interaction strength (Hudson, 2001). A can also obtain from Rehman et al. (2016) with details sediment transport properties

$$A = \frac{d_{50}\left(0.005\left(\frac{d_{50}}{h}\right)^{0.2} + 0.012D_*^{-0.6}\right)}{\left(gd_{50}\left(\frac{\rho_s}{\rho} - 1\right)\right)^{1/3}} \tag{6.8}$$

Where ρ and ρ_s are the density of water and sediment, h is the depth of water, D_* is the dimensionless particle diameter, which can be obtained from

$$D_* = d_{50}\left(\frac{g}{\nu^2}\left(\frac{\rho_s}{\rho} - 1\right)\right)^{1/3} \tag{6.9}$$

where υ = kinematic viscosity of water, g = acceleration due to gravity.

6.2.3.4 Van Rijn approach

Van Rijn (1984) provided a more complex formula by introducing critical threshold velocity in velocity power law formulation (Hudson, 2001).

$$q_b = \begin{cases} Au(|u| - u_{cr})^{2.4} & if \quad u \geq u_{cr} \\ 0 & otherwise \end{cases} \tag{6.10}$$

where u_{cr} is the critical threshold velocity, which can be obtained from following formulation depending upon the median diameter (d_{50}) of sediment particle.

$$u_{cr} = \begin{cases} 0.15\left(d_{50}\right)^{0.1}\log_{10}\left(\frac{2h}{d_{50}}\right) & if \quad 100 \leq d_{50} \leq 500\mu m \\ 8.5\left(d_{50}\right)^{0.6}\log_{10}\left(\frac{2h}{d_{50}}\right) & if \quad 500 \leq d_{50} \leq 2000\mu m \end{cases} \tag{6.11}$$

$$A = \frac{d_{50}\left(0.005\left(\frac{d_{50}}{h}\right)^{0.2} + 0.012D_*^{-0.6}\right)}{\left(gd_{50}\left(\frac{\rho_s}{\rho} - 1\right)\right)^{1.2}} \tag{6.12}$$

D_* is the dimensionless particle diameter as mentioned in Equation 6.9.

6.2.4 Numerical formulation of the governing equation

The shallow water equation (Equation 6.1) is solved by using a first order accurate flux vector splitting finite difference scheme (Anderson, 1995). Equation 6.1 can be re-written as

$$\frac{\delta U}{\delta t} + A_J \frac{\delta U}{\delta x} = S \tag{6.13}$$

where $A_J = \frac{\delta F}{\delta U}$ is the jacobian matrix

To introduce flux-vector splitting, we need matrix properties from linear algebra. Eigenvector associated with a specific eigenvalue λ_j of flux jacobian matrix can be determined by using equation

$$\left[L^j\right]^T \left[A_J(U) - \lambda_j I\right] = 0 \tag{6.14}$$

Where $\left[L^j\right]^T$ is the transverse of column vector $\left[L^j\right]$. For each eigenvalue of flux jacobianmatrix $A_J(U)$, there will be a different eigenvector L_j. A matrix T_e can be formed whose inverse T_e^{-1} has the elements of all the eigenvectors. The matrix T_e has the property of diagonalizing the matrix $A_J(U)$.

$$T_e^{-1} A_J(U) T_e = [\lambda] \tag{6.15}$$

where $[\lambda]$ is a diagonal matrix with the eigenvalues of $A_J(U)$. From Equation 6.15 we have

$$A_J(U) = T_e [\lambda] T_e^{-1} \tag{6.16}$$

From Equation 6.16 we can define A^+ and A^- as

$$A^+ = T_e\left[\lambda^+\right]T_e^{-1} \tag{6.17}$$

$$A^- = T_e\left[\lambda^-\right]T_e^{-1} \tag{6.18}$$

where $\left[\lambda^+\right]$ and $\left[\lambda^-\right]$ are matrices with positive and negative eigenvalues matrix.

$$\left[\lambda^+\right] = \begin{bmatrix} u+c & 0 \\ 0 & 0 \end{bmatrix} \tag{6.19}$$

$$\left[\lambda^-\right] = \begin{bmatrix} 0 & 0 \\ 0 & u-c \end{bmatrix} \tag{6.20}$$

where $c = \sqrt{gh}$. Using the procedure of split normalize Jaccobian matrix we can split the flux vector F into two parts, $F^+$and F^- (Cao and Pender, 2004).

$$A_J(U) = \left(A^+ + A^-\right)A(U) \tag{6.21}$$

$$A^+ + A^- = I \tag{6.22}$$

$$F = \left(A^+ + A^-\right)F \tag{6.23}$$

For bed updating equation (Equation 6.4), first order accurate backward finite difference scheme is used. Bed elevation is calculated simultaneously at every time step and updated bed information is incorporated in the hydrodynamic equation in the next time step.

6.3 Results and Discussions

Results for the numerical simulation of pit migration are presented in this section. The numerical simulations are conducted for various flow characteristics as mentioned in table 6.1. The numerical results are compared with the experimental one.

Table 6.1 Various flow characteristics for numerical experiments

	Shape of the pit and bed material	Numerical Experiments	Discharge, m^3/s	Average depth of flow, m	Froude No.	Reynolds No.
Numerical Set-I (NSet-I)	Rectangular pit (Shape-I), d_{50}= 0.418mm	Exp1	0.0305	0.102	0.299	21109
		Exp2	0.0354	0.1005	0.355	24595
		Exp3	0.038	0.096	0.408	26577
Numerical Set-II (NSet-II)	Trapezoidal pit (Shape-II), d_{50}= 1.1mm	Exp1	0.0442	0.0987	0.455	30740
		Exp2	0.0472	0.1014	0.467	32712
		Exp3	0.0503	0.1038	0.48	34730
		Exp4	0.0535	0.1079	0.482	36674
		Exp5	0.0567	0.1101	0.496	38756

Subcritical flow condition was maintained for each experiment with Froude number less than one as shown in table 6.1. Reynolds numbers for these experiments were observed to be larger than four thousand and indicated high turbulent flow in the flume. The threshold shear stress from Shields criterion is obtained 0.236 N/m^2 for 0.418 mm (d_{50}) sand and 0.69 N/m^2 for 1.1 mm (d_{50}) sand. Proposed numerical model is tested for these flow conditions to verify the performance of the model for simulating mining pit migration and channel bed erosion.

6.3.1 Initial and boundary conditions

The flow conditions mentioned in table 6.1 are used for simulation of numerical model. Flow conditions for all these experiments are at subcritical flow condition. So, we need to specify one boundary condition at upstream and one at downstream (Chaudhry, 2008). At the upstream boundary, constant discharge is applied and at the downstream boundary elevation of water surface is kept constant. Extrapolation technique is applied at both upstream and downstream boundary for calculating bed load sediment transport and channel bed elevation. Initial flow velocity, water depth and bed elevation is defined at each grid for respective experiments. Values adopted for different parameters are g = 9.81 m/s^2, n = 0.03, p = 0.3, ρ = 1000 kg/m^3, ρ_s =2650 kg/m^3, length of channel= 17.2 m, Width of channel = 1 m, S_b =0.0017, spatial grid Δx_n= 0.04 m, temporal grid Δt is specified from satisfying Courant condition less than one.

6.3.2 Simulation of pit migration by using proposed numerical model

Numerical model is run for all the hydraulic conditions listed in table 1 and compared the numerical results with respective experimental profile along the center of the channel.

6.3.2.1 Simulation of bed profile for NSet-I experiment

For this set of experiment, four different bed load transport equations namely Shields approach (1936), Meyer Peter and Mullar (1948), Grass formula (1981) and Van Rijn approach (1984) for the closure of the governing equation are used. The former two are based on shear stress and energy slope approach respectively whereas later two are based on velocity approach. Figure 6.1 shows comparison of experimental and numerical channel bed profile at one hour by using four different sediment transport formulas. Results are presented for 5 m test section. Experimental and numerical bed profile shows erosion at the downstream of the pit. However, same initial and boundary condition shows different quantitative results for different sediment transport formulas. Numerical results by using Shields approach (1936) shows highest migration speed of upstream edge of mining pit and more downstream erosion as compare to the experimental profile.

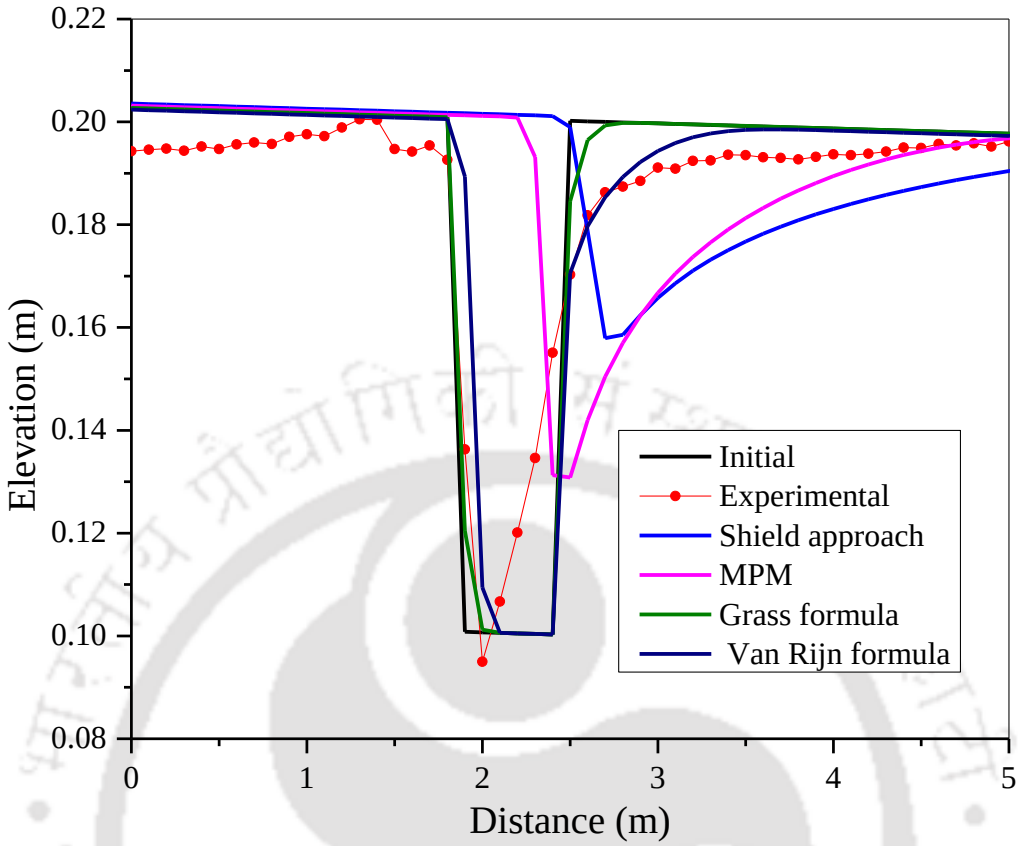

Figure 6.1 Comparison of experimental and numerical profiles after one hour by using different sediment transport formula for Exp3 of NSet-I

Shields formula is based on shear stress approach where erosion is depends on the difference between bed shear stress (τ) and critical shear stress of the bed material. Bed shear stress τ is a function of depth of flow and energy slope. Characteristics of bed shear stress and energy slope of channel having mining pit was discussed in author's previous publication, where it was stated that two different water surface slope occurs at both upstream and downstream of the pit by creating a flow separation zone and thus influence the energy slope of the channel (Barman et al., 2017). So the shear stress approach may not be appropriate for morphological simulation of a mining region. Same is the case for Meyer Peter and Muller (1948) formulation, where formulation is based on energy slope approach. In both this cases we observed an over estimation of mining pit migration. Grass (1981) formulation is based on velocity approach and gives a low migration speed. It underestimates the migration speed of the upstream edge and also

downstream erosion. Figure 6.2 displays experimental and numerical bed profile by using Grass formula (1981) after 4 hours for Exp3.

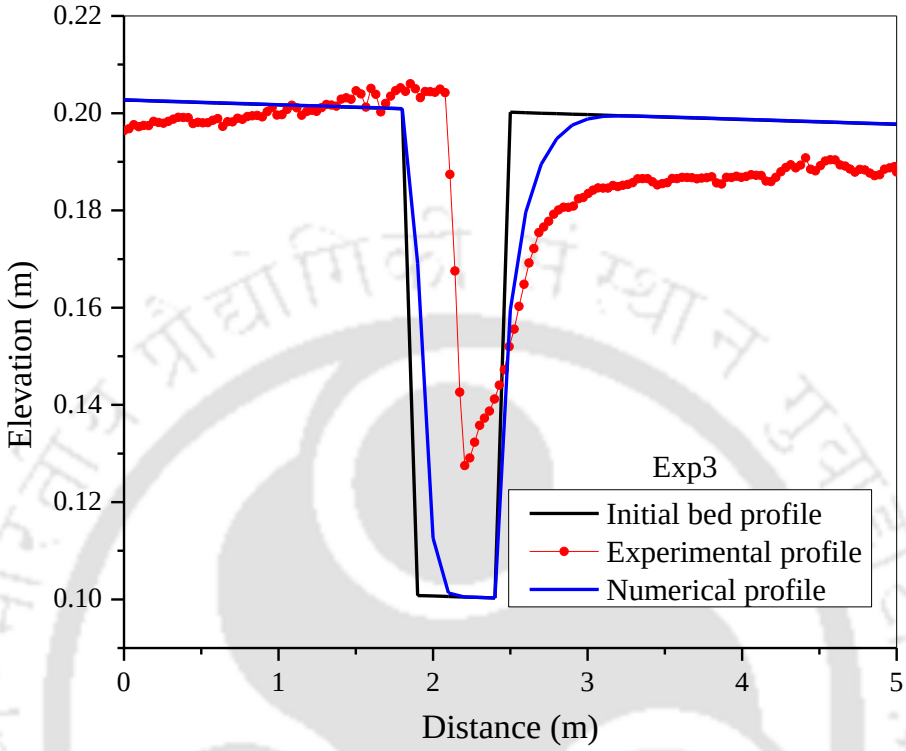

Figure 6.2 Comparison of experimental and numerical profile by using Grass formula after 4 hours for Exp3 of NSet-I

Figure 6.3 shows both experimental and numerical profile by using Van Rijn formula and gives nearly comparable results in terms of migration of upstream edge and also the downstream erosion. Van Rijn introduced a threshold current speed for range of different particle diameter. Partial filling of pit at the bottom does not show a good agreement with experimental one. Adverse slope at the downstream edge of the pit may create recirculation zone inside the pit and may increase the deposition at the bottom of the pit. This phenomenon cannot be capture due to the limitation of the depth averaged one dimensional model. The model is also tested for other two different discharges. Figure 6.4 shows migration of rectangular mining pit for two different discharges.

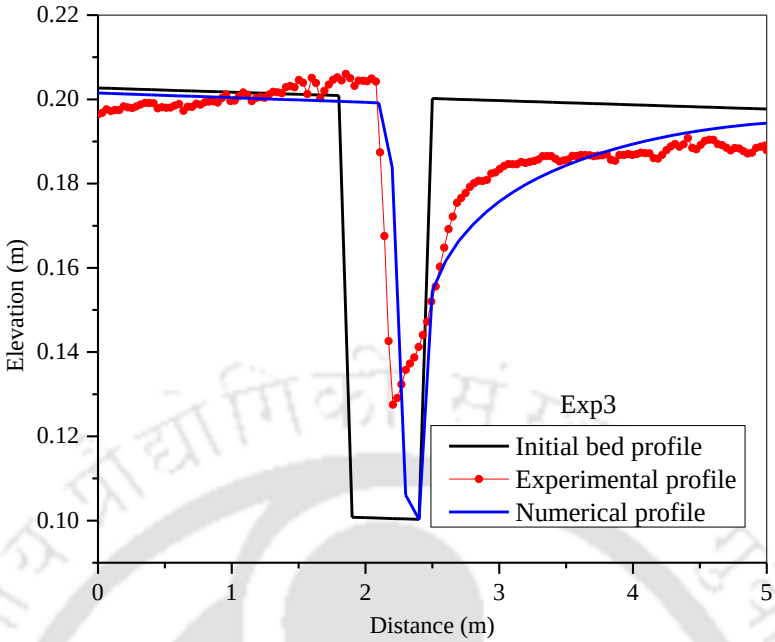

Figure 6.3 Comparison of experimental and numerical profile by using Van Rijn formula after 4 hours for Exp3 of NSet-I

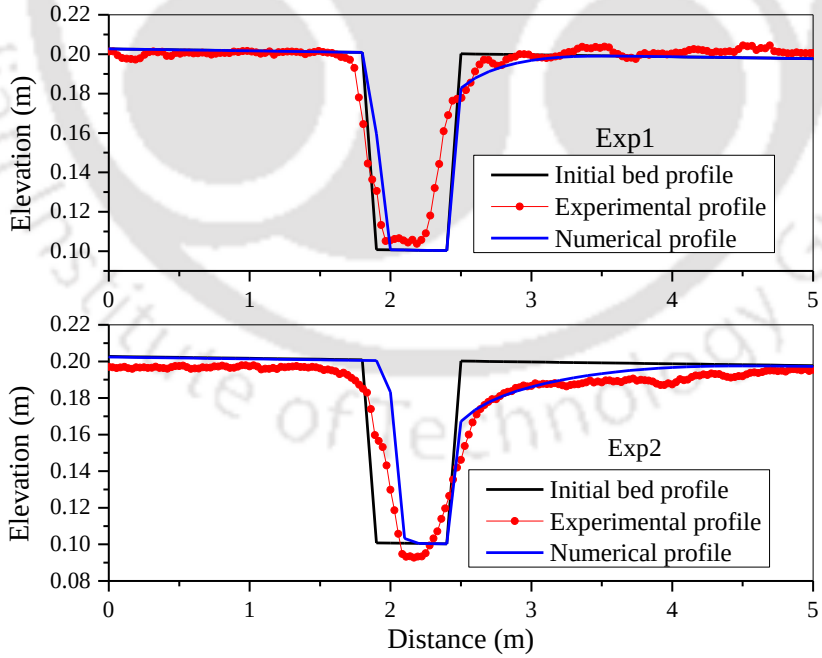

.

Figure 6.4 Comparison of experimental and numerical profile by using Van Rijn formula after 4 hours for Exp1 and Exp2 of NSet-I

Numerical model with Van Rijn formula (1984) for bed load transport shows good agreement with experimental one in terms of time taken to completely filling up of the pit. Figure 6.5 represent both experimental and numerical profiles after filling up of the pit. The numerical result shows migration of erosion towards downstream direction and compared well with experimental one.

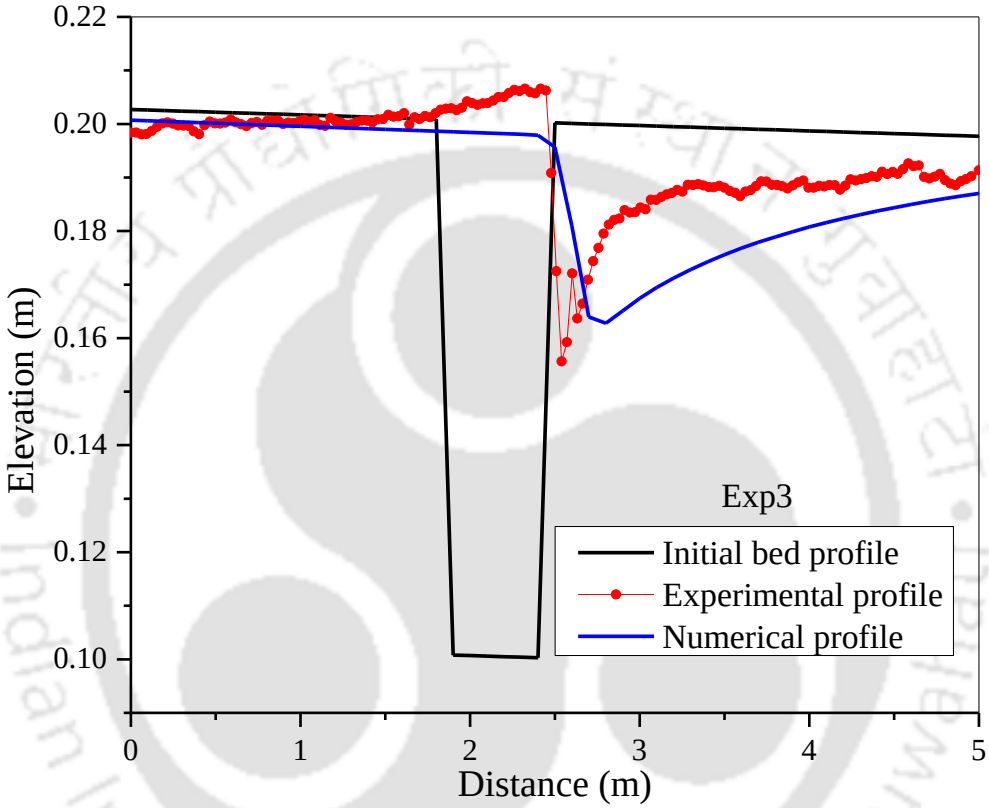

Figure 6.5 Numerical and experimental bed profiles for Exp3 after 7 hours of NSet-I

The proposed model is also tested for the experiment conducted Lee et al. (1993) (Figure 6.6). We have observed similar trend of pit migration from the numerical simulation with maximum 12.7% error in terms of migration of upstream edge of the pit. Lee et al. (1993) measured the bed profile after draining out the water in their experiment. In this present research, we have used ultrasonic ranging system for bed profile measurement. The use of ultrasonic ranging system facilitates us to measure the bed profile under the water, thus provide more accurate representation of bed profile evolution at different time interval.

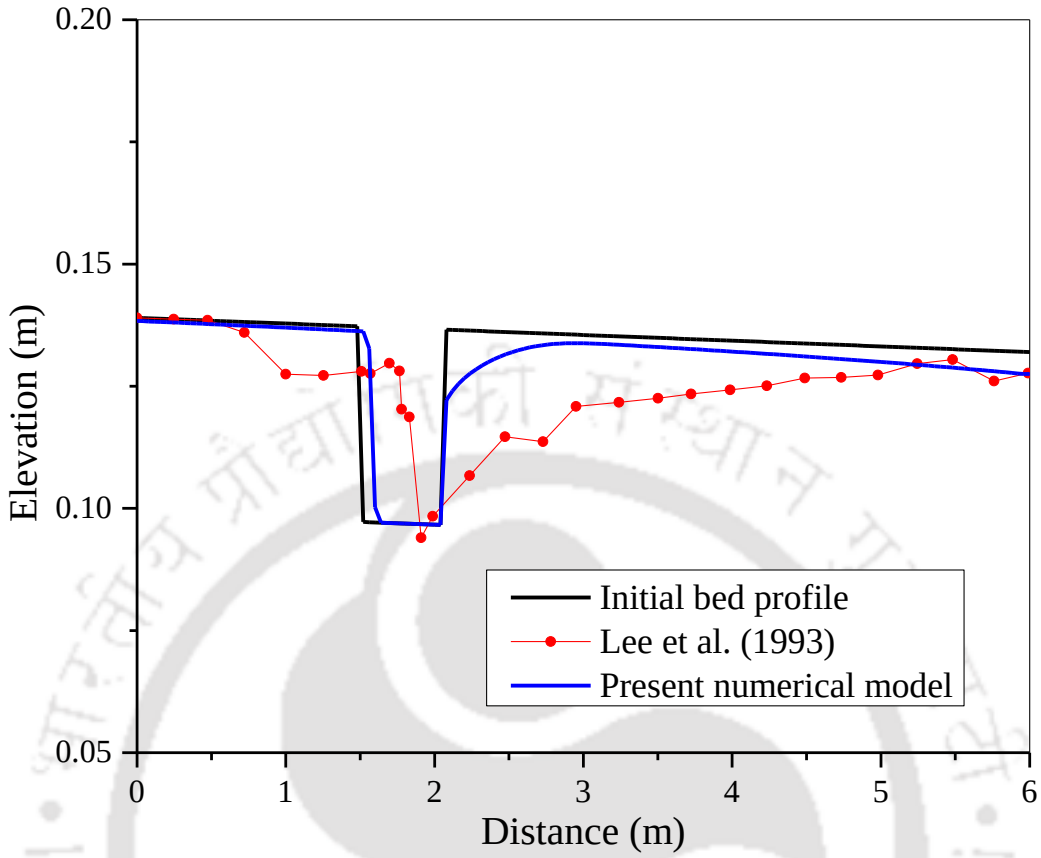

Figure 6.6 Comparison of present model with Lee et al. (1993) experimental results (Time = 2 hours)

The numerical model is also tested for another set of experiment and presented in the following section.

6.3.2.2 Simulation of bed profile for NSet-II experiment

Numerical model is run for the various hydraulic conditions of NSet-II. Here, the comparison of numerically simulated of bed profile with experimental one is presented. Figure 6.7 shows both experimental and numerical profile for five different discharges.

a)

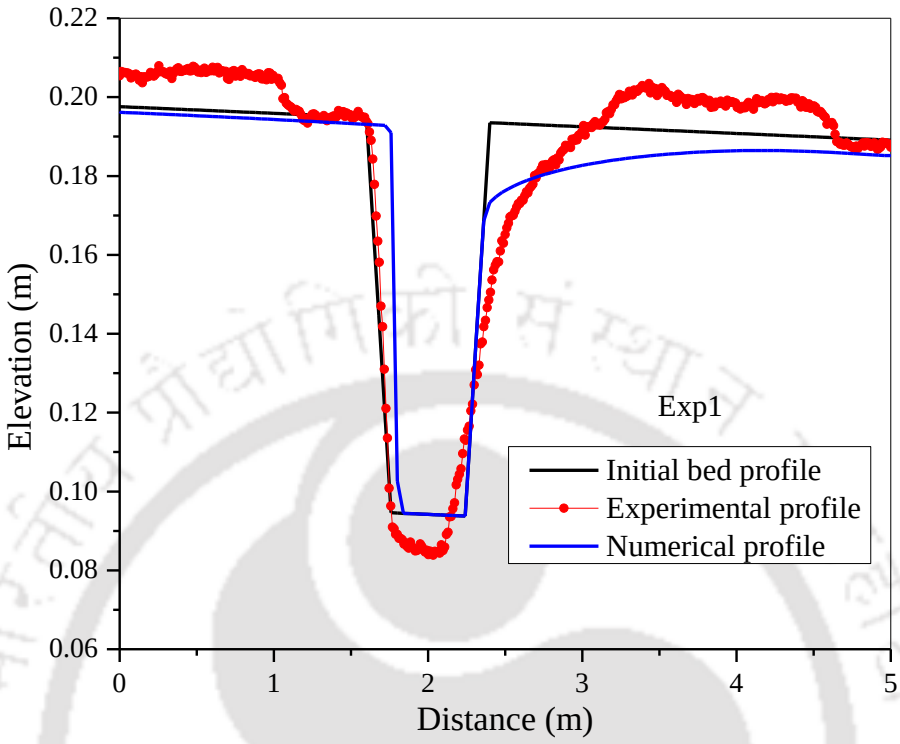

b)

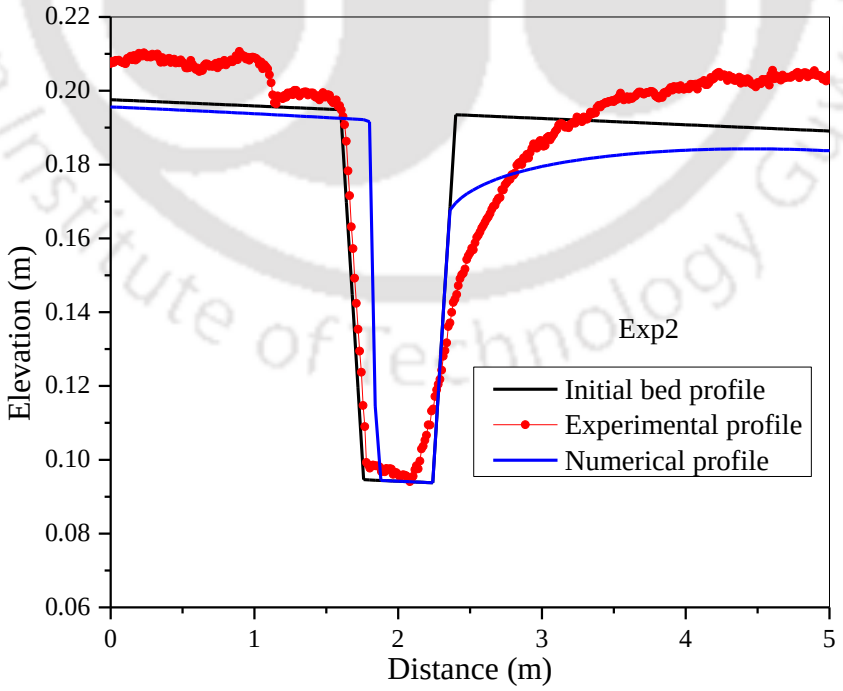

c)

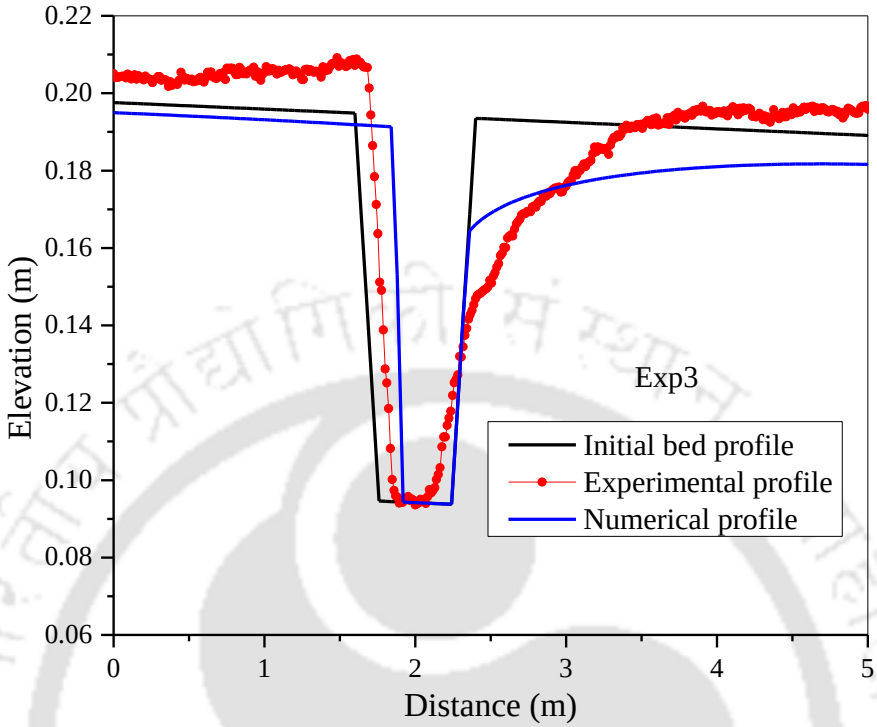

d)

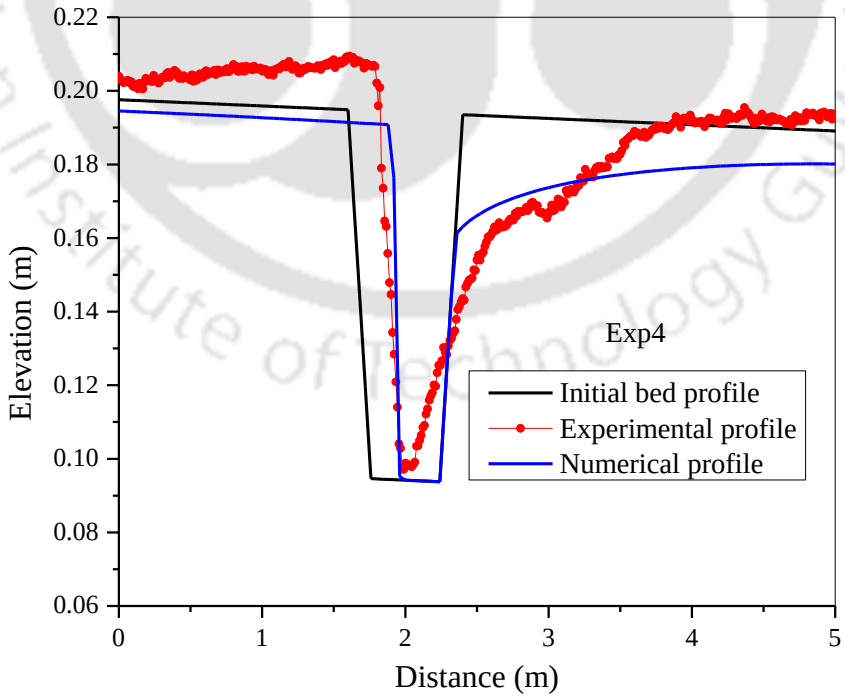

e)

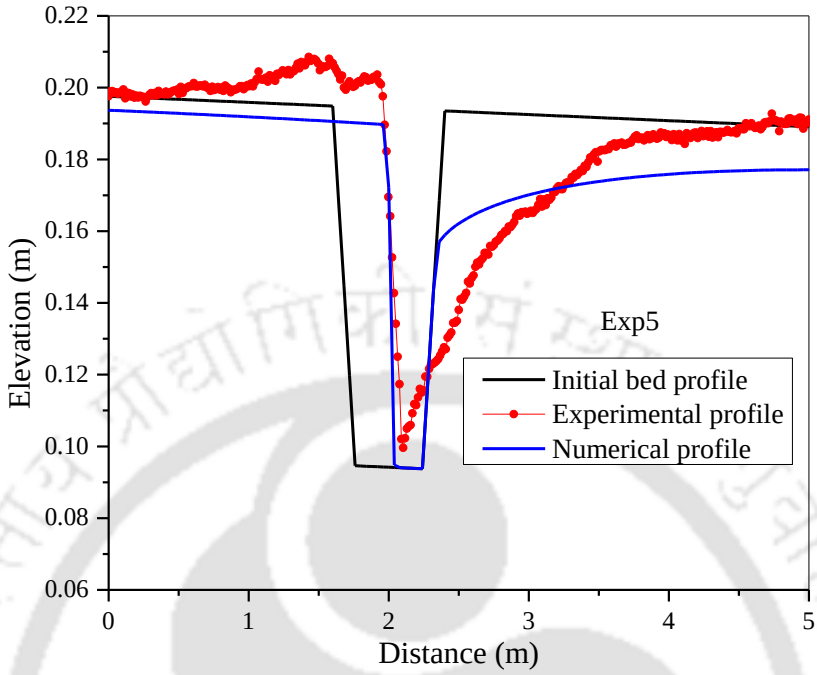

Figure 6.7 Numerical and experimental bed profiles for NSet-II after 4 hours a) Exp1, b) Exp2, c) Exp3, d)Exp4, e) Exp5

Numerical simulation of both sets of experiments shows that proposed model compared well with experimental results in terms of migration of mining pit. The percentage error in numerical results as compared to the experimental one is presented in table 6.2.

Table 6.2 Error in numerical results as compared to the experimental one

	Numerical experiments	Percentage error
NSet-I	Exp1	3.2
	Exp2	11.1
	Exp3	4.8
NSet-II	Exp1	5.7

	Exp2	4.9
	Exp3	12.5
	Exp4	3.2
	Exp5	1.5

6.3.3 Applicability of Equation 4.11 for simulating pit migration

The bed load transport equation developed in this study (Equation 4.11) is also applied for simulating pit migration.

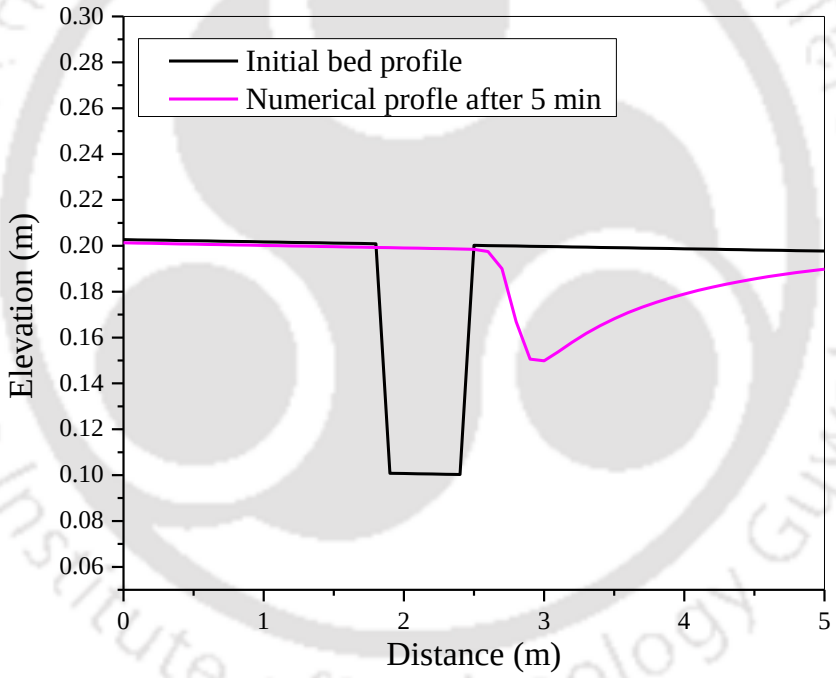

Figure 6.8 Numerical profile after 5 minutes of simulation by using Equation 4.11 (Exp3 of NSet-I)

Similar trend of profile with a very high migration speed leading to filling up the pit at very fast rate is observed due to the application of this equation (Figure 6.8). In the present experiment bed load discharge was collected at the downstream end of the flume. The mining pit in the channel also acts as a sediment entrapper, which collects the sediment transported from the

upstream and thus the migration of upstream edge occurs. The erosion at the downstream of the pit has been observed higher than the upstream and has been already discussed in the previous chapters (Chapter 3 and Chapter 4). The migration of upstream edge of the pit does not depend on the sediment transport rate from the downstream of the pit. The mining pit divide the whole system into two parts, one upstream of the pit and another one is the downstream of it. The bed load discharge data used for developing Equation 4.11 were collected at the downstream end of the flume, which is influenced by the severe erosion at the downstream of the pit and results in higher rate of sediment out flux. So, the use of this equation will definitely give a higher migration speed for the upstream edge of the pit. In this regards a rigorous study on the comparison of sediment transport rate between upstream and downstream of the pit can be recommended as a future work.

6.4 Conclusions

Determination of migration of mining pit is important since it gives the time taken for filling up of a pit of particular volume, which can be used for sustainable mining operation. In this chapter, applicability of a numerical model for simulating mining pit migration has been discussed. A first order flux vector splitting finite difference scheme has been used for the solution of hydrodynamic equation. The simulated result is compared with experimental one for an alluvial laboratory channel. Hydrodynamic and bed elevation changes equations are solved simultaneously by using semi couple methodology. This model allows the use of various sediment transport equations for simulating the propagation of upstream edge of the mining pit and downstream erosion of it. The characteristics of erosion of the channel bed due to the presence of mining pit are observed to be similar irrespective of the use of various sediment transport formulation. However, the migration speed and the downstream erosion are different for different sediment transport formula due to the empirical nature of these formulations. Van Rijn formula has shown a comparable agreement of results in terms of downstream erosion and propagation of upstream edge of the pit. However, more rigorous understanding of empirical nature of sediment transport formulation is necessary, since selection of these formulations has significant influence on the numerical model.

7 Conclusions and Future Recommendations

The present study was conducted to understand the channel response to an external disturbance, named sand mining on its morphology and hydrodynamics. Experimental study was carried out with various hydraulic conditions for five different shaped mining pits. It has been observed that mining pit causes erosion at the downstream of the pit. Important conclusions regarding morphology and hydrodynamics are drawn from this study and are presented below:

7.1 Geomorphic Characteristics in a Mining Affected Alluvial Channel

- Erosion of channel bed at downstream of the pit is observed irrespective of the shape of the pit.
- The upstream edge migrates towards the downstream and the edge maintains an angle nearly equal to the angle of repose of the bed material.
- At downstream no such angle is maintained and the edge is completely washed out.
- The migration of upstream edge increases with increase in discharge into the channel.
- Both longitudinal and cross-sectional profile shows filling up of the pit with time, that is, the depth of the pit decreases with the increase in time.
- In case of the pit constructed along the centerline of the flume leaving bank on both sides, the cross-sectional profiles of it shows erosion of bank and decrease in scour depth with time. The initial dry bed slope of the bank line is distorted and flattening of the cross-sectional slope with time is observed.
- The erosion at the downstream of the pit is not constricted to the width of the pit but spreads to the whole width of the channel by completely destroying the downstream edge of the pit.
- In-stream mining directly alters the channel geometry and bed elevation as shown in the present experimental work, which can further affect the waterway at mining region as well as downstream of it. It also has direct influence on the erosion of foundation level of any hydraulic structures.

7.2 Turbulent Flow Structure and Bed Load Transport Characteristics in a Mining Affected Alluvial Channel

- The maximum values of Reynolds shear stress increases at center of the pit and also at the downstream of it as compared to the upstream of the pit. Linear projection of Reynolds shear stress shows maximum shear velocity at the center of the pit. We also observed higher shear velocity at downstream of the pit as compared to the upstream of it.
- The position of occurrence of maximum Reynolds shear stress from the bed surface is higher in the pit as well as in the downstream of the pit. The increase in the distance of occurrence of maximum Reynolds shear stress attributes to the fact that more turbulence is created due to the oscillation on the top of the pit, which further increases the occurrence of momentum exchange and results in more Reynolds shear stress at those sections.
- Mining pit causes disturbance to the vertical velocity profile in the pit region. At the upstream edge of the pit the velocity profile follows the modified logarithmic law for the inner zone of the flow. At the center of the pit, negative stream-wise flow velocity at the bottom shows the presence of recirculation zone. The negative velocity at the bottom gets recovered at the downstream edge of the pit but velocity profile does not follow the modified logarithmic law at this section.
- Presence of mining pit increases near-bed stream-wise and vertical turbulent intensities in the pit and downstream of it as compared to the upstream section. The flow also shows highly anisotropic in nature.
- The transport of sediment along the flow direction shows the mobile nature of the channel bed and dominance of sweep over ejection in the near bed region is observed in all the sections.
- Contribution of sweep event is observed to as maximum in the mining region and the downstream of it. The increase in the thickness of the sweep dominance zone to the entire *z/h* at downstream section of the pit indicates the increase in the sediment transport at downstream of the pit than upstream.

- Comparison of non-dimensional sediment transport parameter shows higher sediment transport rate for the experiments having mining pit as compared to the plain bed experiment. It indicates a higher rate of sediment transport due to the presence of in-stream mining pit.

7.3 Migration of Mining Pit and Multi-Scale Characterization of Migration

- Migration of upstream boundary with time occurs and the migration speed of upstream edge increases with increase in bank value. It is also observed that migration speed is more sensitive to the flow property than the pit geometry.
- An empirical formulation is derived to determine the migration speed of the mining pit, which is an important factor, required for quantitative understanding of sand mining and can be used for sustainable development.
- Multi-scale statistical characterization of mining pit migration shows decrease in celerity with increase in scale.
- Celerity at each scale and average celerity from the multi-scale analysis shows increase in celerity with increase in length by width ratio of the pit.

7.4 Scope of Applying Numerical Model for Simulating Pit Migration

- In this research, basic objective of numerical modeling was to investigate the scope and limitation of numerical model in simulating pit migration.
- Numerical bed profile shows migration of mining pit and erosion at the downstream of the pit. However, quantitative difference of migration speed and downstream erosion is observed for different sediment transport formula for same initial and boundary condition.
- In this study, Van Rijn (1984) approach shows quantitative agreement with experimental one in terms of pit migration and downstream erosion. However, it cannot be concluded that this formulation is the best fit for simulating pit migration.
- The study reveals that the inherent uncertainty in sediment transport formula added more approximation to the numerical model. Hence, proper understanding of finer details of sediment transport mechanism is required for more robust numerical simulation of pit migration.

7.5 Recommendations for the Future Work

Sand mining is a very common manmade disturbance that occurs in a river and changes the sediment and flow characteristics. The present research on mining pit in an experimental channel leaves wide scope to explore various other factors that are affected by mining activities. Future scope of this work can be summarized as below:

- The flow in the pit region is highly three dimensional; hence more research investigation is required to explore the characteristics of velocity and turbulence in all three directions.
- The effects of boundary roughness on flow characteristics in a mining affected alluvial channel need to be studied in future. Comprehensive study is needed to understand the structure of eddies formation in the pit region and also an elaborate investigation on velocity profile.
- In the present study, we have considered the pit in a straight channel. Therefore, more research is needed to understand the effects of mining pit in meandering and non-prismatic channel.
- The study can also be extended to investigate both in-stream and flood plain mining in a compound channel.
- More research can be carried out to understand the change in morphology and flow characteristics after removal of the natural armor layer.
- The numerical model developed in this study is very nascent in nature. From the analysis of hydrodynamic in the pit region, we have observed change in flow characteristics in that region. A detailed study is required for development of three dimension numerical model for simulating pit migration.
- Study can also be carried out for comparison of sediment transport rate at upstream and downstream of the pit.
- Since sand mining has huge economic benefits and plays important role in infrastructure development, more detailed investigation is required for developing a sustainable management practice.

References

Aberle J, Nikora V, Henning M, Ettmer B, Hentschel B. 2010. Statistical characteristics of bed roughness due to bed forms: A field study in the Elbe River at Aken, Germany. *Water Resource Research*, 46, W03521, doi:10.1029/2008WR007406.

Afzalimehr H, Moghbel R, Gallichand J, Jueyi SUI. 2011. Investigation of turbulence characteristics in channel with dense vegetation. *International Journal of Sediment Research* 26(3): 269-282.

Alfrink BJ, Van Rijn LC. 1983. Two- Equation turbulence model for flow in Trenches. *Journal of Professional Issues in Engineering* 109 (3): 941-958.

Anderson JD.Jr. (1995). *Computational fluid dynamics*. McGraw Hill, India, 497-502.

Beheshti AA, Ataie-Ashtiani B. 2008. Analysis of threshold and incipient conditions for sediment movement. *Coastal Engineering* 55: 423-430.

Brestolani F, Solari L, Rinaldi M, Lollino G. 2015. On morphological impacts of gravel mining: the case of the Orco River. *Engineering Geology for Society and Teritory* 3: 319-322.

Bull WB, Scott KM. 1974. Impact of mining gravel from urban stream beds in the southwestern United States. *Geology* 2: 171-174.

Cao Z, Day R, Egashira S. 2002. Couple and decouple numerical modelling of flow and morphological evolution of alluvial rivers. *J. Hydraul. Eng*. 128: 306-321.

Cao Z, Pender G. 2004. Numerical modelling of alluvial rivers subjected to interactive sediment mining and feeding. *Advances in Water Resources* 27: 533-546.

Calle M, Alho P, Benito G. 2017. Channel dynamics and geomorphic resilience in an ephemeral Mediterranean river affected by gravel mining. *Geomorphology* 285: 333-346.

Cellino M, Lemmin U. 2004. Influence of coherent flow structures on the dynamics of suspended sediment transport in open channel flow. *Journal of Hydraulic Engineering* 130 (11): 1077–1088.

Chaudhry MH. (2008). *Open channel flow*. Second edition, Springer, 323-364.

Chen D, Liu M. 2009. One and Two dimensional modelling of deep gravel mining in the Rio Salado. World Environmental and Water Resources Congress 3462-3470.

Chen D, Acharya K, Stone M. 2010. Sensitivity analysis of nonequilibrium adaptation parameters for modeling mining-pit migration. *J. Hydraul. Eng*. 136: 806-811.

Collins BD, Dunne T. 1989. Gravel transport, gravel harvesting, and channel bed degradation in rivers draining the Southern Olympic Mountains, Washington, U.S.A.. *Environmental Geology* 13: 213-224.

Collins BD, Dunne T. 1990. Fluvial geomorphology and river gravel mining: a guide for planners. *California division of mines and geology*, special publication 98, Sacramento, CA.

de Leeuw J, Shankman D, Wu G, de Boer WF, Burnham J, He Q, Yesou H, Xiao J. 2010. Strategic assessment of the magnitude and impacts of sand mining in Poyang Lake, China. *Regional Environmental Change*, 10(2): 95-102.

Death RG, Winterbourn MJ. 1995. Diversity pattern in stream benthic invertebrate communities: The influence of habitat stability. *Ecology*, 76 (5): 1446-1460.

Deshpande V, Kumar B. 2016. Turbulent flow structures in alluvial channels with curved cross-sections under conditions of downward seepage. *Earth Surface Processes and Landforms* 41: 1073-1087.

Emadzadeh A, Chiew YM, Afzalimehr H. 2010. Effect of accelerating and decelerating flows on incipient motion in sand bed streams. *Advances in Water Resources* 33(9): 1094-1104.

Erskine WD. 1990. Environmental impacts of sand and gravel extraction on river systems. *The Brisbane River: a source book for the future, Australian Littoral Society, Moorooka*, 295-302.

Femmer SR. 2002. *Instream gravel mining and related issues in southern Missouri* (No. 012-02).

Fredsoe J. 1978. Sedimentation of river navigation channels. *Journal of the Hydraulic Division* 104: 223-236.

Gill MA. 1994. Hydrodynamics of mining pits in erodible bed under steady flow. *Journal of Hydraulic Engineering* 120: 1337-1348.

Goring DG, Nikora VI. 2002. Despiking acoustic doppler velocimeter data. *Journal of Hydraulic Engineering* 128 (1): 117–126.

Grass AJ. 1981. Sediment Transport by Waves and Currents - Report No : FL29. London: SERC London Centre for Marine Technology.

Hatva T. 1994. Effect of gravel extraction on groundwater. *IAHS Publications-Series of Proceedings and Reports-Intern Assoc Hydrological Sciences* 222: 427-434.

Hudson J. (2001). *Numerical technique for morphodynamic modeling*. (Doctoral dissertation, Department of mathematics, The University of Reading, Whiteknights).

Ikhsan J, Fujita M, Takebayashi H. 2009. Sustainable sand mining management in Merapi Area using groundsills. Annuals of disaster prevention research institute, Kyoto University, No. 52 B.

Kim C. 2005. Impact analysis of river aggregate mining on river environment. *KSCE Journal of Civil Engineering* 9: 45-48.

Kondolf GM. 1993. The reclamation concept in regulation of gravel mining in California. *Journal of environmental planning and management* 36: 397-409.

Kondolf GM. 1994. Geomorphic and environmental effects of instream gravel mining. *Landscape Urban Planning* 28: 225-243.

Kondolf GM. 1997. Hungry water: effects of dams and gravel mining on river channels. *Environmental Management* 21(4): 533–551.

Kumar P, Foufoula-Georgiou E. 1997. Wavelet analysis for geophysical applications. *Review of Geophysics* 35(4): 385–412.

Lacey RWJ, Roy AG. 2008. Fine-scale characterization of the turbulent shear layer of an in-stream pebble cluster. *Journal of Hydraulic Engineering* 134 (7): 925–936.

Lai X, Shankman D, Huber C, Yesou H, Huang Q, Jiang J. 2014. Sand mining and increasing Poyang Lake's discharge ability: A reassessment of causes for lake decline in China. *Journal of Hydrology* 519: 1698-1706.

Lamelas MT, Marinoni O, Hoppe A., de La Riva, J. 2008. Suitability analysis for sand and gravel extraction site location in the context of a sustainable development in the surroundings of Zaragoza (Spain). *Environmental geology* 55(8): 1673-1686.

Lane EW. 1955. The importance of fluvial morphology in hydraulic engineering, *Proceedings, ASCE*, 81, paper 745, 1-17.

Lee HY, Fu DT, Song MH. 1993. Migration of rectangular mining pit composed of uniform sediment. *Journal of Hydraulic Engineering* 119: 64-80.

Li J, Qi M. 2015. Local scour induced by upstream riverbed level lowering. *Natural Hazards*. DOI 10.1007/s11069-015-1677-y.

Lu J, Liu C, Guan J, Liu L, Liu H. 2015. Sand and gravel mining in upstream of the Yangtze river and its effect on the Three Gorges Reservoir. World environmental and water Resources Congress 1821-1830.

Mallat S. 1998. A Wavelet Tour in Signal Processing, Academic, San Diego, Calif.

Marsh NA, Western AW, Grayson RB. 2004. Comparison of methods for predicting incipient motion for sand beds. *Journal of Hydraulic Engineering* 130 (7): 616–621.

Mas-Pla J, Montaner J, Sola J. 1999. Ground water resources and quality variations caused by gravel mining in coastal stream. *J. Hydraul. Eng*. 216: 197-213.

Mohtar WHMW, Sharil S, Mukhlisin M. 2016. Representative sediment sizes in predicting the bed-material load for nonuniform sediments. *International journal of sediment research* 31 (1): 79-86.

Nepf HM, Vivoni ER. 2000. Flow structure in depth-limited, vegetated flow. *Journal of Geophysical Research*. 150 (12): 28547–28557.

Neyshabouri SAAS, Farhadzadeh A, Amini A. 2002. Experimental and field study of mining pit migration. *International Journal of Sediment Research* 17(4): 323-33.

Nezu I. 1977. Turbulent structure in open channel flow. (PhD thesis, Kyoto University, Kyoto, Japan).

Nezu I, Nakagawa H. 1993. Turbulence in Open Channels, in: IAHR/AIRH Monograph, Balkema, Rotterdam, The Netherlands.

Nikora VI, Sukhodolov AN, Rowinski PM. 1997. Statistical sand wave dynamics in one-directional water flows. *Journal of Fluid Mechanics* 351: 17–39.

Ojha S, Choudhary S. 2017. Qualitative analysis of socio-environmental factors of sand mining on Mithri Tributary of Luni River at Kosana, Pipar Jodhpur Dist. of Rajasthan, India. *International Research Journal of Environmental Sciences* 6(10): 22-31.

Padmalal D, Maya K, Sreebha S, Sreeja R. 2008. Environmental effects of river sand mining: a case from the river catchments of Vembanad lake, Southwest coast of India. *Environmental geology* 54(4): 879-889.

Prasad VR. 1991. *Velocity, Shear and Friction factor studies in rough rectangular open channels for super critical flow*. (Ph.D. thesis, Indian Institute of Science, Bangalore).

Qi M, Kuai YR. 2017. Pier scour under influence of headcut erosion of sand pit. *Journal of Hydraulic Engineering*. DOI: 10.13243 / j.cnki.slxb.20160820.

Ramkumar M, Kumaraswamy K, James RA, Suresh M, Sugantha T, Jayaraj L, Mathiyalagan A, Saraswathi M, Shyamala J. 2015. Sand mining, channel bar dynamics and sediment textural properties of the Kaveri river, South India: implications on flooding hazard and sustainability of the natural fluvial system. *Environmental Management of River Basin Ecosystems*. DOI 10.1007/978-3-319-13425-3_14: 283-318.

Rao AR, Sreenivasulu G, Kumar B. 2011. Geometry of sand-bed channels with seepage. *Geomorphology* 128 (3–4): 171–177.

Rehman K, Cho YS. 2016. Bed evolution under rapidly varying flows by a new method for wave speed estimation. *Water* 8(5), 212.

Rinaldi M, Wyżga B, Surian N. 2005. Sediment mining in alluvial channels: physical effects and management perspective. *River Research and Application* 21: 805-828.

Robinson CT, Minshall GW. 1986. Effect of disturbance frequency on stream benthic community structure in relation to the canopy cover and season. *Journal of North American Benthological Society* 5(3): 237-248.

Rovira A, Batalla RJ, Sala M. 2005. Response of a river sediment budget after historical gravel mining (The lower Tordera, NE Spain). *River Research and Application* 21: 829-847.

Santo EL, Sanchez LE. 2002. GIS applied to determine environmental impact indicators made by sand mining in a floodplain in southeastern Brazil. *Environmental Geology* 41:628-637.

Sear DA, Archer D. 1998. Effects of gravel extraction on stability of gravel-bed rivers: the Wooler Water, Northumberland, UK. *Gravel-bed rivers in the environment. Edited by RL Beschta, PD Komar, and JB Bradley. Water Resources Publications, Highlands Ranch*, Colo, 415-432.

Singh A, Lanzoni S, Wilcock PR, Foufoula-Georgiou E. 2011. Multiscale statistical characterization of migrating bed forms in a gravel and sand bed rivers. *Water Resource Research* 47, W12526, doi:10.1029/2010WR010122.

Singh O., Kumar A. 2017. Sand and gravel extraction from piedmont and floodplain zones of Yamunanagar district in Haryana, India: Environmental tragedy or economic gain? *International Journal of Environmental Studies*: 1-17.

Vade PM, Boix CF, Ollero A. 2010. Incision due to gravel mining: modeling a case study from the Gallego river, Spain. *Geomorphology* 117: 261-271.

Van Rijn LC. 1986. Sedimentation of dredged channels by currents and waves. *Journal of waterway port coastal and ocean engineering* 112 (5): 541-559.

Wilcock PR. 2001. Toward a Practical Method For Estimating Sediment Transport Rates in Gravel Bed Rivers. *Earth Surface Processes and Landforms* 26: 1395-1408.

Wu W. 2004. Depth averaged two dimensional numerical modelling of unsteady flow and nonuniform sediment transport in open channels. *J. Hydraul. Eng*. 130 (10): 1013-1024.

Wu W. 2007. *Computational river dynamics*, Taylor and Francis.

Wu W, Wang SSY. 2008. Simulation of morphological evolution near sediment mining pits using 1-D mixed regime flow and sediment transport model. World Environmental and Water Resources Congress.

Yang CT. 1996. *Sediment transport: theory and practice*. McGraw Hill, Singapore.

Yanmaz AM, Cicekdag O. 2000. Channel mining induced stream bed instability around bridges. *Watershed Management and Operation Management 2000*: 1-8.

Yue X, Mu X, Zhao G, Shao H, Gao P. 2014. Dynamic changes of sediment load in the middle reaches of the Yellow River basin, China and implication for eco-restoration. *Ecological Engineering* 73: 64-72.

Zawiejska J, Wyżga B, Pawlik AR. 2015. Variation of bed material along mountain river modified by gravel extraction and channelization, the Czarny Dunajec, Polish Carpathians. *Geomorphology* 231: 353-366.

Zrostlík Š, Bareš V, Krupička J, Picek T, Matoušek V. 2016. Distribution of velocity and turbulent characteristics in coarse-sediment laden flows above erodible plane bed in open channel. *EPJ Web of Conferences* 114: 02144.